

St. Paul Island, Pribilof Islands, Alaska : geology, volcanic evolution, and volcanic hazards
by Grace Sherwood Winer

A thesis submitted in partial fulfillment of the requirements for the degree of Master of Science in Earth Sciences
Montana State University
© Copyright by Grace Sherwood Winer (2001)

Abstract:
St. Paul Island, Alaska, is a potentially active Pleistocene to Holocene volcanic center located in the Bering Sea about 400 km north of the Aleutian arc front. Previous geological mapping and studies of the geology of St. Paul Island have been done only in reconnaissance. This study has been undertaken in order to make the first detailed geological map of the island, to reconstruct its eruptive history and volcanic evolution, and to assess volcanic hazards that may be associated with future eruptions. New geological mapping covers the entire island at a scale of 1:28,000 and includes 17 volcanic units. Eruptive styles on St. Paul have evolved from early, mostly effusive eruptions of primitive lavas that form the platform of the island, to more explosive monogenetic cinder cones emplaced upon the platform, to the polygenetic centers that are forming large shields from repeated eruptions of evolved low viscosity lavas. Lavas erupted are mainly basalts, basanites, and tephrites with MgO contents ranging from 14 to 4 wt% and phenocryst assemblages of olivine ± clinopyroxene and plagioclase. St. Paul's volcanic system as a whole is trending toward the progressive development of shallow crustal magma chambers where cooling and differentiation are occurring. A new 14C date of 3230 ybp has been obtained on the youngest lava flow on St. Paul. Volcanic hazards associated with a future eruption on St. Paul Island are similar to those from dominantly Strombolian style eruptions at other basaltic lava fields. However, because of St. Paul's unique human and wildlife populations, isolated location, and extreme weather conditions in the Bering Sea, volcanic risks may be exacerbated. Assuming a predictable eruption recurrence interval of 7400 years, the probability of an eruption on St Paul Island in future decades is estimated to be extremely small.

ST. PAUL ISLAND, PRIBILOF ISLANDS, ALASKA:

GEOLOGY, VOLCANIC EVOLUTION, AND VOLCANIC HAZARDS

by

Grace Sherwood Winer

A thesis submitted in partial fulfillment
of the requirements for the degree

of

Master of Science

in

Earth Sciences

MONTANA STATE UNIVERSITY
Bozeman, Montana

April 2001

© COPYRIGHT

by

Grace Sherwood Winer

2001

All Rights Reserved

N378
W7255

APPROVAL

of a thesis submitted by

Grace Sherwood Winer

This thesis has been read by each member of the thesis committee and has been found to be satisfactory regarding content, English usage, format, citations, bibliographic style, and consistency, and is ready for submission to the College of Graduate Studies.

Todd C. Feeley _____ 4-12-01
(Signature) Date

Approved for the Department of Earth Sciences

James G. Schmitt _____ 4-12-01
(Signature) Date

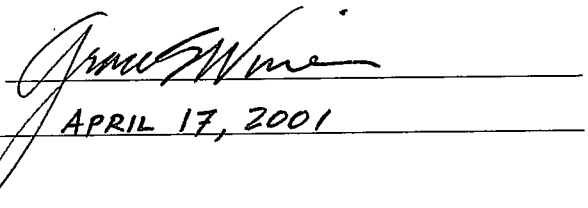
Approved for the College of Graduate Studies

Bruce McLeod _____ 4-18-01
(Signature) Date

STATEMENT OF PERMISSION TO USE

In presenting this thesis in partial fulfillment of the requirements for a master's degree at Montana State University, I agree that the Library shall make it available to borrowers under the rules of the Library.

If I have indicated my intention to copyright this thesis by including a copyright notice page, copying is allowable only for scholarly purposes, consistent with "fair use" as prescribed in the U.S. Copyright Law. Requests for permission for extended quotation from or reproduction of this thesis in whole or in parts may be granted only by the copyright holder.

Signature 

Date APRIL 17, 2001

ACKNOWLEDGEMENTS

Support for this project was generously provided by the National Geographic Society, the Geological Society of America, and Sigma Xi Grants-in-Aid of Research. I am indebted to the people of St. Paul Island for their warm hospitality and assistance, without which our work on St. Paul would have been very difficult indeed. Thank you Phyllis Swetzof, Aquilina Bourdukofsky, Karin Holser, and so many others. Special thanks to Dr. David Lageson for introducing me to the fascinating field of geology and for advice, support and encouragement throughout my undergraduate and graduate years at Montana State University. Thanks to Dr. George Plafker and Dr. Ken Pierce for consultation on Bering Sea tectonics; to Dr. Mel Kuntz for advice on organic carbon sampling; and to Dr. Joseph Ashley for advice on interpretation of aerial photographs and map technicalities. Special thanks to Anne Loi for technical support and encouragement. Thanks to Dr. J.J. Borkowski for consultation on statistics, to the staff at the NOAA National Weather Service station on St. Paul Island for data on weather and tides, and to Peter Gauer for interpretation of weather data. Thanks to my committee members, Dr. Jim Schmitt and Dr. Bill Locke, for their insight and helpful suggestions. My deepest gratitude to my advisor Dr. Todd Feeley for years of patience, helpful discussions, guidance, and advice, both in the field and at MSU. I thank Bernie for unwavering support over the years, my family for their encouragement and confidence in me, and Ruth for introducing me to St. Paul Island.

TABLE OF CONTENTS

1. INTRODUCTION 1

Statement of Purpose 1
Geographic Location and Description of St. Paul Island 2
Regional Geology and Tectonic Setting 4
Geology of St. Paul Island: Previous Work and Current State of Knowledge 7

2. METHODS 16

Mapping and Sample Collection 16
X-ray Fluorescence 17
Petrography 17
Geochronology 18

3. GEOLOGY OF ST. PAUL ISLAND 19

Ages of Rocks on St. Paul Island 19
Classification and Composition of St. Paul Rocks 20
Geological Map of St. Paul Island 34
Descriptions and Interpretations of Map Units 36
Undifferentiated Platform Lavas (UPL) Description 36
Kaminista Description 46
Kaminista Interpretation 48
Undifferentiated Platform Lavas (UPL) Interpretation 50
Undifferentiated Lava Flows (ULF) Description 52
Undifferentiated Lava Flows (ULF) Interpretation 52
PyC Unit Description 52
PyC Unit Interpretation 55
Black Bluffs (BB) Description 56
Black Bluffs (BB) Interpretation 58
Polovina Hill (POL) Description 60
Polovina Hill (POL) Interpretation 64
Hill 404 (404) Description 66
Hill 404 (404) Interpretation 67
North Hill (NoH) Description 67
North Hill (NoH) Interpretation 69
Hill 255 (H255) Description 69
Hill 255 (H255) Interpretation 70
Crater Hill (CH) Description 71
Crater Hill (CH) Interpretation 73

TABLE OF CONTENTS - CONTINUED

Lake Hill (LH) Description 74
Lake Hill (LH) Interpretation 77
Ridge Hill (RiH) Description 77
Ridge Hill (RiH) Interpretation 78
Rush Hill (RuH) Description 79
Rush Hill (RuH) Interpretation 81
Ridge Wall (RW) Description 82
Ridge Wall (RW) Interpretation 85
Hutchinson Hill (HH) and Northeast Point Description 86
Hutchinson Hill (HH) Interpretation 88
Airport Lava Field (ALF) Description 89
Airport Lava Field (ALF) Interpretation 90
Cone Hill Volcanic Complex (CHVC) Description 91
Cone Hill Volcanic Complex (CHVC) Interpretation 95
Bogoslof Hill Volcanic Complex (BHVC) Description 100
Bogoslof Hill Volcanic Complex (BHVC) Interpretation 106
Fox Hill (FXH) Description 109
Fox Hill (FXH) Interpretation 114
Surficial Deposits (Sd) Description 115
Faulting and Fissuring 116
Volcanic and Structural Lineaments 119
Xenoliths in St. Paul Lavas 124

4. SUMMARY 126

Volcanic Evolution of St. Paul Island 126
Platform Building Stage 126
Monogenetic Cinder Cone Stage 128
Polygenetic Shield Stage 133
Compositional and Petrologic Evolution of St. Paul Island 136

5. POTENTIAL VOLCANIC HAZARDS AND RELATED RISKS 140

Introduction and Definitions 140
Hazard Assessment 142
Potential Volcanic Hazards 143
Estimate of Eruptive Intervals and Prediction 144
Volcanic Hazard Characteristics and Associated Risks on St. Paul Island 146
Lava Flows 146

TABLE OF CONTENTS - CONTINUED

Tephra Falls 147
Ballistic Ejecta 148
Volcanic Gases 149
Ground Deformation 149
Earthquakes: Seismicity of Volcanic Origin 149
Tsunami 150
Base Surge 150
Factors That May Exacerbate Risks on St. Paul Island 151
Hazard Mapping 152
Suggestions for Dealing with Future Volcanic Eruptions 154

6. CONCLUSIONS 156

REFERENCES CITED 158

APPENDIX A: RADIOCARBON SAMPLE PREPARATION AND ANALYTICAL TECHNIQUES 168

LIST OF TABLES

Table

1. Major Element, Trace Element, and Modal Analyses of Volcanic Rocks and Xenoliths from St. Paul Island, Alaska 22

2. CIPW Calculated Normative Minerals in Weight Percent and Rock Names 29

LIST OF FIGURES

Figures

1. Location of St. Paul Island 3

2. Tectonic setting of St. Paul Island 5

3. Barth's geologic map of St. Paul Island 9

4. Classification of the rocks 21

5. Pahoehoe flow lobe details 37

6. Lava tube near sea level at Southwest Point 38

7. Lava toes and columnar jointing in lava flow lobes at Reef Point 39

8. Marine and beach sediments at Tolstoi Point 40

9. Lava flows at Tolstoi Point thicken upward 40

10. Schematic diagram of stratigraphy at Zapadni Point 41

11. Schematic diagram of vertical section at Einahnuhto Bluffs on St. Paul's west coast 43

12. Photomicrographs showing textures of platform lavas 45

13. Kaminista ridge with view to the northeast 47

14. Kaminista 49

15. Black Bluffs, the emergent tuff/cinder cone located near the village of St. Paul 57

16. Close-up view of Black Bluffs 57

17. Diagram of Surtseyan eruption at Black Bluffs 59

LIST OF FIGURES - CONTINUED

18. Polovina Hill, a large complex cinder cone, dominates eastern St. Paul Island 60

19. Vertical section on east flank of Polovina Hill is exposed in a quarry 61

20. Bombs from Polovina Hill 62

21. Photomicrograph of trachyte from Polovina Hill (SP98-35) 63

22. North Hill is a complex cinder cone located on northern St. Paul Island 68

23. Olivine-rich North Hill basanite with glassy groundmass 68

24. Crater Hill viewed across a lava flow from Bogoslof Hill 72

25. Photomicrograph of lherzolite xenolith (left) in Crater Hill lava (SP98-50) 73

26. At Lake Hill, vents are located on intersecting NE-SW lineaments 76

27. Schematic diagram of Ridge Hill cinder cone and proposed mechanism for basal cone spreading (Kuntz et al., 1982) 79

28. Schematic diagram of section through Rush Hill and Einahnuhto Bluffs on the west coast of St. Paul Island (Barth, 1956) 80

29. Praying Aleut 84

30. Photomicrograph of Ridge Wall olivine basalt (SP98-42) 84

31. Photomicrograph of granitoid xenolith (left and upper right) in Ridge Wall lava (SP98-43X) 85

32. Hutchinson Hill located on Northeast Point 87

LIST OF FIGURES – CONTINUED

33. Photomicrograph of crystal-rich Hutchinson Hill basalt (SP98-04) 88

34. View from Kittiwake Lake caldera looking northeast along the Cone Hill ridge 92

35. Fissure on Cone Hill ridge 93

36. Exposure of feeder dike in Cone Hill ridge 93

37. Collapsed lava tube on southwestern Cone Hill ridge 94

38. Photomicrograph of glomeroporphyritic CHVC lavas 95

39. Proposed mechanism for formation of lava dome in Cone Hill volcanic complex 99

40. Profile of Bogoslof Hill as seen from Lake Hill 100

41. Northwest cone on Bogoslof Hill 101

42. Fissure in lava tongue on east flank of Bogoslof Hill strikes E-W across Bogoslof summit 103

43. Photomicrographs of BHVC lavas 105

44. Fox Hill cinder cone and lava flow (FXH) 110

45. Sample site for ^{14}C in layer of sediment beneath Fox Hill lava flow (SP98-64) 111

46. Segments of the breached Fox Hill cinder cone that have been rafted along on the Fox Hill lava flow 111

47. Fox Hill lava flow at Southwest Point 112

48. Photomicrograph of fractionated Fox Hill lava 113

49. Faulting of platform lavas on Tolstoi Point 117

LIST OF FIGURES - CONTINUED

50. Fissure on Bogoslof Hill 118

51. Volcanic and structural lineaments on St. Paul Island and surrounding area 120

52. Lineaments of volcanic vents, fissures, and faults on St. Paul Island 121

53. Rose diagrams showing directional trends of A: fissures, B: cone breaching, C: faults, and D: vent alignments 123

54. Platform lavas on the west coast 127

55. Schematic diagram of a monogenetic volcanic field 129

56. Relationship of Village Hill cinder cone to platform lavas 131

57. Remnant of scoria cone on lava flows on east Reef Point 132

58. Schematic diagram of coalescing dikes forming a shallow magma chamber beneath Bogoslof Hill 135

59. Variation diagrams showing increasing evolution and fractionation of lavas from platform to monogenetic to polygenetic centers 137

60. Area of possible future lava flows from Bogoslof Hill volcano 153

LIST OF PLATES

Plates

1. Geological Map of St. Paul Island, Alaska..... Pocket

2. Cone Hill Volcanic Complex (CHVC) ..... Pocket

ABSTRACT

St. Paul Island, Alaska, is a potentially active Pleistocene to Holocene volcanic center located in the Bering Sea about 400 km north of the Aleutian arc front. Previous geological mapping and studies of the geology of St. Paul Island have been done only in reconnaissance. This study has been undertaken in order to make the first detailed geological map of the island, to reconstruct its eruptive history and volcanic evolution, and to assess volcanic hazards that may be associated with future eruptions. New geological mapping covers the entire island at a scale of 1:28,000 and includes 17 volcanic units. Eruptive styles on St. Paul have evolved from early, mostly effusive eruptions of primitive lavas that form the platform of the island, to more explosive monogenetic cinder cones emplaced upon the platform, to the polygenetic centers that are forming large shields from repeated eruptions of evolved low viscosity lavas. Lavas erupted are mainly basalts, basanites, and tephrites with MgO contents ranging from 14 to 4 wt% and phenocryst assemblages of olivine ± clinopyroxene and plagioclase. St. Paul's volcanic system as a whole is trending toward the progressive development of shallow crustal magma chambers where cooling and differentiation are occurring. A new ^{14}C date of 3230 ybp has been obtained on the youngest lava flow on St. Paul. Volcanic hazards associated with a future eruption on St. Paul Island are similar to those from dominantly Strombolian style eruptions at other basaltic lava fields. However, because of St. Paul's unique human and wildlife populations, isolated location, and extreme weather conditions in the Bering Sea, volcanic risks may be exacerbated. Assuming a predictable eruption recurrence interval of 7400 years, the probability of an eruption on St Paul Island in future decades is estimated to be extremely small.

INTRODUCTION

Statement of Purpose

Previous studies of the volcanic geology, including petrology and petrography, of St. Paul Island have been done mostly in reconnaissance (Stanley-Brown, 1892; Barth, 1956; Cox et al., 1966; Hopkins, 1976; Lee-Wong et al., 1979; Moll-Stalcup, 1994a, 1994b). Past workers have not made a detailed investigation of the eruptive history of the island correlated with changes in magma composition, nor have they presented any studies related to volcanic hazards in the event of a future eruption. However, they have suggested that volcanic eruptions on St. Paul have been a regular occurrence for about the last 300-400 Ka with eruptions taking place within the last 10,000 years, and the most recent occurring only a few thousand years ago (Cox et al., 1966; Hopkins,1976). Cox et al. (1966) and Hopkins (1976) agree that future volcanic eruptions on St. Paul Island are to be expected. Therefore, this field study of the volcanic geology of St. Paul Island and investigation of petrography and compositional trends of St. Paul magmas is undertaken for the purpose of: (1) increasing knowledge of the stratigraphy of St. Paul Island by field mapping and use of petrography and geochemistry to correlate eruptive units, (2) documenting the age and character of (a) the layered lava flows that form the platform of the island and (b) the morphologically younger units on the island's surface, (3) describing and interpreting the volcanic geology of St. Paul Island, especially the most recent volcanism, and (4) using 1-3 to make a general prediction of possible future

eruptions, their probable locations and styles, and to make an assessment of associated volcanic hazards on St. Paul Island. This work builds upon previous studies of St. Paul by Winer and Feeley (1997) and Feeley and Winer (1999), which show evidence for the development of shallow crustal magma chambers beneath the island.

The volcanic hazard assessment at St. Paul island is not only relevant because of its human inhabitants, but also because St. Paul is the seasonal breeding ground for nearly a million northern fur seals [the world's largest herd of marine mammals (Johnson, 1982)], the nesting site for large colonies of seabirds, home to a herd of several hundred reindeer, and port for the Central Bering Sea fishing fleet. Because of its rich wildlife, St. Paul Island, in spite of its remote location, is also an international tourism destination.

Geographic Location and Description of St. Paul Island

St. Paul Island is located in the Bering Sea about 440 km north of the Aleutian Island chain and 500 km west of the Alaska mainland at approximately 57° 07' N Latitude, 170° 16' W Longitude (Fig. 1). St. Paul is situated on the southern edge of the shallow and extensive Bering Sea shelf, near the 180 m depth contour, which represents a sharp break in bottom topography between the shelf and the abyssal Bering Sea (Fig. 1). St. Paul Island is the largest (40.4 mi^2; 104 km^2) of the Pribilof Islands, which consist of St. Paul and St. George, the two largest islands, and three islets located near St. Paul. The islets are Otter Island, about 1 km in length, and two smaller rocky outcrops, Sea Lion Rock and Walrus Island, over which the sea breaks in stormy weather. St. George and St. Paul,

the only inhabited islands, are each about 20 km long and are separated by 70 km. They have an arctic marine climate and the area is infamous for fog and inclement weather.

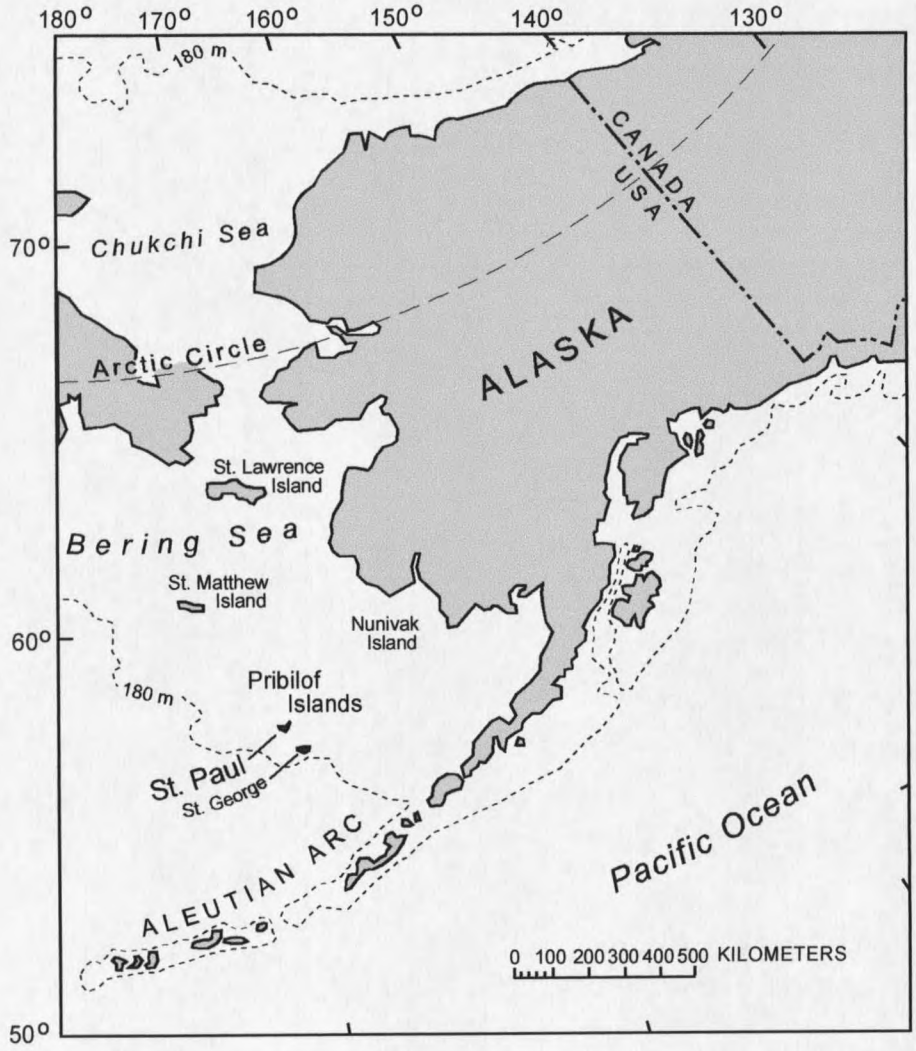


Figure 1. Location of St. Paul Island. Index map showing St. Paul Island, the Pribilof Islands, and their location on the southern edge of the Bering sea shelf. The approximate position of the shelf edge is marked by the dashed 180 m depth contour.

The Pribilof Islands, the hauling grounds for the great herds of northern fur seals, were uninhabited by humans until 1786, when they were discovered by the Russian mariner, Gehrman Pribylov (Elliott, 1881). Soon after their discovery, the Russians brought a number of Aleut people from the Aleutian Islands to the Pribilof Islands for the purpose of harvesting seal furs (Johnson, 1982). Descendents of these early settlers live on St. Paul today in the largest Aleut community (population ~750) in the world and the center of Aleut culture.

Scientific studies of the Pribilof Islands, also known as the Seal Islands, began soon after the United States acquired the territory of Alaska in 1867. Because St. Paul is the main breeding ground of the great fur seal herds, this small, remote island was the focus of many early studies, not only in geology, but also in zoology, botany, and paleontology (Hanna, 1919).

Regional Geology and Tectonic Setting

St. Paul Island is a locus of young and persistent basaltic volcanism situated in the Bering Sea about 440 km north of the Aleutian arc front. St. Paul Island, and the other Pribilof Islands, are constructed of basaltic lavas extruded onto the Pribilof Ridge, a northwest trending structural arch on the southern Bering Sea shelf (Marlow et al., 1976; Marlow et al., 1994) (Fig. 2). Volcanic eruptions in the Pribilof Islands began at St. George Island about 2.1 Ma and continued there for about 0.6 Ma (Cox et al., 1966). About 1 Ma after the initial eruption at St. George, volcanic eruptions began building St.

Paul Island, and have continued nearly to the present (Cox et al., 1966). Dredge samples from the Pribilof Ridge between St. George and St. Paul Islands have yielded basalts of an age intermediate between dates from St. George and St. Paul (Simpson et al., 1979), suggesting a northwest progression in volcanism.

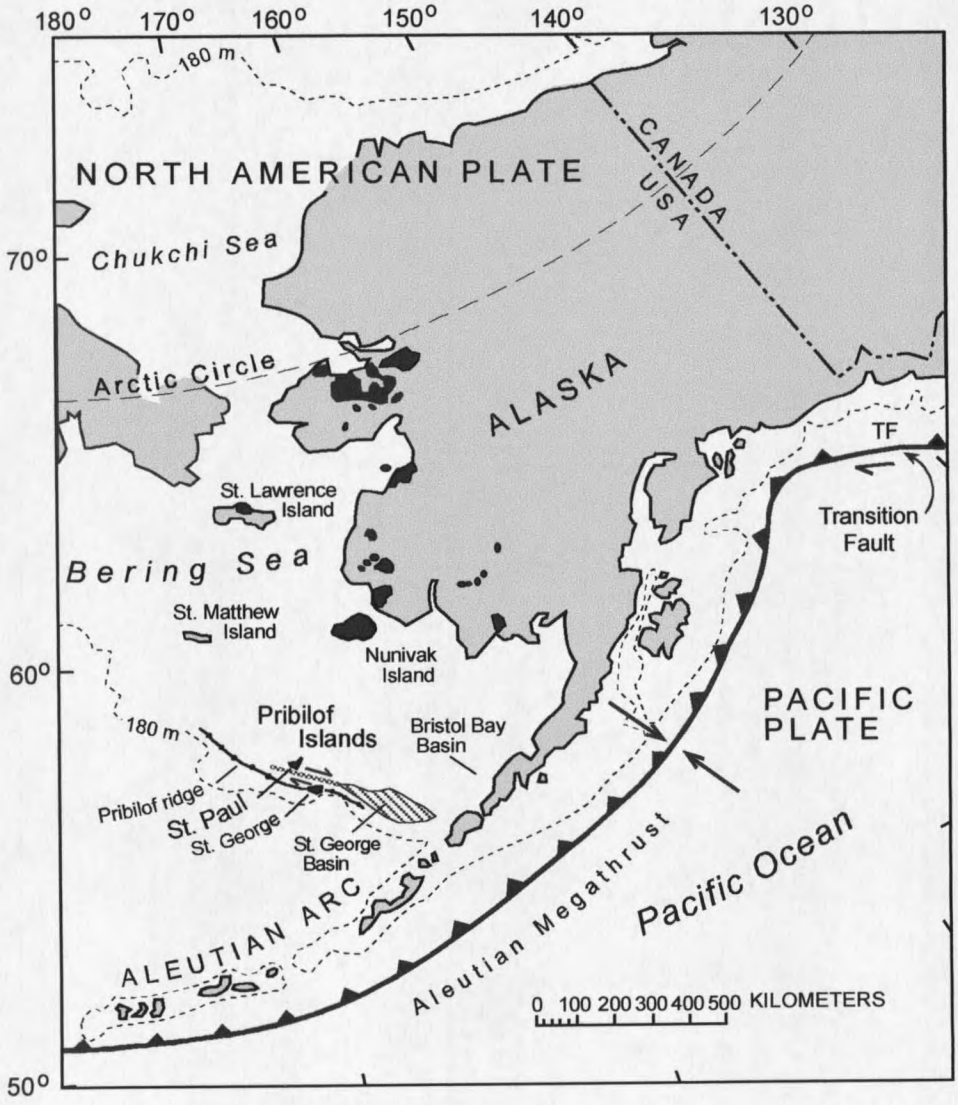


Figure 2. Tectonic setting of St. Paul Island. Black areas represent volcanic fields of the Bering Sea Basalt province. Adapted from Moll-Stalcup (1994a).

Pleistocene to Holocene in age, St. Paul is the youngest eruptive center in the Bering Sea basalt province, a group of approximately 15 late Cenozoic (<6 Ma) volcanic fields that are widely distributed behind the Aleutian arc front as eruptive centers along the Bering Sea coast of western Alaska and as islands on the Bering Sea shelf (Moll-Stalcup, 1994a, 1994b) (Fig. 2). Intraplate volcanism in the Bering Sea basalt province is associated with extension on the Bering Sea shelf and, in the Pribilof area, with extensional deformation and collapse of the Bering shelf margin (Marlow et al., 1976; Worrall, 1991; Cooper et al., 1992; Marlow et al., 1994; Plafker and Berg, 1994b; Moll-Stalcup, 1994a).

The Bering shelf margin was an active margin prior to early Tertiary time, when subduction of the Kula plate ceased (Marlow and Cooper, 1980; Plafker and Berg, 1994a; Marlow et al., 1994). Motion on the Beringian margin ceased about 50 Ma when subduction stepped to the south where the Pacific plate began to subduct beneath Alaska, trapping a fragment of the Kula plate behind the growing Aleutian arc (Hillhouse and Coe, 1994).

The North American and Pacific plates have since undergone dextral-oblique convergence along the northwest trending Transition fault and orthogonal convergence along the northeast trending Aleutian arc margin (Plafker and Berg, 1994a) (Fig. 2). Pacific plate motion is presently northwest relative to Alaska at rates from >4.9 cm/yr in southeastern Alaska to 7.7 cm/yr at the western end of the Aleutian arc (Plafker and Berg, 1994a). Some manifestations of the Pacific-North American plate interactions are (1) development of the Aleutian subduction zone and magmatic arc in early Tertiary time,

(2) basin formation associated with wrench faulting on the margin of the Bering Sea shelf, and (3) basaltic volcanism of the Bering Sea basalt province (Plafker and Berg, 1994a, 1994b) (Fig. 2).

Volcanism on the Bering Sea shelf margin appears to be controlled by mantle melting events related to continued extension and deep wrench faulting (Marlow and Cooper, 1980). The extension and wrench faulting have resulted in the formation of grabens such as St. George basin, which has developed along a margin-parallel dextral shear zone (Worrall, 1991; Cooper et al., 1992; Marlow et al., 1994; Plafker and Berg, 1994b) (Fig. 2). This shear zone strikes toward St. Paul Island, where the east-west orientation of tensional faults and eruptive centers suggests that this fault system, with a long history of past movement, is still active (Hopkins, 1976). Therefore, it appears that Quaternary volcanism on St. Paul Island is related to the ongoing interaction between the Pacific and North American plates (Cooper et al., 1992; Plafker and Berg, 1994a, 1994b; Plafker et al., 1994; Marlow et al., 1994).

Geology of St. Paul Island: Previous Work and Current State of Knowledge

St. Paul Island formed from both effusive and explosive eruptions of basaltic lavas. Early eruptions constructed a platform of nearly horizontal, stacked lava flows that rise to about 60 m above the sea. Barth (1956) suggested that these platform-building eruptions were mostly from subsequently buried fissures. Between the layered lava flows, in minor amounts, are intercalated layers of pyroclastic materials and sediments mixed with

reworked tephra, evidence that explosive eruptions were also a part of the early eruptive history of St. Paul Island (Barth, 1956).

The surface of St. Paul consists of more than fifteen scoria and spatter cones that rise 30 to 100 m above their bases and are surrounded by small shields of coalescing low viscosity lava flows (Fig. 3). St. Paul has a shoreline of headlands, sandy beaches, and wave-eroded cliffs. Seaward of the coastal cliffs are narrow beaches of angular to well-rounded basaltic boulders and, at some sites, the tessellated horizontal surfaces of eroded columnar basalt flows. Sandy beaches are located in areas where lava flows are too near sea level to form coastal cliffs. Three promontories, Reef Point, Tolstoi Point, and Zapadni Point, extend seaward from the southern shore of the island. These promontories, composed of layers of older platform lavas, are extensively faulted and tilted in contrast to the younger lava flows on the island's surface (Cox et al., 1966; Hopkins, 1976).

A central highland spans the island from east to west. Hopkins (1976) suggests that the eruptive centers aligned along this highland are rift related. The youthful volcanic topography of the central highland is marked by sharp, undissected cinder cones (Cox et al., 1966) where volcanic rocks have been little modified by mass wasting and erosion is minimal (Cox et al., 1966). Astride the highland, in the center of the island, Bogoslof Hill rises to a height of 180 m (590 feet). Bogoslof Hill was credited by Stanley-Brown (1892) with being the source of the most voluminous lava flows on the island. Surfaces of the lava flows on St. Paul have been fractured into boulders by frost-riving during intervals of more severe climate in the past, and the sharp outlines of the cinder cones

continue to be softened by geliturbation (Hopkins and Einarsson, 1966). There is no evidence that St. Paul has ever been glaciated (Hopkins and Einarsson, 1966).

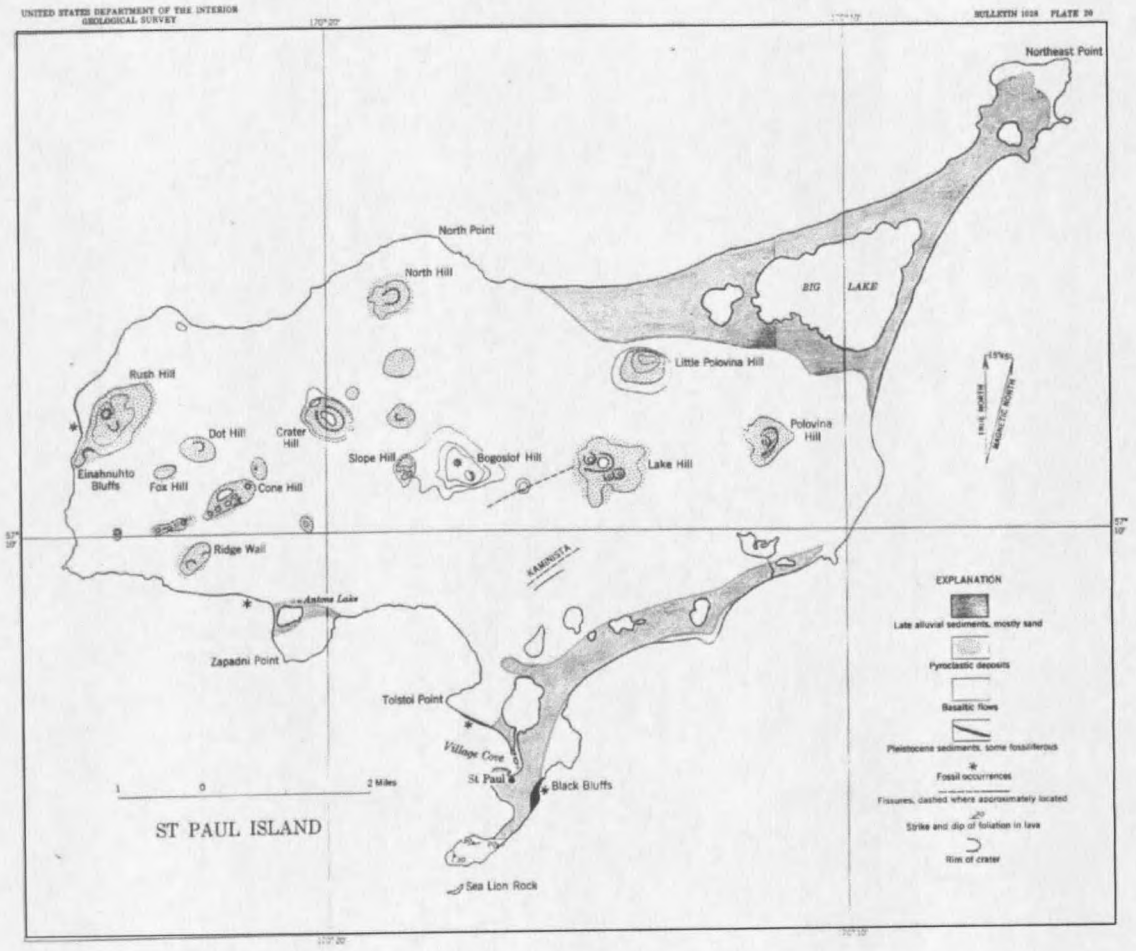


Figure 3. Barth's geologic map of St. Paul Island. From Barth (1956).

Evidence for a hydromagmatic eruption at Black Bluffs, a wave-eroded cone just east of the village of St. Paul, was noted by Stanley-Brown (1892) and Dawson (1894). These workers describe the stratification of the cone as well as the fossiliferous fragments of marly clay-rock, or calcareous argillite, torn from the sea floor during the eruption and

distributed throughout the layers of basaltic scoria and ash of the cone. Barth (1956) noted the polymict character and cross-bedding of deposits at Black Bluffs, and interpreted them as sediments transported by ice and deposited in water.

Sedimentary deposits on St. Paul Island range from layers of marine, eolian, and colluvial sediments intercalated in the layers of platform lavas, to extensive covers of eolian silt on most of the lava flows, to coastal sand dunes occurring on the eastern portion of the island (Barth, 1956; Cox et al., 1966; Hopkins, 1967a; Hopkins, 1976). The dunes, now mostly stabilized by vegetation, do not appear to have been faulted (Hopkins, 1976). Hopkins attributes the source of the eolian sediments to the Bering land bridge that was exposed during times of lowered sea level. During the platform building stage, marine transgressions related to glacial intervals deposited fossiliferous marine and beach gravel sediments on St. Paul Island (Cox et al., 1966; Hopkins, 1967a). The oldest of the marine sediments are from the Anvilian transgression (probably <1.9 to >0.7 Ma) (Hopkins, 1967). Fossiliferous marine sediments, probably of Anvilian age, are exposed on St. Paul Island at Tolstoi Point and are possibly incorporated into the base of the tuff cone at Black Bluffs (Hopkins, 1967a). A third possible location of this sedimentary deposit is beneath the village hill. In 1818, a well drilling operation, located near the north end of St. Paul village, bored into a layer of "gray marl" at 3 m above sea level (Hanna, 1919). However, a relationship between the calcareous, fossil-bearing clay blocks in Black Bluffs (described by Stanley-Brown, 1892), the marl under the village hill (Hanna, 1919), and the Anvilian sediments at Tolstoi Point (Hopkins, 1967a) has not been established.

The type locality for the middle Pleistocene Einahnuhtan transgression [<300 ka and >100 ka (Hopkins, 1976a)] is on western St. Paul Island at Einahnuhto Bluffs where marine sediments are emplaced over the stratigraphically lowest lava flow exposed beneath the bluffs (Hopkins, 1967a) [this lava flow was dated at 0.360 ± 0.10 Ma by Cox et al. (1966)]. At Einahnuhto Bluffs, fossiliferous beach and littoral Einahnuhtan sediments are interbedded with pillow lavas (Hopkins, 1967a; Lee-Wong et al., 1979) and unconformably overlain by younger boulder beach gravel of Kotzebuan age (~175 Ka) (Hopkins, 1967a). Hopkins (1967a) describes a wave-cut scarp as high as +33 m on Tolstoi Point as being carved during the Kotzebuan transgression. Fossiliferous marine sediments from the Einahnuhtan transgression are also exposed in sea cliffs at Tolstoi Point and Zapadni Point (Hopkins, 1967a). Fauna in Einahnuhtan sediments are, with few exceptions, modern (Hopkins, 1967a). Dawson (1894) described a chain of dunes southeast of Big Lake that appear to follow the subtle break-in-slope, which he attributed to changing sea level. Sea level has remained near its present level since about 3,000 BC (Hopkins, 1967a). The interested reader is directed to Hopkins (1976a) for an in-depth discussion of the various changes in sea level that affected St. Paul Island. Marine sediments and fossils of St. Paul Island are also described in some detail in earlier works (Stanley-Brown, 1892; Dall, 1899; Hanna, 1919; Washington and Keyes, 1930; Hopkins, 1967a; Hopkins, 1976).

St. Paul Island has no surface streams, as the highly permeable volcanic rocks allow the infiltration of most precipitation (Hopkins and Einarsson, 1966). However, fresh water is found in lakes, located most often in or near the sand dunes. A few small lakes

have formed in the craters of volcanic cones such as Crater Hill and Lake Hill. The largest body of fresh water, Big Lake, formed inside the tombolo that connects Northeast Point to the main body of St. Paul Island. Formation of this tombolo was completed in historic time, as early settlers on St. Paul, in the late 1700's, required boats to travel from the main island to Northeast Point (Elliott, 1881; Father Michael Lestenkof, 2000, personal commun.). Northeast Point was formerly called "Novastoshnah", from the Russian meaning, "of recent growth" (Elliott, 1881). Antone Lake, on the northwest part of Zapadni Point, was likely formed by the sea ice crowding boulders into a rampart, as described by Stanley-Brown (1892), and forming the dam that contains the lake.

In previous work on St. Paul, Barth (1966), who published the first geologic map of the island (Fig. 3), recognized multiple volcanic vents, but did not map any separate lava flows. Barth's (1956) map merely distinguishes lavas from sand dunes and shows the locations of some vents with pyroclastic deposits on St. Paul. A preliminary report by Lee-Wong et al. (1979) includes an unpublished reconnaissance sketch map of St. Paul by Hopkins and Einarsson, dated 1965. This map shows faults and breaks out volcanic rocks into four units: (1) Rush Hill, (2) Bogoslof Hill, and lavas both (3) older and (4) younger than Bogoslof Hill, the latter including the Fox Hill lava flow. Cox et al. (1966) mapped some faults and eruptive centers, including Fox Hill and the Fox Hill lava flow, while studying geomagnetic polarity epochs on St. Paul lavas and collecting samples for K-Ar radiometric age determinations. In an investigation of geologic hazards related to locating an oil pipeline and oil trans-shipment facility on St. Paul, Hopkins (1976) studied the history and frequency of faulting and volcanic eruptions on the island.

Hopkins' (1976) study of the fault history of St. Paul Island cited no clear evidence that faulting has affected stabilized sand dunes. Hopkins (1976) estimates the ages of the dunes to be around 10,000 to 12,000 years old and the rate of displacement on individual faults to be approximately one meter per 10,000 years. [Despite considerable effort, Hopkins' (1976) fault map from this study could not be obtained.] Hopkins (1976) concluded that faulting is an ongoing process and estimated a 10,000 year eruptive interval for volcanic activity on St. Paul Island.

Petrographic and compositional studies have been done on St. Paul rocks by several workers (Washington and Keyes, 1930; Barth, 1956; Cox et al., 1966; Kay et al., 1978; Lee-Wong et al., 1979). Magmas erupted at St. Paul have been classified by Barth (1956) as alkalic basalts and basanites, both containing phenocrysts of olivine and augite ± plagioclase, with occasional inclusions of olivine nodules. Cox et al. (1966) reported not only frequent ultramafic inclusions, but also granitic xenoliths, with both types sometimes occurring together. In a singular finding, Barth (1956) located a small amount of rhyolitic pumice (SiO_2 = 69.09 wt%: Barth's (1956) analysis) high on the east slope of Polovina Hill. Pribilof basalts were early recognized as having chemistry comparable to that of ocean island basalts in the Pacific Ocean by Washington and Keyes (1930). This was corroborated by Kay et al. (1978), who found that Pribilof basalts were isotopically similar to seamount lavas erupted in an intraplate environment; they attributed the Pribilof magma source region to the underlying asthenospheric mantle. Lee-Wong et al. (1979) conducted petrographic and geochemical studies using previously collected samples of St. Paul rocks. They interpreted the wide range of MgO values (4.85 to

14.64 wt%) for the silica-poor (44.23 to 46.79 wt%) rocks as reflecting substantial differentiation. Lee-Wong et al. (1979) noted a trend of decreasing MgO content with decreasing age of St. Paul magmas; they also commented on the consistently low MgO content of the Bogoslof Hill lavas. More recently, Moll-Stalcup (1994a, 1994b) described St. Paul Island as a part of the Bering Sea basalt province, the product of intraplate volcanism related to regional north-south extension in the Bering Sea region (Moll-Stalcup, 1994a). Moll-Stalcup (1994a) suggested that the rock underwent little, if any, differentiation. Most recently, Winer and Feeley (1997) and Feeley and Winer (1999) described petrographic and geochemical evidence for fractionation of Quaternary basalts on St. Paul, and argued for the development of shallow crustal magma chambers beneath the island.

Ages of rocks erupted on St. Paul Island are all within the Bruhnes chron of normal polarity (<780 ka) (Cox et al., 1966). Absolute and relative age determinations by Cox et al. (1966) put the ages of lavas on St. Paul Island from 0.360 ± 0.10 Ma to nearly the present [radiometric age determinations from Cox et al. (1966) are discussed below in Chapter 3]. A sediment core from the lake in the Lake Hill crater yielded a radiocarbon age determination of >17,800 years BP (Colinvaux, 1981). This age is poorly constrained because of the introduction of groundwater into the sediment (Colinvaux, 1981). Washington and Keyes (1930) cited a report by Landgrebe (1855) of "flames rising from the sea" northeast of the Pribilof Islands, and also of a submarine eruption recorded as occurring in the vicinity of St. George Island (Sapper, 1917). Barth (1956) also cited Landgrebe (1855), but regarded any assertions of such recent volcanic activity

in the area as inconclusive. The fact that lava has flowed from a crater on Bogoslof Hill was noted by Stanley-Brown (1892) and Barth (1956). However, no historic eruptions have occurred at St. Paul Island.

METHODS

Mapping and Sample Collection

Fieldwork on St. Paul Island was done during three weeks in June 1998, and one week in September 2000. Field relations were mapped using NOAA map # 16382 (1:50,000) as a base map and aerial color photographs (1:24,000), acquired June, 1993, by Aeromap, Anchorage, Alaska. The base map was enlarged for use in the field. The aerial photographs were studied at Montana State University prior to fieldwork, and were utilized in the field. Where possible, individual lava flows and their source vents were mapped. Mappable eruptive units include an assemblage of volcanic products inferred to have erupted from a single common vent, from several closely spaced vents, or from several more widely spaced vents related by structural continuity. For volcanic centers with a series of eruptive events from a common center, to the extent possible, separate flows are delineated on the geological map (Plate 1). Access to some coastal locations was limited by not only the steepness of the near vertical cliffs, but also by the presence of large, territorial, and belligerent northern fur seal bulls on their breeding grounds. The geologic map made in the field has been converted into digital form.

In total, seventy-eight samples were collected. Of these samples, 72 are volcanic rock samples of 1 to 2 kg each; four are beach sand; one is about 4 kg of organic carbon-containing sediment; and one is fossil shells. Rock samples were collected from the densest and freshest rocks available and trimmed of weathered surfaces as necessary.

X-ray Fluorescence

Approximately 100 grams of each of 37 selected rock samples were sent to the WSU GeoAnalytical Laboratory at Washington State University, Pullman, Washington. These samples were analyzed by X-ray fluorescence (XRF) for major element oxides and trace elements (Table 1) with all Fe expressed as FeO. XRF was done using techniques outlined by Johnson et al. (1999).

Petrography

Seventy-two billets were sent to Wagner Petrographic, Provo, Utah, for preparation as petrographic thin sections. Thin sections were examined using a polarizing petrographic microscope. Microscopic data consists of two types: qualitative textural data (described below) and quantitative modal data (Table 1). Modal phenocryst percentages were determined by point counting 1100 to 1200 points per thin section. Phenocrysts are defined as crystals $\geq$ 0.3 mm in the longest dimension. Because these basaltic rocks are all vesicular to some extent, vesicles were included in the modal analysis and then their proportion was subtracted from the total numbers of counts to give the dense rock equivalent.

Geochronology

One sample (SP98-64) of organic carbon-containing sediment, exposed beneath a lava flow, was collected with a shovel and stored in a sealed plastic bag. Sediment was collected from the upper one third of the deposit, but not from the top few centimeters, where complete combustion of organic matter occurs (Kuntz et al., 1986b). Beta Analytic Inc., Radiocarbon Dating Services, Miami, Florida, analyzed the carbon sample. They found that the amount of carbon in the sample was very small, requiring them to convert the sample carbon to graphite and then to count the radiocarbon atomically using an accelerator mass spectrometer (AMS). This method provided sufficient carbon for reliable measurements and all analytical steps went normally. Details of the analytical procedures are explained in Appendix A.

GEOLOGY OF ST. PAUL ISLAND

This chapter on the geology of St. Paul Island includes geochronology, chemical classification of the rocks, major and trace element compositions, modal and normative minerals, rock names, and the new geological map. Map units are described and interpreted.

Ages of Rocks on St. Paul Island

Ages of rocks on St. Paul Island are bracketed by two events, a geomagnetic polarity transition and the eruption of the youngest lava flow on the island. Geomagnetic polarity studies conducted by Cox et al. (1966) determined that all volcanic rocks forming St. Paul Island erupted during the Bruhnes chron of normal polarity, 780 Ka to the present. Using K-Ar determinations on the island platform lavas, Cox et al. (1966) also obtained intermediate dates ranging from 0.36 ± 0.10 Ma to 0.096 ± 0.10 Ma. A new radiometric age-date from this study verifies that St. Paul Island has erupted in the very recent geologic past. A high-precision AMS radiocarbon age-date obtained on organic carbon-bearing sediments located beneath the Fox Hill lava flow, shows that the youngest eruption on St. Paul Island occurred 3,230 ± 40 years before the present at Fox Hill.

Classification and Composition of St. Paul Rocks

Most volcanic rocks erupted on St. Paul Island range from basanites and tephrites to trachybasalts and basalts (Fig. 4). In addition, one rare trachyte magma erupted from Polovina Hill. All volcanic rocks are alkaline according to the nomenclature of MacDonald and Katsura (1964). Samples were collected from eighteen eruptive centers as well as from lava flows for which source vents were not identified. Due to emplacement mechanisms and in-flow mixing of very low viscosity pahoehoe lava flows (Hon et al., 1994; Peterson et al., 1994; Calvari and Pinkerton, 1999; Kilburn, 2000), each sample is considered to be representative of the lava flow as a whole. As a test of this premise, four samples from the Fox Hill lava flow (SWPT1, SWPT2, SWPT3, and FXH1) were analyzed. Within analytical error, all are identical in chemical composition. Most samples, except for those collected along the sea cliffs and those from eruptive centers where only tephra was exposed, were taken from flow surfaces; cross-sections of inland lava flows do not exist, due to little erosion.

Major and trace element analyses of St. Paul rocks are presented in Table 1. Because of the limited range of SiO_2 (43.11 to 47.30 wt%) and larger range of MgO contents (14.39 to 4.25 wt%), the basaltic rocks are ordered by decreasing MgO content. Modal mineralogy is included in Table 1. Also included in the table are analyses of the rare trachyte magma (SP98-35), erupted from Polovina Hill, and two xenoliths (SP98-51X and SP98-43X). Modal minerals are presented in Table 1 and normative minerals and rock names are presented in Table 2.

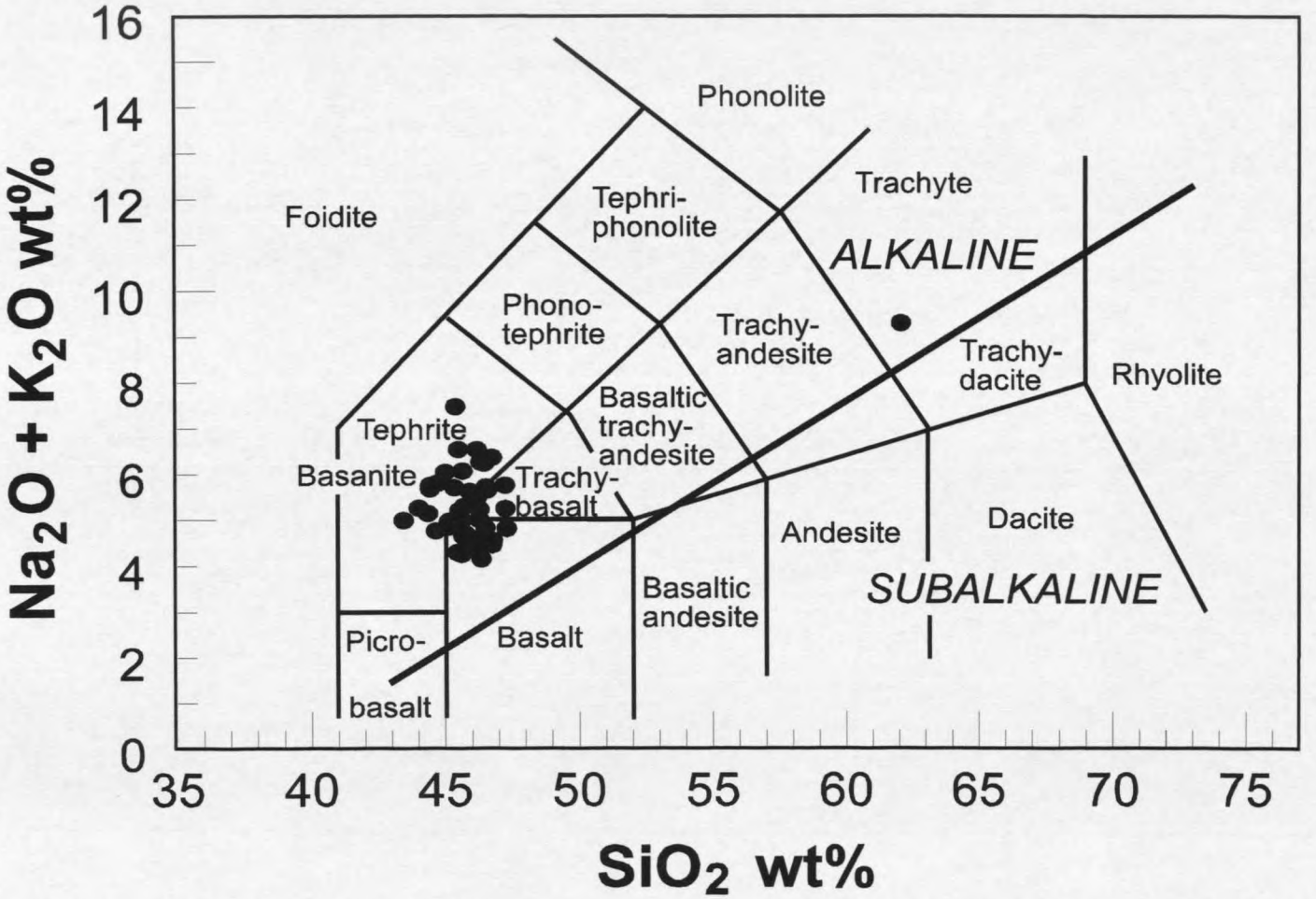


Figure 4. Classification of the rocks. Chemical classification scheme and nomenclature of St. Paul volcanic rocks using the total alkalis versus silica (TAS) diagram of le Maitre et al. (1989). The straight heavy line separates alkalic from subalkalic rocks (MacDonald and Katsura (1964).

Table 1. Major element, trace element, and modal analyses of volcanic rocks and xenoliths from St. Paul Island, Alaska

Map unit	UPL	UPL	UPL	NoH	RW	POL	UPL	UPL
Sample #	9825	9870	9816	9837	9843	POL 1	SWPB 1	9822
Major element oxides (wt%)								
MgO	14.39	13.95	12.45	12.36	12.09	12.02	11.95	11.88
SiO_2	45.08	45.61	45.67	44.01	45.11	43.11	44.35	45.82
Al_2O_3	12.41	12.52	13.20	12.95	12.96	13.29	13.22	13.39
TiO_2	2.241	2.134	2.325	2.825	2.534	3.006	2.376	2.377
[1]FeO	11.01	10.88	11.40	12.30	11.83	12.30	12.16	11.50
MnO	0.172	0.175	0.169	0.174	0.173	0.172	0.168	0.169
CaO	9.38	9.59	9.58	9.38	9.65	9.78	9.86	9.97
K_2O	1.31	1.16	1.28	1.60	1.33	1.39	1.45	1.21
Na_2O	3.47	3.03	3.31	3.60	3.51	3.59	3.63	3.25
P_2O_5	0.497	0.430	0.394	0.592	0.450	0.566	0.523	0.438
Total	99.96	99.48	99.78	99.79	99.63	99.22	99.69	100.01
Trace elements (ppm)								
Ni	356	345	276	268	272	241	270	239
Cr	535	460	479	377	356	332	521	438
Sc	23	21	23	27	22	28	31	21
V	251	243	241	266	240	295	263	253
Ba	174	116	118	159	187	291	272	132
Rb	13	12	13	17	17	17	16	13
Sr	618	500	488	680	509	663	675	522
Zr	170	154	159	190	156	190	181	146
Y	18	18	19	19	21	19	19	19
Nb	40.5	35.0	39.1	47.8	45.3	48.5	44.2	38.1
Ga	16	17	20	20	23	20	16	20
Cu	44	47	50	47	57	45	49	30
Zn	81	88	89	93	98	91	82	87
Pb	1	3	3	3	1	0	2	2
La	16	11	19	14	14	41	30	20
Ce	41	29	39	48	55	49	50	41
Th	5	2	5	2	6	7	7	2
[3]Modal percent phenocrysts								
plag	0.4	0.1	0.1	0	0	0.4	1.1	3.1
olivine	21.3	22.9	17.3	17.9	17.1	15.0	17.9	19.6
cpx	3.2	5	0.8	2.7	0.1	7.3	0.9	0.3
oxide	0.4	0	0	0	0	0.3	0.5	0
total	25.3	28	18.2	20.6	17.2	23.0	20.4	23

[1] Total Fe expressed as FeO

[3]Crystals with greatest dimension greater than or equal to 0.3mm counted as phenocrysts

† Denotes values >120% of highest standards

Table 1. Continued

	RW 9842	UPL 9814	UPL 9810	LH 9833	UPL ERP 2	RiH 9877	CH 9851
MgO	11.76	11.68	11.60	11.20	11.06	11.04	10.91
SiO_2	45.62	46.24	46.18	45.53	45.93	45.73	45.14
Al_2O_3	13.21	13.24	13.39	13.20	13.42	13.81	13.74
TiO_2	2.572	2.360	2.367	2.687	2.522	2.549	2.650
^1FeO	11.24	11.81	11.79	11.76	12.54	10.24	11.74
MnO	0.175	0.171	0.173	0.176	0.173	0.172	0.186
CaO	9.81	9.70	9.58	9.80	9.51	10.27	9.81
K_2O	1.34	1.21	1.15	1.36	1.30	1.61	1.16
Na_2O	3.59	3.05	3.35	3.43	3.15	3.63	3.75
P_2O_5	0.460	0.451	0.448	0.545	0.494	0.567	0.466
Total	99.78	99.92	100.02	99.69	100.1	99.62	99.55
Ni	266	239	238	241	228	229	226
Cr	360	325	322	323	289	368	281
Sc	29	25	22	27	25	28	27
V	241	227	229	241	239	279	244
Ba	194	157	147	195	270	160	164
Rb	18	12	13	16	13	12	14
Sr	515	551	540	569	542	731	554
Zr	160	153	152	173	160	184	171
Y	22	20	20	22	21	21	21
Nb	45.4	39.5	38.9	47.8	43.2	40.4	40.8
Ga	20	22	20	21	23	19	17
Cu	60	45	49	50	56	42	51
Zn	94	99	95	103	104	87	100
Pb	0	0	2	4	0	3	0
La	19	16	17	19	21	18	23
Ce	47	46	56	50	52	58	49
Th	5	6	5	5	5	6	6
plag	0	30.3	21.3	0.4	9.1	3.7	0.9
olivine	18.5	17.1	14.8	11.7	15.1	17.4	9.7
cpx	0	6.9	3.2	0.4	1.2	4.1	1.7
oxide	0	2.1	0	0	0	0	0
total	18.5	56.4	39.3	12.5	25.4	25.2	12.3

Table 1. Continued

	KAM KAM 1	UPL ERP 1	UPL 9813	H404 9853	H255 9840	Hill 255 9841	PyC 9845
MgO	10.87	10.68	10.55	10.52	10.32	10.09	9.99
SiO_2	45.46	45.77	46.50	44.65	46.78	46.76	46.35
Al_2O_3	13.51	13.54	13.87	14.03	13.59	13.63	13.47
TiO_2	2.455	2.525	2.481	2.846	2.373	2.427	2.304
^1FeO	13.48	13.47	11.50	10.80	12.04	12.02	12.58
MnO	0.171	0.176	0.172	0.180	0.176	0.177	0.168
CaO	9.62	9.45	9.58	10.68	9.55	9.65	9.38
K_2O	1.22	1.21	1.19	1.57	1.06	1.01	0.88
Na_2O	3.01	3.41	3.58	3.13	3.44	3.39	3.21
P_2O_5	0.469	0.484	0.456	0.548	0.454	0.444	0.365
Total	100.26	100.72	99.88	98.95	99.78	99.60	98.70
Ni	216	211	202	191	211	205	197
Cr	308	292	314	326	266	265	250
Sc	21	26	24	31	21	28	20
V	229	231	237	295	220	240	207
Ba	244	249	146	179	130	128	98
Rb	14	13	13	14	11	10	8
Sr	581	547	528	669	511	474	414
Zr	165	163	155	189	150	148	135
Y	20	21	20	21	21	21	20
Nb	38.9	41.5	37.5	47.2	36.6	35.9	28.8
Ga	20	20	19	20	19	21	20
Cu	48	52	48	44	57	66	45
Zn	101	98	96	89	101	104	99
Pb	1	1	2	0	0	4	3
La	16	13	25	30	17	12	23
Ce	48	58	37	67	37	50	35
Th	5	3	3	5	3	3	5
plag	39.7	13.6	41.3	0	0.8	0	9.8
olivine	19.0	13.9	17.6	10.2	12.6	9.7	11.9
cpx	24.4	2.1	14.4	3.5	0.1	0	8.3
oxide	5.9	0	3.5	0	0	0	0
total	89.0	29.6	76.8	13.7	13.5	9.7	30

Table 1. Continued

	PyC 9854	UPL 9871	Upl 9819	PyC 9852	ALF 9831	ALF 9875	CHVC 9846
MgO	9.66	9.43	8.89	8.74	8.23	8.05	7.56
SiO_2	45.34	46.27	47.25	45.00	45.53	45.91	46.28
Al_2O_3	14.69	14.23	14.79	14.77	15.16	15.28	15.24
TiO_2	2.781	2.558	2.474	3.037	2.879	2.941	2.886
^1FeO	10.67	11.23	10.90	11.26	12.02	11.55	11.25
MnO	0.175	0.173	0.169	0.174	0.173	0.174	0.172
CaO	9.54	9.91	9.55	10.22	9.56	9.74	10.56
K_2O	1.75	1.20	1.49	1.72	1.52	1.63	1.50
Na_2O	3.90	3.75	3.70	4.26	3.62	3.93	3.67
P_2O_5	0.575	0.492	0.401	0.651	0.549	0.560	0.540
Total	99.08	99.25	99.62	99.83	99.24	99.76	99.66
Ni	189	155	151	136	73	67	84
Cr	272	304	297	233	215	227	199
Sc	23	29	26	26	27	23	30
V	257	257	247	286	266	266	281
Ba	215	135	125	211	163	156	160
Rb	20	11	17	19	13	15	14
Sr	672	571	515	744	697	714	635
Zr	206	165	197	204	205	198	192
Y	23	22	21	22	21	21	22
Nb	53.1	37.3	45.1	49.5	45.5	42.8	43.0
Ga	22	20	21	21	24	23	22
Cu	47	37	46	39	32	30	57
Zn	90	103	92	89	99	97	91
Pb	1	1	2	1	2	3	2
La	25	24	20	29	27	19	8
Ce	66	42	58	66	57	48	49
Th	4	4	6	5	2	4	3
plag	0	53.8	19	1.3	22	25.7	14
olivine	11.4	16.3	11	10.1	11.1	8	7.2
cpx	5.1	17.5	0.4	5	2.2	5.3	6.3
oxide	0	2	0	0	0	1.2	0
total	16.5	89.6	30.4	16.4	35.3	40.2	27.5

Table 1. Continued

	HH 9804	CHVC 9856	FXH SWPT 2	FXH FXH 1	RuH 9878	FXH SWPT 3	FXH SWPT 1
MgO	7.54	7.42	7.40	7.40	7.36	7.27	7.20
SiO_2	47.30	46.19	44.73	44.43	45.80	44.43	44.52
Al_2O_3	15.40	15.35	15.02	15.09	15.93	15.06	15.06
TiO_2	2.534	2.865	3.394	3.402	3.045	3.405	3.394
^1FeO	11.27	11.20	13.07	12.83	11.12	12.64	13.07
MnO	0.174	0.175	0.168	0.169	0.180	0.169	0.169
CaO	10.22	10.33	9.71	9.65	9.12	9.67	9.63
K_2O	1.13	1.54	1.77	1.80	2.39	1.72	1.78
Na_2O	3.62	3.90	3.98	3.89	3.61	3.90	3.93
P_2O_5	0.463	0.556	0.550	0.558	0.779	0.564	0.561
Total	99.65	99.53	99.79	99.22	99.34	98.83	99.31
Ni	86	83	68	71	96	70	69
Cr	234	162	122	119	139	118	115
Sc	25	27	24	23	24	27	30
V	239	283	294	299	260	274	292
Ba	123	140	269	280	294	314	291
Rb	14	14	15	16	24	14	15
Sr	535	642	673	677	†931	676	677
Zr	174	195	196	198	246	198	200
Y	24	23	21	21	23	22	21
Nb	39.3	43.5	43.2	45.3	64.5	44.3	43.7
Ga	23	24	24	26	23	22	23
Cu	41	56	28	43	24	42	37
Zn	100	93	93	98	91	94	96
Pb	0	0	0	1	4	0	2
La	27	20	17	21	28	16	29
Ce	51	64	54	49	78	42	63
Th	6	5	5	3	5	2	4
plag	22.4	13.5	3.5	3.6	0.8	1.1	7.1
olivine	6.6	9.7	10.4	11.3	5.7	8.3	8.1
cpx	3.4	4.2	0.4	2.0	0.4	0.3	1.5
oxide	0	0	0.4	0.2	0	0	0.6
total	32.4	27.4	14.7	17.1	6.9	9.7	17.3

Table 1. Continued

	RuH 9818	CHVC 9858	CHVC 9849	RuH 9823	CHVC 9857	BHVC 9847	BHVC 9873
MgO	6.91	6.80	6.72	6.46	6.40	6.01	5.69
SiO_2	45.49	46.38	46.52	45.37	46.50	46.89	46.45
Al_2O_3	16.00	15.77	15.71	16.23	15.85	15.97	16.37
TiO_2	3.046	2.955	2.941	3.241	2.995	3.042	3.208
^1FeO	11.15	10.67	11.11	11.10	10.99	10.64	10.99
MnO	0.174	0.176	0.173	0.181	0.174	0.170	0.173
CaO	9.68	10.23	10.06	8.79	10.18	10.62	9.91
K_2O	2.29	1.58	1.58	2.52	1.64	1.63	1.85
Na_2O	4.19	3.99	4.08	4.94	4.02	4.07	4.33
P_2O_5	0.713	0.571	0.579	0.861	0.591	0.574	0.645
Total	99.65	99.12	99.47	99.70	99.34	99.61	99.61
Ni	52	70	72	58	65	32	23
Cr	103	114	105	78	101	119	79
Sc	24	23	22	17	19	24	26
V	275	283	272	262	280	290	288
Ba	205	157	157	287	153	148	186
Rb	17	13	13	24	14	15	18
Sr	†895	648	651	†950	661	718	†799
Zr	233	200	198	262	203	210	214
Y	23	24	22	24	23	22	21
Nb	56.7	45.3	44.9	67.5	46.3	46.2	47.3
Ga	24	23	21	26	20	23	21
Cu	25	57	65	18	63	47	30
Zn	88	92	94	91	94	95	92
Pb	4	2	2	5	0	1	4
La	29	16	22	32	29	21	28
Ce	72	59	71	80	61	66	62
Th	4	3	5	2	6	4	2
plag	0.4	12.4	7.3	2.2	13.9	30	27.3
olivine	5.2	5.9	5	5.2	5.4	2.7	4.8
cpx	1.7	2.2	0.1	0	0.3	13.8	2.5
oxide	0	0	0	0	0	0	0
total	7.3	20.5	12.4	7.4	19.6	46.5	34.6

Table 1. Continued

	BHVC 9826	BHVC 9872	BHVC 9827	POL 9835	Crater Hill 9851X	Ridge W. 9843X
MgO	5.37	5.29	4.25	1.15	4.70	0.26
SiO_2	46.31	46.75	46.18	62.06	50.28	74.05
Al_2O_3	16.35	16.49	15.51	16.72	19.32	15.46
TiO_2	3.244	3.310	3.877	0.890	1.671	0.058
[1]FeO	11.70	10.65	12.43	4.42	8.24	0.57
MnO	0.170	0.174	0.187	0.081	0.145	0.005
CaO	9.94	10.05	9.69	4.10	9.12	4.92
K_2O	1.87	1.87	2.22	4.34	0.39	0.52
Na_2O	4.33	4.44	4.26	4.89	4.64	4.05
P_2O_5	0.660	0.649	0.784	0.208	0.192	0.037
Total	99.95	99.68	99.39	98.86	98.70	99.93
Ni	19	18	4	4	14	10
Cr	62	65	36	0	34	0
Sc	28	24	20	12	25	9
V	280	287	324	60	234	15
Ba	193	182	194	690	35	82
Rb	14	14	21	47	3	10
Sr	†819	735	685	451	747	465
Zr	223	221	260	147	78	43
Y	24	23	28	24	11	2
Nb	50.0	50.6	61.2	8.8	8.1	4.5
Ga	25	23	27	19	21	14
Cu	32	32	39	32	72	26
Zn	97	99	112	43	76	2
Pb	0	2	3	6	0	3
La	15	28	42	15	7	0
Ce	77	62	86	28	22	31
Th	9	2	7	0	0	0
plag	30.1	19	8.9	17.4		
olivine	2.9	4.1	2.1	0.1		
cpx	5.1	0.9	0.6	0.1		
oxide	0.4	0	0	2.1		
total	38.5	24	11.6	19.7		

Table 2. CIPW Calculated Normative Minerals in Weight Percent and Rock Names

Map Unit	UPL	UPL	UPL	NoH	RW	POL	UPL	UPL	RW	UPL
SAMPLE	9825	9870	9816	9837	9843	POL 1	SWPB 1	9822	9842	9814
Normative										
Q	0.00	0.00	0.00	0.00	0.00	0.00	0.00	0.00	0.00	0.00
or	7.72	6.87	7.55	9.43	7.86	8.24	8.56	7.12	7.90	7.13
ab	11.55	14.81	14.88	10.01	13.45	8.93	9.53	15.55	14.68	18.22
an	14.37	17.16	17.35	14.42	15.67	16.10	15.48	18.30	15.94	18.81
lc	0.00	0.00	0.00	0.00	0.00	0.00	0.00	0.00	0.00	0.00
ne	9.60	5.89	7.09	11.04	8.80	11.68	11.47	6.41	8.47	4.07
kal	0.00	0.00	0.00	0.00	0.00	0.00	0.00	0.00	0.00	0.00
C	0.00	0.00	0.00	0.00	0.00	0.00	0.00	0.00	0.00	0.00
di	22.85	22.00	21.94	22.42	23.31	22.96	23.98	22.42	23.56	20.97
hy	0.00	0.00	0.00	0.00	0.00	0.00	0.00	0.00	0.00	0.00
wo	0.00	0.00	0.00	0.00	0.00	0.00	0.00	0.00	0.00	0.00
ol	23.13	22.94	20.34	19.70	19.22	18.51	19.65	19.08	17.61	19.72
ac	0.00	0.00	0.00	0.00	0.00	0.00	0.00	0.00	0.00	0.00
mt	5.41	5.28	5.54	6.26	5.85	6.55	5.62	5.60	5.89	5.58
il	4.24	4.06	4.41	5.35	4.81	5.73	4.51	4.50	4.88	4.47
hem	0.00	0.00	0.00	0.00	0.00	0.00	0.00	0.00	0.00	0.00
ti	0.00	0.00	0.00	0.00	0.00	0.00	0.00	0.00	0.00	0.00
ap	1.15	1.00	0.91	1.37	1.04	1.32	1.21	1.01	1.06	1.04
Rock type*	basalt	basalt	basalt	basanite	basalt	basanite	basanite	basalt	basalt	basalt

*According to Le Maitre (1989)

Table 2. Continued

	UPL	LH	UPL	RiH	CH	KAM	UPL	UPL	H404	H255
SAMPLE	9810	9833	ERP 2	9877	9851	KAM 1	ERP 1	9813	9853	9840
Q	0.00	0.00	0.00	0.00	0.00	0.00	0.00	0.00	0.00	0.00
or	6.77	8.03	7.64	9.51	6.86	7.16	7.07	7.01	9.34	6.25
ab	18.05	15.96	17.92	13.29	15.30	16.69	17.20	19.67	12.17	21.67
an	18.03	16.59	18.55	16.63	17.24	19.62	17.87	18.21	19.72	18.48
lc	0.00	0.00	0.00	0.00	0.00	0.00	0.00	0.00	0.00	0.00
ne	5.52	7.06	4.66	9.44	8.91	4.67	6.14	5.71	7.84	4.01
kal	0.00	0.00	0.00	0.00	0.00	0.00	0.00	0.00	0.00	0.00
C	0.00	0.00	0.00	0.00	0.00	0.00	0.00	0.00	0.00	0.00
di	21.09	22.65	20.19	24.24	22.65	19.94	20.43	20.93	23.75	20.74
hy	0.00	0.00	0.00	0.00	0.00	0.00	0.00	0.00	0.00	0.00
wo	0.00	0.00	0.00	0.00	0.00	0.00	0.00	0.00	0.00	0.00
ol	19.46	17.30	19.34	14.88	16.92	20.52	19.67	16.96	14.13	17.71
ac	0.00	0.00	0.00	0.00	0.00	0.00	0.00	0.00	0.00	0.00
mt	5.58	6.06	5.80	5.87	6.02	5.70	5.77	5.76	6.34	5.61
il	4.48	5.10	4.77	4.84	5.03	4.63	4.74	4.70	5.44	4.50
hem	0.00	0.00	0.00	0.00	0.00	0.00	0.00	0.00	0.00	0.00
ti	0.00	0.00	0.00	0.00	0.00	0.00	0.00	0.00	0.00	0.00
ap	1.03	1.26	1.14	1.31	1.08	1.08	1.11	1.05	1.28	1.05
Rock type	basalt	basalt	basalt	trachy-basalt	basalt	basalt	basalt	basalt	basalt	basalt

Table 2. Continued

Map Unit	H255	PyC	PyC	UPL	UPL	PyC	ALF	ALF	CHVC
SAMPLE	9841	9845	9854	9871	9819	9852	9831	9875	9846
Q	0.00	0.00	0.00	0.00	0.00	0.00	0.00	0.00	0.00
or	5.97	5.25	10.39	7.12	8.80	10.14	9.01	9.61	8.86
ab	22.28	23.26	14.94	19.67	21.17	12.58	18.80	17.89	18.56
an	18.99	19.93	17.49	18.52	19.35	16.05	20.69	19.20	20.66
lc	0.00	0.00	0.00	0.00	0.00	0.00	0.00	0.00	0.00
ne	3.47	2.25	9.87	6.59	5.49	12.66	6.47	8.29	6.76
kal	0.00	0.00	0.00	0.00	0.00	0.00	0.00	0.00	0.00
C	0.00	0.00	0.00	0.00	0.00	0.00	0.00	0.00	0.00
di	20.84	19.84	20.85	22.04	20.30	24.05	18.66	20.26	22.48
hy	0.00	0.00	0.00	0.00	0.00	0.00	0.00	0.00	0.00
wo	0.00	0.00	0.00	0.00	0.00	0.00	0.00	0.00	0.00
ol	17.12	18.64	13.57	14.15	13.51	10.72	13.25	11.46	9.62
ac	0.00	0.00	0.00	0.00	0.00	0.00	0.00	0.00	0.00
mt	5.69	5.57	6.24	5.90	5.76	6.56	6.37	6.43	6.35
il	4.61	4.42	5.31	4.88	4.70	5.75	5.49	5.57	5.48
hem	0.00	0.00	0.00	0.00	0.00	0.00	0.00	0.00	0.00
ti	0.00	0.00	0.00	0.00	0.00	0.00	0.00	0.00	0.00
ap	1.03	0.85	1.34	1.14	0.93	1.50	1.28	1.29	1.25
Rock type*	basalt	basalt	basanite	basalt	trachy-basalt	basanite	basanite	basanite	trachy-basalt

Table 2. Continued

Map Unit	HH	CHVC	FXH	FXH	RuH	FXH	FXH	RuH	CHVC	CHVC
SAMPLE	9804	9856	SWPT 2	FXH 1	9878	SWPT 3	SWPT 1	9818	9858	9849
Q	0.00	0.00	0.00	0.00	0.00	0.00	0.00	0.00	0.00	0.00
or	6.67	9.10	10.43	10.67	14.15	10.23	10.54	13.52	9.38	9.35
ab	23.80	18.39	14.91	14.84	17.41	15.85	15.24	14.01	20.11	20.44
an	22.42	19.84	17.84	18.45	20.25	18.63	18.23	18.07	20.54	19.90
lc	0.00	0.00	0.00	0.00	0.00	0.00	0.00	0.00	0.00	0.00
ne	3.69	7.92	10.11	9.85	7.15	9.41	9.80	11.60	7.47	7.65
kal	0.00	0.00	0.00	0.00	0.00	0.00	0.00	0.00	0.00	0.00
C	0.00	0.00	0.00	0.00	0.00	0.00	0.00	0.00	0.00	0.00
di	20.26	22.21	21.36	20.76	15.92	20.78	20.86	20.13	21.23	20.98
hy	0.00	0.00	0.00	0.00	0.00	0.00	0.00	0.00	0.00	0.00
wo	0.00	0.00	0.00	0.00	0.00	0.00	0.00	0.00	0.00	0.00
ol	11.43	9.49	10.57	10.54	10.92	10.11	10.47	8.66	7.81	8.31
ac	0.00	0.00	0.00	0.00	0.00	0.00	0.00	0.00	0.00	0.00
mt	5.85	6.33	7.08	7.13	6.60	7.16	7.11	6.59	6.49	6.44
il	4.81	5.44	6.43	6.48	5.80	6.51	6.46	5.78	5.64	5.59
hem	0.00	0.00	0.00	0.00	0.00	0.00	0.00	0.00	0.00	0.00
ti	0.00	0.00	0.00	0.00	0.00	0.00	0.00	0.00	0.00	0.00
ap	1.07	1.29	1.27	1.30	1.81	1.32	1.30	1.65	1.33	1.34
Rock type[2]	basalt	tephrite	basanite	basanite	basalt	basanite	basanite	tephrite	tephrite	trachy-basalt

Table 2. Continued

Map Unit	RuH	CHVC	BHVC	BHVC	BHVC	BHVC	BHVC	POL
SAMPLE	9823	9857	9847	9873	9826	9872	9827	9835
Q	0.00	0.00	0.00	0.00	0.00	0.00	0.00	8.53
or	14.87	9.71	9.63	10.92	11.01	11.03	13.13	25.88
ab	14.42	20.44	20.50	20.13	19.53	20.89	21.32	41.76
an	14.64	20.40	20.48	19.75	19.57	19.51	16.65	10.95
lc	0.00	0.00	0.00	0.00	0.00	0.00	0.00	0.00
ne	14.79	7.40	7.54	8.93	9.18	9.01	7.99	0.00
kal	0.00	0.00	0.00	0.00	0.00	0.00	0.00	0.00
C	0.00	0.00	0.00	0.00	0.00	0.00	0.00	0.00
di	18.50	21.02	22.62	20.04	20.25	20.64	21.09	6.56
hy	0.00	0.00	0.00	0.00	0.00	0.00	0.00	0.64
wo	0.00	0.00	0.00	0.00	0.00	0.00	0.00	0.00
ol	7.77	7.43	5.56	5.83	5.95	4.19	2.83	0.00
ac	0.00	0.00	0.00	0.00	0.00	0.00	0.00	0.00
mt	6.86	6.53	6.58	6.82	6.85	6.96	7.80	3.50
il	6.15	5.70	5.77	6.09	6.14	6.28	7.37	1.71
hem	0.00	0.00	0.00	0.00	0.00	0.00	0.00	0.00
ti	0.00	0.00	0.00	0.00	0.00	0.00	0.00	0.00
ap	1.99	1.37	1.33	1.49	1.52	1.50	1.82	0.49
Rock type	tephrite	trachy-basalt	trachy-basalt	tephrite	tephrite	tephrite	tephrite	trachyte

Geological Map of St. Paul Island

The new map of the volcanic geology of St. Paul Island (Plate 1) covers the entire island at a scale of 1:28,000. Seventeen different volcanic units are mapped in addition to greater than 40 vents (Plate 1). Because this study has focused on the volcanic geology of St. Paul Island, thin and discontinuous coverings of eolian sediments are not illustrated on the map. Undifferentiated lavas (UPL) and (ULF) are those with source vents that are either no longer preserved or have not been located. The platform lavas (UPL) are best exposed on the southern promontories and near vicinity where they have been extensively faulted. The oldest lava flows in this unit may not be shown on the map (Plate 1) because they are exposed near sea level at the base of nearly vertical sea cliffs. Undifferentiated lava flows (ULF) are located inland and have not undergone apparent large magnitude faulting. Pyroclastic cones with no identified lava flows are grouped together in the PyC unit; this unit includes Black Bluffs, the remnant of a Surtseyan volcano. The Bogoslof Hill and Cone Hill volcanic complexes (BHVC and CHVC) are polygenetic volcanoes, and the remainder of the units (the majority) are monogenetic scoria cones and their associated lava flows. Monogenetic volcanoes are defined as volcanoes that are formed during one eruptive episode, usually lasting for less than a year, and then become extinct, while polygenetic volcanoes may erupt repeatedly from the same central vent, or group of closely spaced vents and have life spans of up to 1 Ma.

Relative and numerical dating methods were used to construct the geological column for St. Paul Island (Plate 1). Relative age determinations of units were made using a

combination of three methods: (1) stratigraphic relationships between volcanic deposits, (2), faulting, and (3) cover of sediment and vegetation on lava flows. Relative age determinations are, where possible, corroborated by radiometric dating. Petrographic and geochemical similarities were used to confirm field evidence and to correlate volcanic deposits.

Stratigraphic relationships between stacked lava flows exposed in cross-section in sea cliffs are locally obvious. Faults and fissures cut several of the volcanic units on St. Paul Island. [The term *fissure* is used to designate a fracture or crack in the rocks along which there is a distinct separation (Jackson, 1997).] On the island surface, age relationships may or may not be clear. In some areas, younger lava flows clearly cover older deposits and also flow around the bases of pyroclastic cones. Pyroclastic deposits may also cover older lava flows. Excellent examples of such stratigraphic relationships are located at the Fox Hill cinder cone and its associated lava flow (FXH) on western St. Paul Island (Plate 1). In other areas, contacts between adjacent lava flows are less clear because they are obscured by thin covers of sediment and vegetation. The thickness of eolian sedimentation and cover of vegetation on volcanic deposits was sometimes useful in distinguishing the relative ages of lava flows. Along contacts, the older flows are less well exposed, with sediments and tundra vegetation occupying the interstices between the flow-surface boulders.

Descriptions and Interpretations of Map Units

Descriptions and interpretations of the mapped units are presented below according to inferred stratigraphic order. Rock names (see Figure 4 and Table 2) and brief descriptions of petrography are included in unit descriptions. The weight percent of MgO in the rock (Table 1) distinguishes unevolved (>10%) from moderately evolved (10 to 8%) from evolved (<8%).

Undifferentiated Platform Lavas (UPL) Description

Undifferentiated platform lavas (UPL) are composed of multiple, often faulted, basaltic lava flows that form the base of St. Paul Island. These older lavas are more extensively faulted than the morphologically younger volcanic units emplaced upon them. Platform lavas are exposed along the wave eroded coastal cliffs where the steepness of the cliffs often precludes illustrating them on the geological map. Upland exposures occur along the southern coast and inland on south central St. Paul at Kaminista. Kaminista, an enigmatic, positive topographic area of faulted platform lava, is discussed below.

The most complete and accessible exposures of the platform lavas occur at four locations. These are (1) Reef Point, the southernmost part of the island, (2) Tolstoi Point, on southern St. Paul, (3) Zapadni Point, on the southwestern coast, and (4) Einahnuhto Bluffs, along the west coast. At these locations, vertical sections of stacked, generally horizontal, pahoehoe lava flows are exposed from sea level to the top of the volcanic pile.

Individual lava flows range in thickness from <1 m to > 20 m. They appear to be both compound and simple and are often laterally discontinuous over short distances. Ropy flow surfaces and vesicular flow tops are commonly preserved and pipe vesicles often occur in flow bases (Fig. 5, A and B). Evidence for emplacement of some platform lavas by tube flow is located at Southwest Point, where a lava tube is exposed near sea level beneath stacked lava flows (Fig. 6).

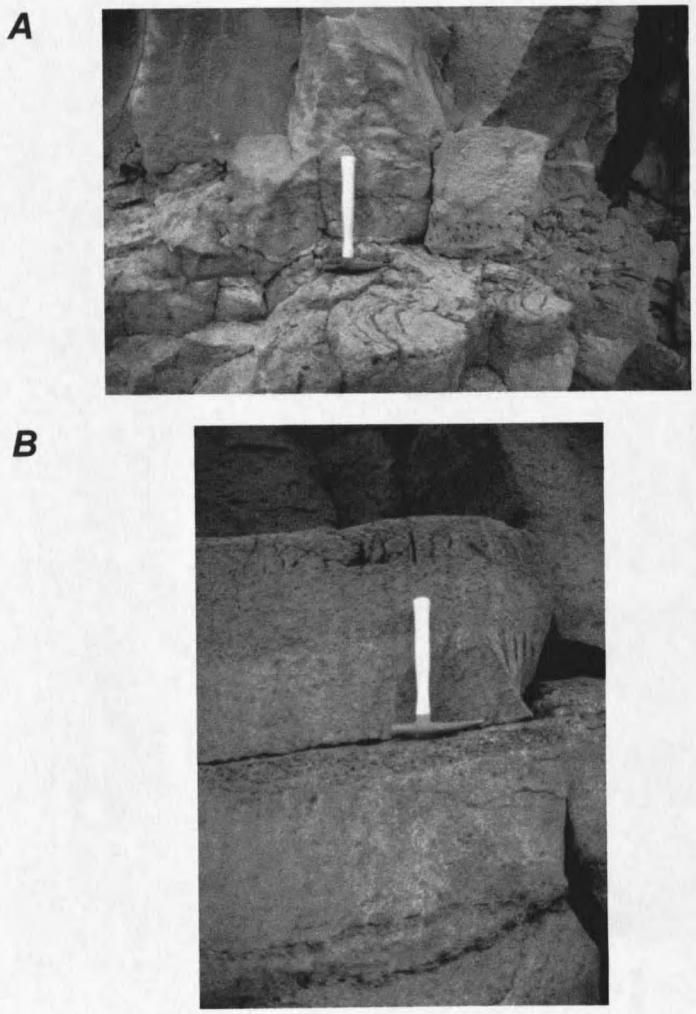


Figure 5. Pahoehoe flow lobe details. A. Pahoehoe ropes and pipe vesicles. B. Thin flow lobes with pipe vesicles at base and vesicles in flow tops. Hammer for scale is 33 cm in length.

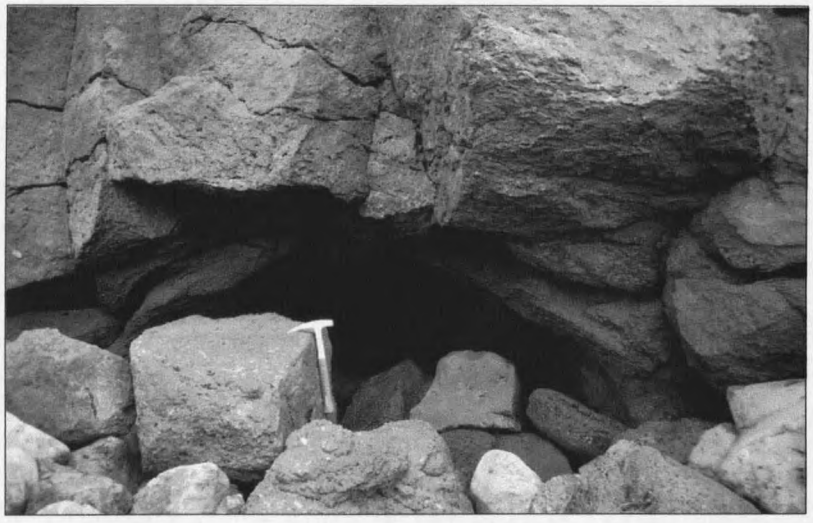


Figure 6. Lava tube near sea level at Southwest Point. Hammer is about 33 cm in length.

At the extremity of Reef Point, at least two lava flows are exposed in the sea cliff. The base of the lower flow is not exposed, however, the flow is at least 3 m thick and it is overlain by a second flow approximately 5 m thick. These columnar jointed lava flows appear unweathered, with well-preserved pahoehoe features of ropes and toes between flows (Fig. 7). The upper flow has pipe vesicles in its base and also closely spaced (5 to 10 cm apart), meter long, segregation or degassing structures. Reef Point flows (lower flow, SP98-09; upper flow, SP98-10) are crystal-rich and petrographically very similar to flows sampled on Tolstoi Point (SP98-14, SP98-15). Samples SP98-10 and SP98-14 are compositionally indistinguishable basalts (Table 1).

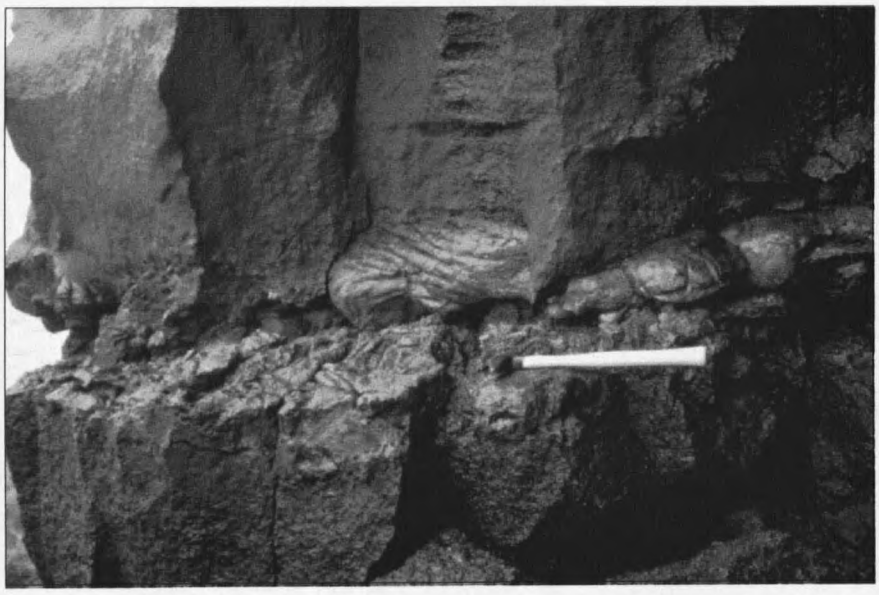


Figure 7. Lava toes and columnar jointing in lava flow lobes at Reef Point. Hammer is about 33 cm in length.

More extensive examples of the stratigraphy of the platform basalts are exposed in vertical-section in the cliffs along the south side of Tolstoi Point and on western Zapadni Point. Basalt flows on Tolstoi Point were emplaced over marine and beach sediments that are variously fossiliferous, clast-rich with well-rounded basaltic clasts, and cross-bedded with reworked tephra (Fig. 8). On southern Tolstoi Point the thickness of the early platform lava flows are estimated to be 0.5 to 15 m, with thinner flows toward the bottom and the thickest, most massive flow at the top of the section (Fig. 9). The upper flow at Tolstoi Point is a massive simple flow, about 30 m thick, with distinctive platy jointing.



Figure 8. Marine and beach sediments at Tolstoi Point.



Figure 9. Lava flows at Tolstoi Point thicken upward. Thicknesses of lava flows are indicated by bars on left side of figure. Geologist is at lower center for scale. The object in the foreground is a shipwreck.

A similar, thick (approximately 25 m), massive flow with platy jointing is exposed on the highest level of the steep southwest facing cliff at Zapadni Point (Fig. 10). Both this flow and the massive flow at Tolstoi Point are distinctive in that they have the highest proportions of modal plagioclase (41% (SP98-13) and 54% (SP98-71); see Table 1) on the island. MgO content in lavas at Zapadni Point decreases upsection, from 14 wt% in the lower flow (SP98-70) to 9.5 wt% in the upper flow (SP98-71). In the thick, platy-jointed lava flows at Tolstoi Point and Zapadni Point, the vast majority of plagioclase crystals are lath-shaped and have lengths ranging up to 1.5 mm. They are frequently

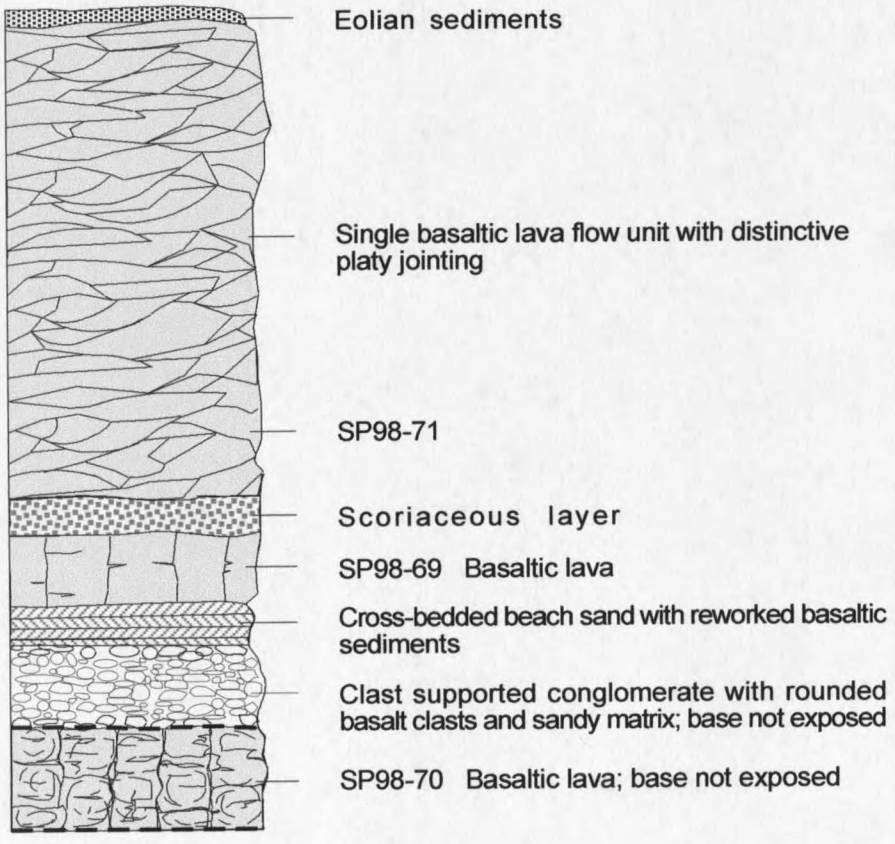


Figure 10. Schematic diagram of stratigraphy at Zapadni Point. Approximately 40 m of vertical section is exposed in west-facing cliff. Sample numbers show approximate collection sites.

aligned, giving a trachytic texture to the rock. The presence of these plagioclase laths may reflect slow, late-stage crystallization due to the thickness of the units. Although similar field appearance and petrography, the two massive units may represent separate flows because the Tolstoi Point flow (SP98-13) is slightly less evolved (10.55 wt% MgO) than the flow at Zapadni Point (SP98-71; 9.43 wt% MgO).

At Einahnuhto Bluffs the stratigraphy of the eruptive sequence is more complex than on Tolstoi Point and Zapadni Point. Among the lower units beneath Einahnuhto Bluffs is basaltic lava that appears to have intruded into wet marine sediments. Evidence for this is the presence of pillow lavas, some as great as 3 m in diameter, embedded in a brecciated matrix of quenched and hydrofractured basaltic lapilli and tuff plus sandy sediments. This unit is interpreted as a peperite formed during intrusion and quenching of basaltic magma in water-saturated sediments. Overlying this unit are compound pahoehoe lava flows similar to those described at other platform outcrops (Fig. 11). Exposed in the sea cliff beneath Rush Hill is a platy-jointed, tabular body of lava (sample SP98-18) that cuts up-section through a layer of sediments before its near-horizontal intrusion into a layer of scoriaceous lapilli-sized tephra. This lava body was also described by Barth (1956), who attributed its origin to an intrusive dike that was emplaced following the explosive eruption of Rush Hill. Lava flows at Einahnuhto Bluffs are overlain by the large and complex Rush Hill cinder cone and associated lava flows. Lava flows exposed in the cliffs at Einahnuhto Bluffs and the northern west coast generally decrease in MgO content upsection.

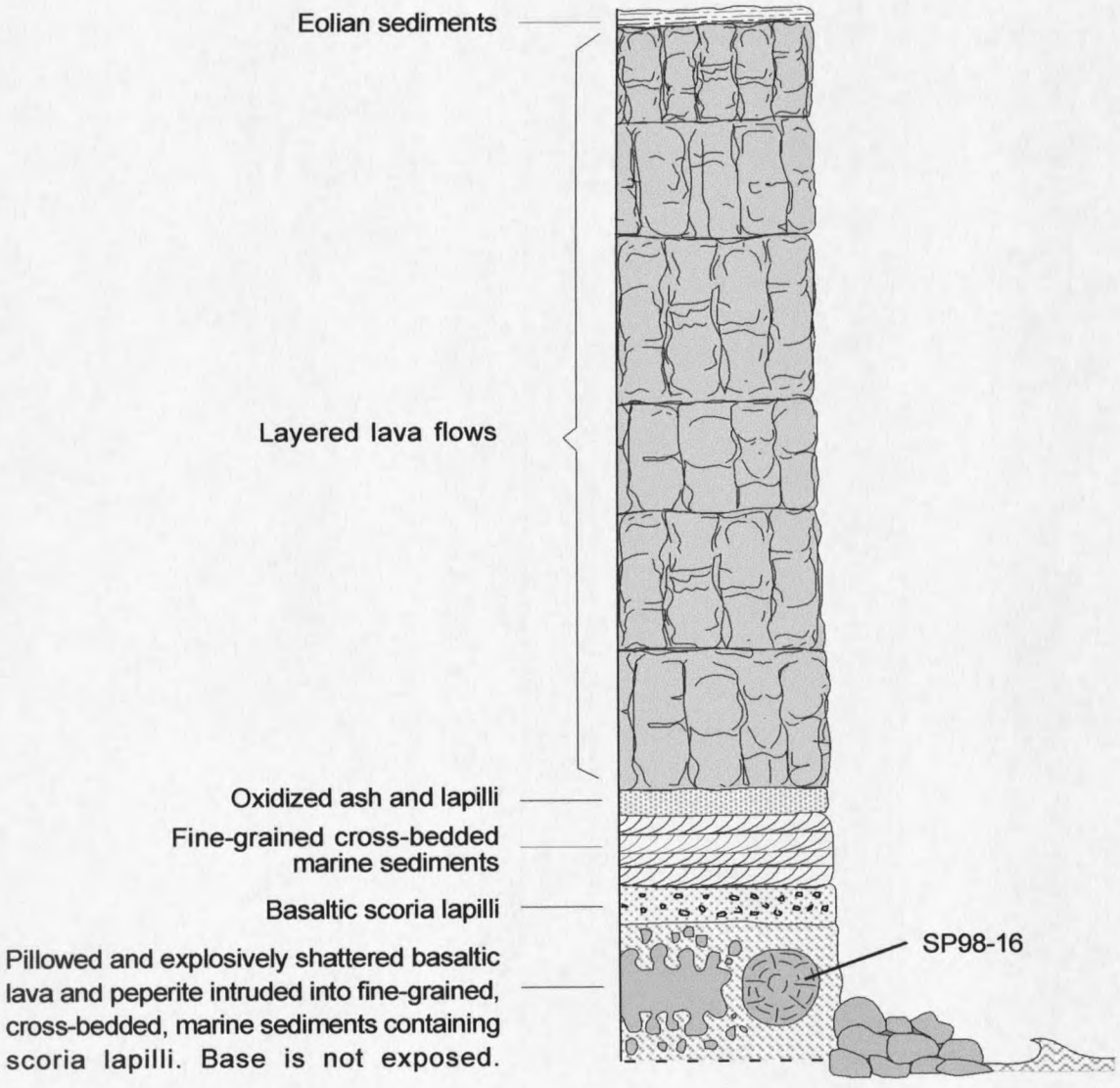


Figure 11. Schematic diagram of vertical section at Einahnuhto Bluffs on St. Paul's west coast. Height of section is about 75 m.

Locations of source vents for UPL's are unknown. On most of the island's surface there is a puzzling lack of geomorphically old cinder cones [such as those on south central and southernmost St. Paul Island, e.g., Telegraph Hill and those south of it] that may be considered as source vent for some of the platform lavas.

Platform lavas are primarily basalts and basanites, with one occurrence of trachybasalt, that range in composition from unevolved (MgO wt% >10) to moderately evolved (MgO wt% 8 to 10), although most are unevolved, and some have MgO contents as great as 14.39 wt%. Compositions of the platform lavas do not display any trends with respect to geographic position, however, MgO contents generally decrease upsection at any given locality. They all contain abundant phenocrysts of early crystallizing olivine (11 to 23 modal %) and have widely varying contents of clinopyroxene and plagioclase (0 to 24 modal % and 0 to 54 modal % respectively). Platform lavas, like many St. Paul lavas, have opaques of Fe-Ti oxides in their groundmasses, but these are usually too small to count as phenocrysts. Olivine phenocrysts in platform lavas have large variations in size and habit, from euhedral megacrysts to subhedral crystals and embayed skeletal forms. Groundmasses range from mostly glassy to intersertal and intergranular textures composed of microcrystalline plagioclase, clinopyroxene, olivine, and opaques. Some are dense and others have varying degrees of vesicularity. The most phenocryst-rich of the platform lavas are located at Kaminista and on the southern promontories. In these lavas modal olivine remains high (≥14%) and modal clinopyroxene is variable (1 to 24%), however, modal plagioclase is remarkably high (21 to 54%). Most of the plagioclase phenocrysts occur in euhedral laths, but a few are more equant, often

subhedral, and zoned. Photomicrographs of various platform lava textures are shown in Figure 12.

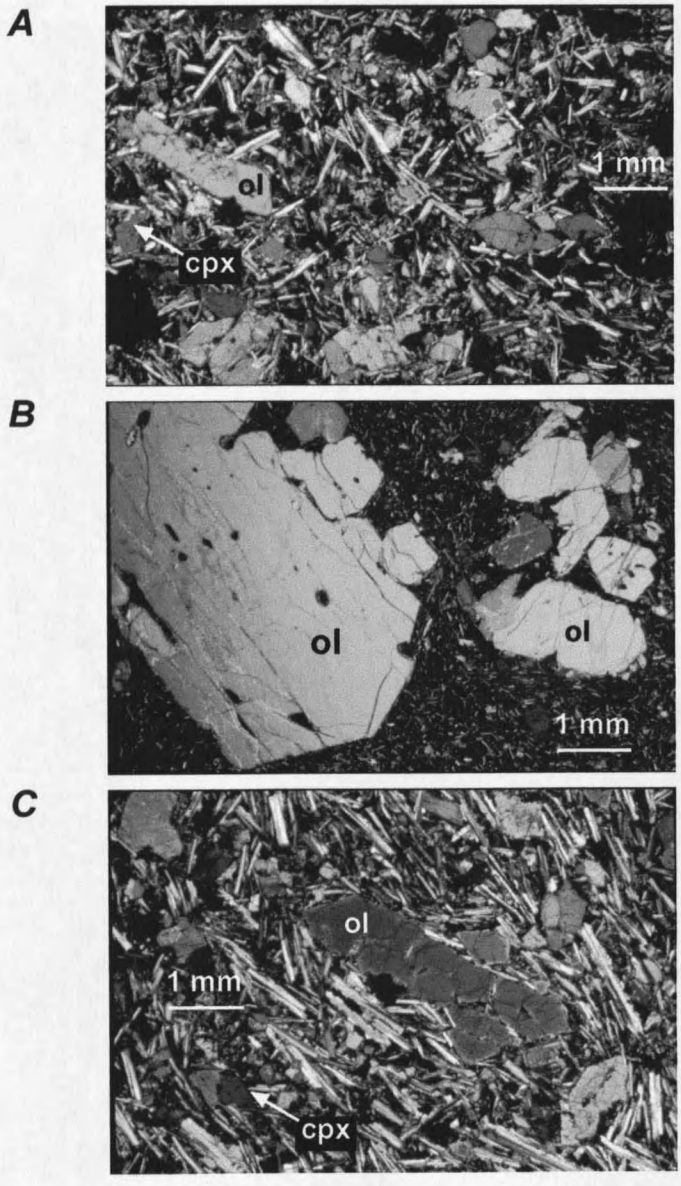


Figure 12. Photomicrographs showing textures of platform lavas. All views with crossed polars. A. Many platform lavas are characterized by their holocrystalline nature and high phenocryst content (SP98-14). B. Olivine megacrysts are common in the most MgO-rich platform lavas (SP98-70). C. Very high phenocryst contents (especially of large plagioclase laths) and trachytic texture is characteristic of lavas with platy jointing (SP98-71).

Kaminista Description. Faulted platform lavas are exposed at Kaminista, an elevated and topographically defined area located between Telegraph Hill and Bogoslof Hill. Kaminista is given special consideration here because of previous descriptions in the literature (Barth, 1956; Cox et al., 1966). Barth's (1956) brief account of Kaminista described lava flows that appeared to originate from a system of fissures. Cox et al., (1966) wrote of large fissures of probable tectonic origin in lavas at Kaminista. Kaminista is included with the platform lavas, based on composition, petrography, and faulting of the rocks. Specifically, lava at Kaminista (KAM-1) has relatively high MgO content (11 wt%) and is crystal-rich with modal plagioclase (40%), olivine (19 %), and clinopyroxene (24%). KAM-1 is petrographically and compositionally similar to UPL lava from Tolstoi Point (SP98-13).

The most prominent feature of Kaminista is a slightly curved ridge of lava that trends northeastward and southwestward; at its center it dips at 27° to 32° to the southeast (043°). Kaminista is seen from the southeast as a planar, rocky ridge (Fig. 13) that rises abruptly to 50 m above the adjacent undifferentiated lava flows (ULF). The ridge rises more steeply at the southwest end and it tapers and broadens toward the northeast (Fig. 14A). Located on this slope is a series of terrace-like features, only a few meters wide, with nearly horizontal surfaces composed of loose boulders (Fig. 14B).



Figure 13. Kaminista ridge with view to the northeast. The ridge rises abruptly from the lowland to the southeast (right). Terrace-like feature in lower left.is described in text.

A curved, trench-like feature [fissure of Barth (1956) and Cox et al. (1966)] adjacent to the northwest side of the high ridge of Kaminista, separates the ridge from the topographically lower and larger expanse of the Kaminista lava field where faulting is extensive. The trench, or fissure, is a natural feature that has been minimally changed by excavations related to a quarry at its southern end (Fig. 14A) (A. Bourdukofsky, 2000, personal commun.). A low graben-like feature is located in the center of Kaminista and extensional fissures are located toward the edges (Fig. 14A).

A vertical section of the Kaminista lava pile is exposed in the quarry wall, where it is about 50 m thick and is composed of at least four flow layers or lobes (Fig 14C). Individual units of Kaminista's compound lava flow have vesicular tops with ropy surfaces and no deposits of sediment or soil between them. These lavas resemble the older platform basalts in that lower flows have columnar to blocky fracture while the top

layer has the platy fracture pattern seen at Tolstoi Point and Zapadni Point. No evidence (e.g., tephra) was found to suggest that Kaminista is a primary volcanic feature.

Kaminista Interpretation. The following interpretation is a possible scenario to explain the geologic features of Kaminista. After emplacement of old platform lavas in the Kaminista area, faulting uplifted the lava flows to a level that prevented them from being covered by younger units. Possibly, motion on orthogonal faults had combined elements of oblique dip-slip, dextral strike-slip, and extension. The oblique strike-slip motion impinged on a curved fault causing compression that uplifted and tilted the southeastern part of the Kaminista lava and shoved it into a high ridge with the original planar flow surface dipping steeply to the southeast (Fig. 14A). Stress on the planar slope opened a series of crevasses that filled with boulders and formed the terrace-like features (Fig. 14B); some oblique dip-slip motion may also have occurred along these fissures. The oblique sense of motion changed to nearly pure strike-slip on the northeast exposure of the fault where the ridge slope tapers off gently. The proposed extensional component dilated the center of the Kaminista structure, forming a graben-like feature and a series of extensional fissures or cracks on the flow surface. The trench-like feature that separates the raised southeast ridge of lava from the collapsed main body of the unit follows the main strike-slip fault trace (Fig. 14A). Fissure-like features on the northeast end of Kaminista are interpreted as splays of the strike slip fault. The direction of extension at Kaminista parallels that on Tolstoi Point, suggesting that both may be part of a larger fault system buried beneath younger lava flows on the central highland (Plate 1).

This interpretation contrasts with that of both Barth (1956) and Cox et al. (1966), who suggested that Kaminista is an eruptive fissure.

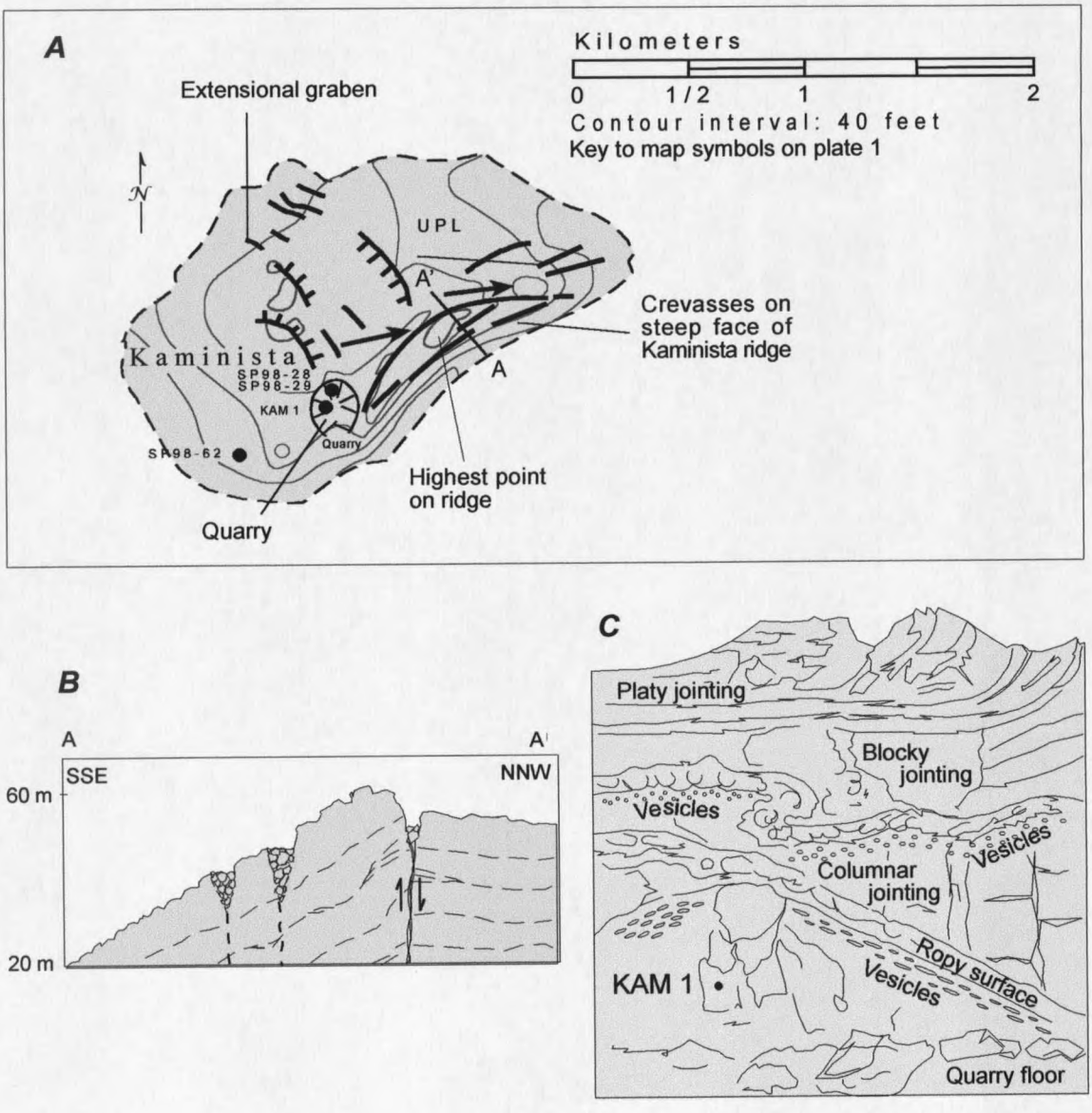


Figure 14. Kaminista. A. Kaminista area in plan view. B. Schematic cross section illustrating uplift and rotation of platform lavas and boulder-filled terraces or crevasses on tilted surface. Arrows show dip-slip component of fault; strike-slip component is dextral. C. Schematic cross section of Kaminista quarry wall. Sample sites are shown in A and C.

Undifferentiated Platform Lavas (UPL) Interpretation

The above description of platform lavas on St. Paul Island suggests that their style of eruption and emplacement is very similar to the plains style volcanism of the Eastern Snake River Plain (ESRP), Idaho, as described by Greeley (1977a) and Hughes et al. (1999). Several lines of evidence lead to this interpretation. First, lavas that form the platform of St. Paul Island are mostly compound, often discontinuous, relatively flat-lying pahoehoe flows, composed of sequences of thin units from the same eruptive episode (e.g., at Reef Point), which generally behave as individual cooling units (Walker, 1972; Greeley, 1977a; Walker, 2000). These compound pahoehoe flows are interpreted as products of low effusion rate eruptions of volatile-poor, low viscosity lavas (Greeley, 1977a; Walker, 2000). Second, platform lavas include tube- and toe-fed flows with varying degrees of vesicularity and with vertical jointing (Greeley, 1977a). The thicker flows at the top of the pile (e.g., at Tolstoi and Zapadni Points) are massive with platy jointing (Greeley, 1977b). The third, and perhaps the strongest evidence for plains style volcanism, is the lack of visible source vents in the form of cinder cones, combined with the meager amounts of associated tephra. This suggests that effusive eruptions from fissures and perhaps low monogenetic shields (since buried by more recent volcanic deposits) with minimal amounts of tephra and larger amounts of effusive lava, are the source of the platform lavas that form the base of St. Paul Island, and that early eruptive activity at St. Paul Island was very similar to volcanism that formed the ESRP.

Platy jointing in the thick, simple flows at the top of Tolstoi and Zapadni Points may be related to the crystallization and slow cooling of the thick flows that developed high

viscosity as they flowed, causing shearing and alignment of late-forming plagioclase laths. An increase in the effusion rate of lava is suggested by this change from compound to simple lava flows up section (Walker, 1972).

The source of at least some platform lavas may have been from central vents marked by old eroded cinder cones on southern St. Paul Island (see description below under PyC unit), but this relationship has not been established and, in any case, it is unlikely that these centers could account for all of the stacks of layered lavas exposed in the sea cliffs around the island.

Barth (1956) suggested that many lava flows on St. Paul were from fissure eruptions and that the fissures have subsequently been buried. The fissure origin of at least some of the early flows is admittedly speculative; however, eruptive fissures are common in basaltic lava fields, for example, the ESRP (Greeley, 1977a; Kuntz et al., 1988; Hughes et al., 1999), and the Trans-Mexican volcanic belt (Alaniz-Alvarez et al., 1998). In regions of extension such as St. Paul Island, the initial pathway for the ascent of magma is presumed to be a fissure (Nakamura, 1977). Undifferentiated platform lavas are interpreted as early monogenetic eruptions of primary, generally unevolved, unfractionated lavas from linear fissure systems and central vents located along these fissure, analogous to plains style volcanism of the ESRP.

Undifferentiated Lava Flows (ULF) Description

Undifferentiated lava flows (ULF) of uncertain origin differ from the UPL unit in that, where exposed, they have not undergone obvious faulting. Discontinuous layers of eolian sediments and a thick growth of tundra vegetation extensively mantle these lava flows, obscuring source vent-flow relationships. Sample SP98-55, taken from a ULF outcrop near Low Hill, is petrographically similar to crystal-rich platform lavas. Clinopyroxene is more plentiful than olivine in this sample and it frequently occurs as glomerocrysts about 2.5 mm in diameter. XRF analysis was not done on this sample.

Undifferentiated Lava Flows (ULF) Interpretation

The source of the undifferentiated lava flows, like the platform lavas, is unknown. The major difference between the ULF and UPL is in the degree or lack thereof, of faulting. In this study, a previously mapped fault in the ULF (Hopkins, 1976) is interpreted as a flow front, not a fault. The site of this flow front is adjacent to the northeast part of Low Hill where sample SP98-55 was collected.

PyC Unit Description

Pyroclastic cones with no identified associated lava flows (PyC) include the older eroded cones located on southern St. Paul, as well as several morphologically younger cones, such as Little Polovina Hill on northeastern St. Paul and cones on the central highland. The older cones located on southern St. Paul are Telegraph Hill, the hill on

which the older part of the village of St. Paul is located (locally called "Village Hill"), and a cone remnant located east of the Salt Lagoon. The latter is locally known as "Black Diamond Hill" because of the large black augite glomerocrysts, which weather out of the scoria there. Among these older cones in the PyC unit is Black Bluffs, the lone example on St. Paul Island of a Surtseyan eruption; Black Bluffs is described below. The older cones are partially or completely surrounded by sedimentary deposits and all are near or adjacent to the older platform lavas. They may represent source vents for some of the platform lavas, although this is speculative.

Little Polovina Hill, located on eastern St. Paul Island, is a cinder cone with a breached crater rim. Sand deposits have since covered any lava flows that may have issued from Little Polovina Hill and dunes have been emplaced around the lower slopes of the cone base. The dunes that surround Little Polovina Hill postdate the construction of the cone.

On the central highland are located PyC units that have been surrounded and/or partially buried by younger deposits from nearby volcanoes. The only cone that does not appear to have either a breached cone or crater is the small, symmetrical cone adjacent to the Crater Hill cone.

Two PyC units on the central highland are faulted. One is a puzzling, unnamed PyC edifice located on the eastern side of the Cone Hill volcanic complex. It is an older, welded, cinder/agglutinate cone with extensional faults that may be related to collapse due to loading of the cone with subsequent deposits from Cone Hill eruptions (see below). A somewhat elongated cinder cone, located adjacent to the southern part of the

faulted cone, is locally known as "Bread Loaf Hill" because of its shape (A. Bourdukofsky, 2000, personal commun.). The second faulted PyC cone is Slope Hill.

Slope Hill, located just west of Bogoslof Hill, is a small (greatest diameter is about 0.75 km) scoria cone that rises about 60 m above the younger Bogoslof Hill lava flow that surrounds it. The cone, constructed of unconsolidated scoria, is lower and elongated to the south. A small flow of grey, olivine-rich basalt issues from a breach in the southwestern cone rim, but beyond the cone it is either absent or is covered by younger lava flows. The lower and elongated southern portion of Slope Hill is transected by a fault that is nearly along strike to a fissure that crosses Bogoslof Hill (see Plate 1).

The eruption that formed Slope Hill is interpreted as a typical Strombolian-style eruption, having both an explosive and an effusive phase. During the initial explosive phase, the eruption of volatile-rich magma built a simple scoria cone. This phase appears to have been followed by the effusive eruption of volatile-poor magma. During the effusive phase the crater rim breached as lava rose in the vent and at least some of the lava flowed out, eroding the lip of the breached crater rim. Any lava flowing away from the cone, including that which may have burrowed out from the base of the cone, has since been buried by lava flowing from Bogoslof Hill. Although Slope Hill appears to be situated on the west flank of Bogoslof Hill, it predates lavas from Bogoslof Hill, which have buried its base.

The lowering and elongation of the southern portion of Slope Hill appears to be related to offset following construction of the cone. The fault or fissure that cuts the Slope Hill cone is on a nearly direct trend with open fissures that pass eastward through

Bogoslof Hill. The fault in Slope Hill may be related to the shallow emplacement of dikes on the flanks of Bogoslof Hill (Vergniolle and Mangan, 2000; Hughes et al., 1999).

PyC samples from Slope Hill (SP98-52) and Low Hill (SP98-54) are basanites with euhedral to subhedral phenocrysts of olivine and clinopyroxene in glassy to fine-grained groundmasses. Basalt from the partially exposed scoria cone on the eastern side of the Cone Hill volcanic complex (SP98-45) has olivine phenocrysts that are often skeletal-columnar in form and slightly embayed along with very small (0.3 to 0.5 mm) clinopyroxene phenocrysts in an intergranular groundmass. Olivine phenocrysts as large as 5 to 7 mm in greatest diameter occur in these samples.

PyC Unit Interpretation

The emplacement of monogenetic pyroclastic cones on St. Paul Island has been an ongoing process since early in the island's history. The ages of cones in the PyC unit appear to range from shortly after the time when St. Paul Island emerged from the sea (e.g. the old eroded cones on south-central St. Paul Island), to more recently formed cones on the central highland (e.g., Slope Hill and Low Hill). The apparent size of PyC cones may be misleading as the older cones on south-central St. Paul have undergone major erosion while the bases of cones on the central highland have been partially buried by younger lava flows.

Black Bluffs (BB) Description

Black Bluffs, the product of a Surtseyan eruption is an emergent tuff/cinder cone located near the village of St. Paul. The term "Surtseyan" is used for a volcano erupting through seawater (Vespermann and Schmincke, 2000). Surtseyan eruptions are characterized by violently explosive eruptions resulting from the interaction of basaltic magma and seawater (Kokelaar, 1983). Francis (1996) defines Surtseyan volcanism as equivalent to wet Strombolian eruptions. Surtseyan eruptions are named for the 1963 submarine volcanic eruption that became emergent and formed the island of Surtsey near Iceland.

The face of Black Bluffs is a cliff that rises nearly vertically from a sand and boulder beach to a height of about 22 m (Fig. 15). At Black Bluffs, the major part of the cone, including the summit, has been eroded by wave action, and tephra beds in the preserved portion of the cone dip landward to the north. The lowest layers of the cone are composed of well-consolidated, thinly stratified tephra of rounded and angular basaltic lapilli and accretionary lapilli in an ashy matrix. Relative proportions of ash, lapilli, and scoria grade up-section from (1) ash > lapilli, to (2) lapilli > ash > blocks to (3) lapilli > blocks. The color of the deposits changes from gray-brown to red-brown up-section. The red-brown layer is sharply overlain by crudely stratified black scoria with block-rich layers (Fig. 16A). The black scoria continues to the top of the cone, except for an intercalated layer of thin (about 0.25 m) layer of tan palagonite located in it. The face of Black Bluffs is also faulted with offsets as great as 2 m (Fig. 16A). Bedding-plane sags

related to block and bomb impacts are numerous in the lower, gray-brown portion of the cone (Fig. 16B).



Figure 15. Black Bluffs, the emergent tuff/cinder cone located near the village of St. Paul. Rapid erosion and mass wasting of Black Bluffs is caused by exposure to the heavy surf of the Bering Sea. Note the change in color near the cone base that marks the change from the palagonitic tuff to cinders. Small figure on the horizon at upper right shows scale.

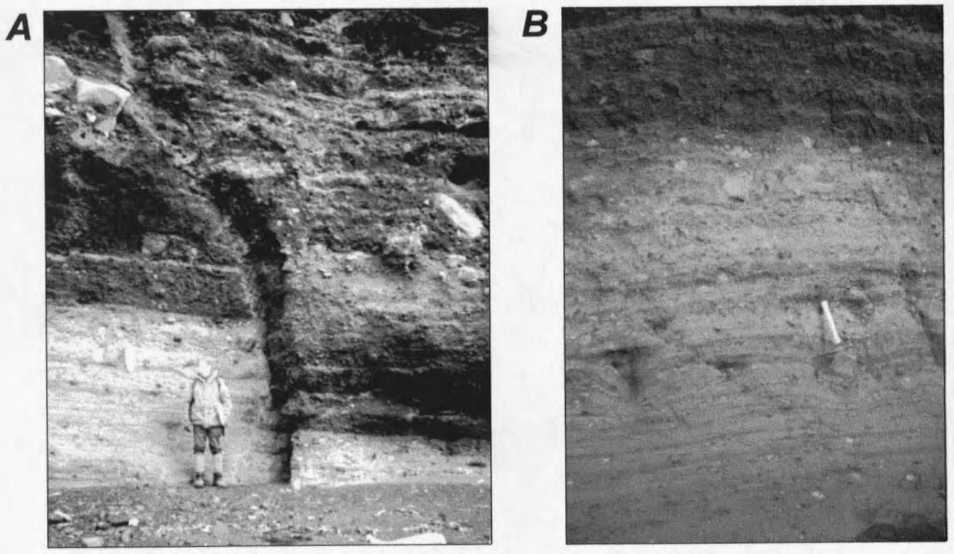


Figure 16. Close-up view of Black Bluffs. A. Faulting in the base of Black Bluffs offsets tuff and cinder strata by about 2 m. Note sharp transition from light colored hydroclastic surge deposit to black, crudely bedded scoria containing large blocks. B. Impact structures are common in the very thinly bedded hydroclastic deposit in the cone base. Transition from surge deposit to scoria marks the change in eruptive style from Surtseyan to Strombolian.

Blocks of friable grey claystone are scattered throughout the lower layers of the cone. Previous workers have described the fossiliferous nature of mudstone clasts in Black Bluffs (Stanley-Brown, 1892; Dawson; 1894; Dall, 1899; Emerson, 1904; Hanna, 1919). Black Bluffs cone is rapidly undergoing mass-wasting as large blocks fall off its vertical face on the seaward side, a consequence of basal sapping from wave action. As it retreats inland its precipitous cliff edge is receding toward the community cemetery located on top of Black Bluffs. The inhabitants of St. Paul today speak of the rapid erosion of Black Bluffs in their lifetimes (conversation with villagers, 1998).

Black Bluffs (BB) Interpretation

Black Bluffs is interpreted as an emergent volcano with its vent located seaward of its preserved flank on St. Paul's insular shelf. Initial eruptions at the Black Bluffs vent were characterized by magma-water interaction of the Surtseyan type when seawater flooded into the top of an open vent. Construction of the volcanic edifice began with submarine explosions, which excavated muddy gray sediments from the seafloor and deposited them in a growing cone of hyaloclastic debris and bedded tephra (Fig. 17). Bedding-plane sags (Fig. 16B) were formed by the impact of blocks and bombs in the wet and plastic Surtseyan surge deposits (Cas and Wright, 1987). Well-bedded hyaloclastic surge deposits changed to crudely bedded scoria, as the eruptive center became emergent and water was excluded from the vent (Kokelaar, 1983; Kokelaar, 1986; Walker, 2000). This change in the nature of the deposits marks the change from hydromagmatic to Strombolian activity. The change in scoria color from red to black up-section coincides

with the emergence of the cone, after which seawater was no longer mixing with the magma and causing oxidation of the tephra. The thin layer of intercalated palagonite in the black scoria probably represents a short interval of renewed Surtseyan activity, perhaps because a temporary breach in the cone permitted water to once again be admitted into the vent. After construction, the littoral location of the cone led to rapid mass wasting. The hydrovolcanic deposits in the base of Black Bluffs are less resistant to the heavy surf than adjacent basalt flows to the north, allowing differential erosion that is beginning to form a small cove in the coastline just north of East Landing. Ainsfield (1990) describes a similar phenomenon in Hawaii.

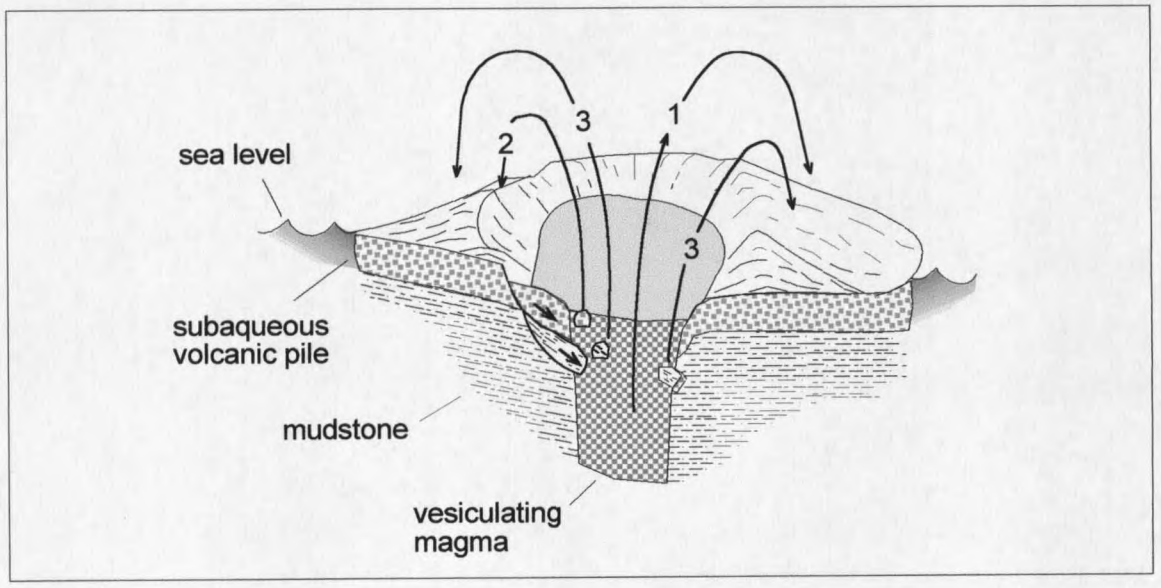


Figure 17. Diagram of Surtseyan eruption at Black Bluffs. Schematic diagram of explosive hydrovolcanic eruption showing entrainment of mudstone from seafloor into the eruptive column and its emplacement in the cone. The numbered paths represent first-cycle juvenile clasts (path 1), recycled juvenile clasts (path 2), and accidental lithic particles derived from seafloor sediments in the vent walls (path 3). From Houghton and Smith (1993) and Kokelaar (1983).

Polovina Hill (POL) Description

The Polovina Hill cinder cone complex, one of the largest monogenetic centers on St. Paul, is two kilometers in diameter at its base and rises 120 m above the surrounding lava shield, dominating the eastern half of St. Paul Island (Fig. 18). A major part of eastern St. Paul Island slopes away in all directions from this large cinder cone. Polovina Hill is

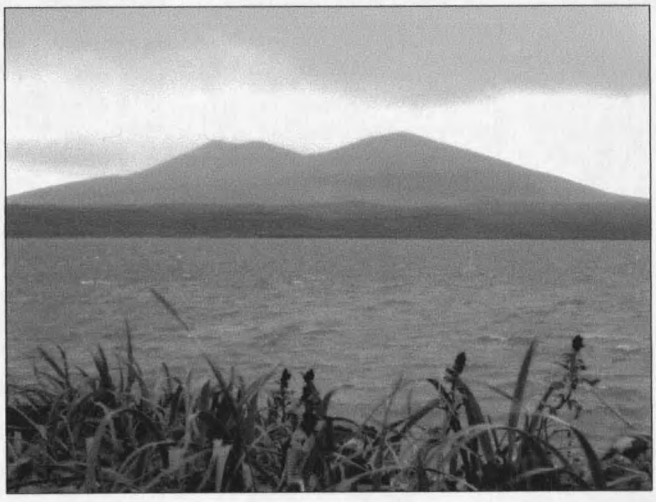


Figure 18. Polovina Hill, a large complex cinder cone, dominates eastern St. Paul Island. Polovina Hill is viewed here from the northwest; Big Lake is in the foreground.

a nested scoria cone with two, or possibly three, overlapping, breached craters. The northeastern crater contains a small marshy pond. A major portion of the cone wall of the first-formed and largest of the craters, the southern crater, is missing and no intact remnants of the cone appear to be preserved on the lava flows surrounding the cone. A portion of the west flank of Polovina Hill is exposed in cross-section in a quarry (Fig. 19). The exposed section is composed of crudely stratified, unconsolidated, black and red, scoriaceous lapilli and bombs (some greater than one meter in diameter). The bombs

are often round or spindle-shaped with cracked, breadcrust surfaces (Fig. 20A). The largest bomb observed was spindle-shaped and approximately 2 m in length (Fig. 20B). Some of the upper layers exposed in the quarry have abundant, large (≤1 m in diameter), dense, black, tachylyte blocks and bombs.



Figure 19. Vertical section on east flank of Polovina Hill is exposed in a quarry. The scoria here is red from oxidation, possibly from water in volatiles escaping from the magma feeder plane located beneath this area of the cone. To the right of the photograph, scoria color changes abruptly to black. Scoria quarried here is used for road building.

Exposed in the quarry wall is an abrupt change in color from black to red scoria that does not appear to be related to the strata, but cuts vertically across the scoria layers. Exposed in the southeastern wall of the quarry, near the cone surface is a thin (<0.5 m) layer of dense lava. Upslope from the red scoria and from the thin lava flow is a depression on the crater rim, from which a small lava flow may have issued. Aligned

with this depression is a second depression on the opposite side of the crater and also a large breach of an earlier formed section of this complex cone.

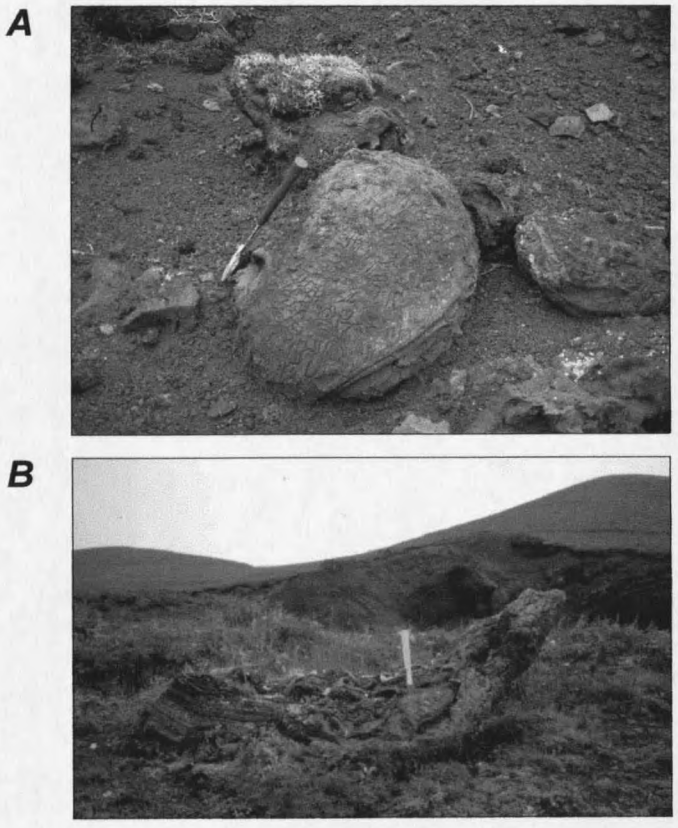


Figure 20. Bombs from Polovina Hill. A. Breadcrust bomb in Polovina quarry. B. Large spindle bomb on east flank of Polovina Hill. Rock hammers are about 33 cm in length. Breadcrust and spindle bombs are common products of Strombolian eruptions.

Polovina Hill's lava flows form a shield that extends to the east coast where the lava is exposed in the sea cliff (SP98-07). At this exposure, the simple lava flow is 7 to 10 m thick, with poorly developed columnar jointing and a rubbly top. The flow base is not exposed. On the surface, the lava shield is extensively covered with a layer of sediment

and tundra vegetation. From the north and west, a dune field encroaches on the Polovina lavas and cinder cone.

High on Polovina's main crater rim a small scattering of buff-colored, finely vesiculated, scoriaceous material was collected (SP98-35). [Barth (1956) reported finding a small amount of rhyolitic pumice on Polovina Hill in the same area.] Compositionally, samples of this unusually vesicular scoria are trachyte (Fig. 4; Table 1), and they are coated with basanite lava that composes the more abundant dark scoria of Polovina Hill. In the Polovina Hill trachyte (SP98-35) (Fig. 21), often euhedral phenocrysts of plagioclase, alkali feldspar, and small opaques are set in a vesicular, glassy groundmass. Due to its extremely rare occurrence, the trachyte was not studied in detail.

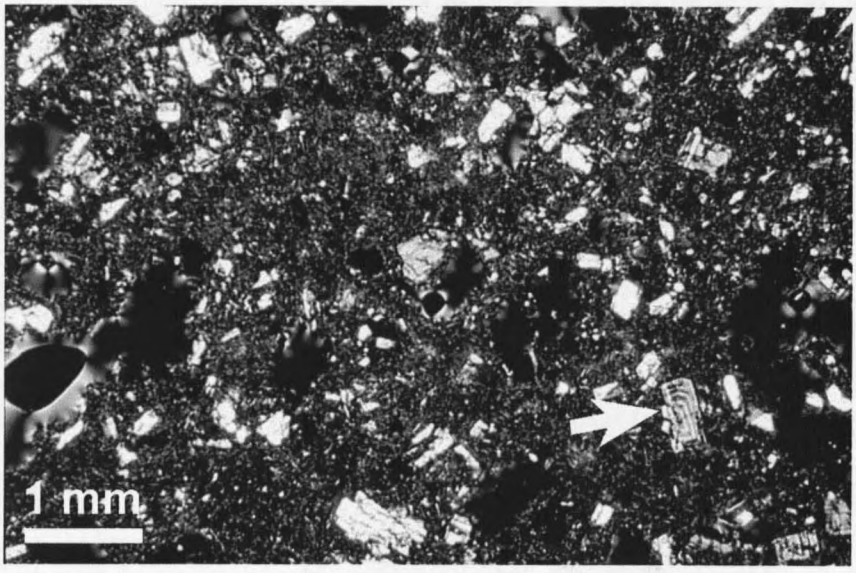


Figure 21. Photomicrograph of trachyte from Polovina Hill (SP98-35). Alkali and plagioclase feldspar phenocrysts are in a glassy, vesicular groundmass. Vesicles are black. Arrow points to zoned plagioclase phenocryst. Crossed polars.

Basanite samples from Polovina Hill tephra (POL 1, SP98-36) and Polovina lava from Polovina Point (SP98-07) have euhedral to subhedral olivine and clinopyroxene phenocrysts (≤2 mm largest diameter) in a glassy to fine-grained groundmass that in places shows slight alignment of plagioclase microlites (plagioclase phenocrysts are rare). The presence of spongy texture in clinopyroxene and common columnar and skeletal forms of olivine are indicative of rapid cooling, especially in tephra samples from the Polovina Hill cone (POL 1 and SP98-36). Increased growth of groundmass microlites in the Polovina Point lava sample (SP98-07) suggests slower cooling in the lava flow than in the tephra.

Polovina Hill (POL) Interpretation

Explosive eruptions of ash and scoriaceous lapilli, blocks, and bombs from two or three closely spaced vents built the Polovina Hill cinder cone complex. The earliest phase of explosive eruptions built the southern part of the cone before the vent (or vents) to the northeast became active. The fact that there is no cone wall to the west of this vent may be explained by two different scenarios: either (1) the cone wall was breached and rafted away on a lava flow, or (2) a lava flow was established early in the eruption and carried away the pyroclasts as they fell so that no cone wall was constructed at that site (Kuntz et al., 1982). If the first scenario is correct, then the fragments of the breached cone wall were either very small, or they eroded away, because they are not evident on the surface of the flow today.

Cone-building eruptions at Polovina Hill are interpreted to have been of the classic Strombolian style, having multiple discrete explosions as large gas bubbles (<1 to >10 m in diameter) rose to the surface of magma in the conduit, expanding rapidly as pressure was released, and exploding with great force, initiating the vertical ejection of an expanding cloud of gas and incandescent pyroclasts (Blackburn et al., 1976; Houghton and Schmincke, 1989; Cas and Wright, 1995). [In Strombolian style eruptions, discrete explosive bursts may occur as frequently as several times per second, or they may be separated by several hours (Blackburn et al., 1976; Cas and Wright, 1995).]

At Polovina Hill, as in other cinder cones, the crude stratification of scoria-fall deposits, represents the changes in energy of explosions during the course of the eruption (Wood, 1980a; Vespermann and Schmincke, 2000). Variations in the vigor and frequency of the explosive bursts is related to gas content in the magma and this, in turn, affects the size of the pyroclasts, e.g., an increase in exsolved gases results in increased explosivity and a higher rate of fragmentation of the magma (Head and Wilson, 1989). Layers of smaller pyroclasts were deposited during periods of high gas flux and increased fragmentation. The tachylyte blocks and bombs that are concentrated in some layers of the cone may have been ejected during a decrease in gas flux when the period between explosions was long enough to allow a crust to form on the surface of the magma, or during vent clearing explosions (Blackburn et al., 1976; Cas and Wright, 1986; Houghton and Schmincke, 1989).

The coinciding aligned depressions on the Polovina Hill crater rim, the direction of breaching, and also the change in scoria color from black to red, may have a common

cause. According to Tibaldi (1995), not only the locations of depressions on crater rims, but also the direction of breaching, have a direct correlation to the strike of the magma feeding plane beneath pyroclastic cones in transtensional environments, such as St. Paul Island (Nakamura et al., 1980). Areas of structural weakness in the cone wall are related to the geometry of the feeding plane (Tibaldi, 1995). Lending credence to this observation is the presence of the color change from black to red in tephra, as this may be related to oxidation by volatiles rising into the scoria along strike of the magma-filled feeding plane beneath the volcano (Tibaldi, 1995). This is significant because, in basaltic magma, while the exsolution of CO_2 begins a few tens of kilometers below the surface, significant amounts of S and H_2O only begin to exsolve within a few hundred meters of the surface (Vergniolle and Mangan, 2000).

The manner in which the land surface slopes away from Polovina in every direction, suggests that the Polovina lava shield is located not only where mapped, but also extends toward Big Lake and Little Polovina Hill. However, in this area sand dunes and eolian sediments cover it to the extent that no outcrops of lava were found.

Hill 404 (H404) Description

Hill 404 is a breached cinder cone that is mostly surrounded by younger lava from Bogoslof Hill. The crater rim and the cone are breached to the northeast and a small lava flow appears to have issued from this breach. Younger lavas of Bogoslof Hill cover an unknown portion of the lava flow. The 404 lava flow approaches the base of Low Hill and appears to be younger than this cone in the PyC map unit.

Scoriaceous basalt from the summit of Hill 404 is very vesicular (50% vesicles) with euhedral to subhedral olivine and clinopyroxene phenocrysts (≤2.5 mm greatest diameter) in a glassy to fine-grained groundmass. Spongy texture in clinopyroxene and somewhat skeletal forms of olivine phenocrysts suggest rapid quenching upon eruption.

Hill 404 (H404) Interpretation

Hill 404 is a simple, monogenetic volcano with a breached cinder cone and an associated lava flow.

North Hill (NoH) Description

North Hill is a medium sized cinder cone complex located on northern St. Paul Island. It has a basal diameter of about 1 km and rises 110 m above its surrounding low shield of poorly exposed lava flows (Fig. 22), which form a cape on the north-central coast (Plate 1). The cone complex is elongated in a NE-SW direction and has three overlapping craters, also aligned NE-SW. Lava issued from multiple breaches in the southwestern part of the cone and a lava flow lobe issuing from the breached cone, extends to, and appears to lap onto, the north side of Low Hill. One section of the breached cone wall remains remarkably intact and it has been moved outward, rotated clockwise, and following the translation and rotation, incorporated into the wall of the third and most southwesterly crater. The surfaces of North Hill lava flows are extensively weathered and covered with vegetation.

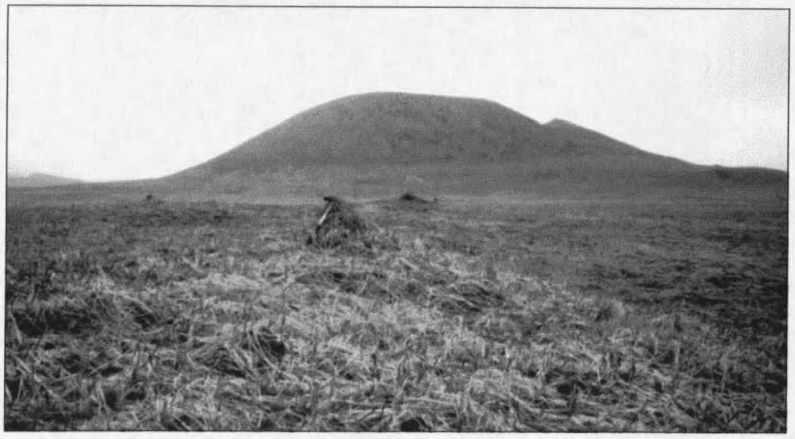


Figure 22. North Hill is a complex cinder cone located on northern St. Paul Island. The North Hill lava shield, in the foreground, has a heavy cover of tundra vegetation.

Basanite lava from North Hill is the least evolved (12.36 wt% MgO) and richest in olivine (18 modal %) of the monogenetic centers. North Hill lava (SP98-37) has a seriate texture with olivine (ranging in size from 0.3 to 6 mm in diameter) and clinopyroxene phenocrysts in a glassy groundmass with sparse plagioclase microlites (Fig. 23).

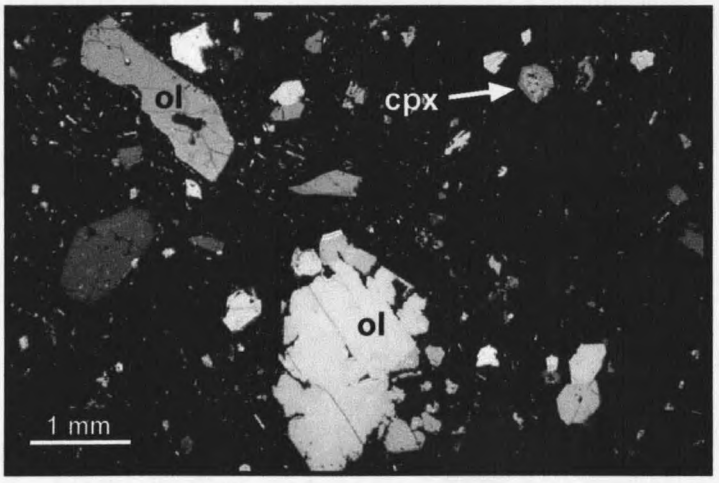


Figure 23. Olivine-rich North Hill basanite with glassy groundmass.

North Hill (NoH) Interpretation

North Hill is a monogenetic volcano with a complex eruptive and breaching history. The coinciding NE-SW elongation of the cone with the alignment of vents suggests that the cone-building eruption initiated along a fissure with the same trend and localized to vents at the three aligned craters (Tibaldi, 1975; Wood, 1980a). [Localization of vents along an erupting fissure is a common occurrence in basaltic volcanism (Wylie et al., 1999).] An extension of the SW trend of North Hill vents strikes toward Ridge Hill and Fox Hill eruptive centers, suggesting that the same fissure, or trend of crustal weakness, may extend to those centers as well.

The arrangement of cone rims, crater walls, breaches, and lava flows at North Hill suggests that explosive crater forming eruptions and the cone-breaching effusive eruption of lava flows were contemporaneous or penecontemporaneous. Based on the sediment-supported cover of vegetation, North Hill lavas are noticeably older than lavas of the central highland. This observation appears to be supported by the less evolved composition of its lava, which is similar to the older platform lavas.

Hill 255 (H255) Description

Hill 255 is a small spatter/cinder cone located near Southwest Point. Its base is about 0.25 km in diameter and it rises approximately 30 m above the younger lava flows that surround it. A lava flow extends southwest from a notch in the low spatter rim around its shallow crater, but only a small area of the surface of this flow is exposed near the cone.

The majority of the H255 lava is covered by Ridge Hill (RiH) lava which is in turn covered by the young Fox Hill lava flow (FXH) between Hill 255 and the coast. At the coast at Southwest Point, all three of these lava flows appear to be exposed, with the Fox Hill flow (SWPT1, SWPT 2, SWPT3) overlying the Ridge Hill flow (SP98-39), which overlies the Hill 255 flow (SP98-40). Hill 255 is locally called the "Halibut's Tail" because of its notched profile (J.R. Merculief, 1998, personal commun.).

Samples from the top of Hill 255 (SP98-41), and from Southwest Point (SP98-40), are petrographically and compositionally (Table 1) similar basalt; compositional differences are within analytical error. Both are unevolved basalt (wt% MgO 10.09 and 10.32 respectively). They have seriate texture with euhedral to anhedral and columnar olivine phenocrysts (10 to 12 modal %), some as large as 5 mm in diameter, set in a fine-grained glassy groundmass well peppered with small opaques. They have few vesicles. The groundmass in SP98-40 is slightly less fine-grained than SP98-41, which may indicate slower cooling in the lava flow than in the more rapidly cooled tephra at the cone summit.

Hill 255 (H255) Interpretation

The eruption that formed Hill 255 is interpreted to have been mildly explosive, building a cone of cinders and spatter. As the explosive phase of the eruption waned, there formed a rim of agglutinated spatter around the cone crater, which filled with a lava pond. Breaching of the southwest crater rim allowed the lava pond to drain and form a flow, which, based upon the compositional and petrographic similarity of a lava flow

exposed at the coast at Southwest Point, extended to the sea. Based on stratigraphy, this lava flow, except for a small part near the cone, was subsequently covered by a lava flow from Ridge Hill. About 3230 years before the present (^{14}C age dating), lava from Fox Hill flowed from the north and separated to flow around Hill 255. The base of Hill 255 is probably partially buried by these younger lava flows.

Crater Hill (CH) Description

Crater Hill is a complex eruptive center located on west central St. Paul Island between Cone Hill and Low Hill. Crater Hill has a large, deep crater and a sharp and ragged cone rim that gives it a distinctive morphology and silhouette, compared to other volcanoes on the island (Fig. 24A). A tongue of lava approximately 50 m thick flows from the breached northwest wall of the cone. Two spatter/cinder cones are located inside the crater, one on either side of the breach in the cone wall. The floor of the crater is greater than 200 feet below the cone rim, which is unusually deep compared with other craters on St. Paul. The crater contains a lake of muddy water. The cone rim is conspicuously sharp and dips steeply ($\leq 40°$) both outward and inward (Fig. 24B). An outward dipping layer of agglutinated spatter 1-3 m thick overlies the outer surface of the cone rim. Agglutinated spatter also extends downslope on the crater walls from near the rim. Xenoliths of ultramafic and granitic composition were found in close proximity on the west crater wall in the vicinity of the SP98-51 sample site. Clinopyroxene, plagioclase, and quartz xenocrysts up to 1 cm in diameter were also found in the same

location. Sample SP98-50, from the Crater Hill lava tongue, contains a lherzolite xenolith (Fig. 25).



Figure 24. Crater Hill. A. Crater Hill viewed across a lava flow from Bogoslof Hill. Note the ragged silhouette of the truncated crater rim. B. Armor of welded spatter on the sharp crater rim is in outward dipping layers. Geologist G. Winer.

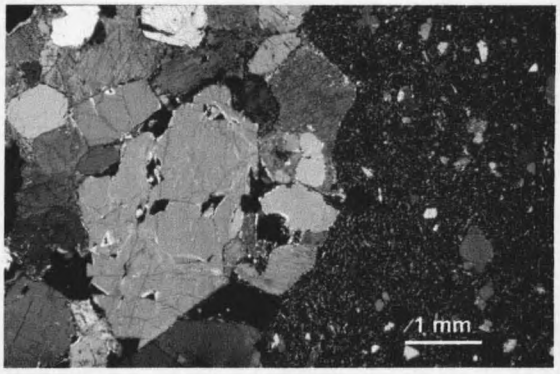


Figure 25. Photomicrograph of lherzolite xenolith (left) in Crater Hill lava (SP98-50).

Crater Hill basalt (SP98-51) is unevolved (10.91 wt% MgO) with seriate texture and fine-grained somewhat glassy groundmass. Olivine is by far the dominant phenocryst phase (10 modal %) and crystals are generally relatively small, ranging in size from 0.3 mm to a few as large as 2.5 mm. Plagioclase (1 modal %) and clinopyroxene (2 modal %) often appear to be undergoing fine-grained alteration both in rims and cores. This sample contains a small (2 mm) altered granitoid xenolith.

Crater Hill (CH) Interpretation

It is inferred that the formation of Crater Hill occurred in five steps: (1) rapidly rising magma entrained ultramafic and basement xenoliths as it ascended from its mantle source and erupted explosively to build a scoria/spatter cone; (2) the scoria cone was armored with a carapace of rootless agglutinated and clastogenic lava flows on the cone rim and crater walls, as the explosive phase waned; (3); a violent eruption reamed out the crater and truncated the cone rim; (4) degassed lava rose into the crater and the cone breached

to the northwest where lava flowed out in a thick tongue-shaped lobe; and (5) mildly explosive lava formed two spatter/cinder cones on the crater floor on either side of the breach in the cone wall.

The Crater Hill crater appears to have been enlarged and deepened by a powerful explosion in a manner that differs from the normal progression expected for the construction of scoria cones (Wood, 1980a). The nature of the explosion that reamed out the crater may be related to the interception of the volcanic conduit by groundwater; it may have been phreatic or phreatomagmatic. However, no palagonite, which may be expected in a phreatomagmatic explosion, was seen, making this interpretation speculative. Material ejected may have been shattered and hurled beyond the cone walls where it was buried by younger lava flows, such as the flow from Bogoslof Hill (BHVC) that partially surrounds Crater Hill. Slumping is not considered as a suitable mechanism for enlarging the interior of the crater as the cone is well reinforced with spatter and agglutinated lava and no signs of slumping (e.g., slump blocks) were seen.

Lake Hill (LH) Description

Lake Hill is a complex eruptive center of nested and overlapping scoria cones with intersecting craters located between Polovina Hill and Bogoslof Hill. A small satellite vent with no crater is located on northwestern Lake Hill. Of the three most recently formed craters, one contains a quarry where scoria has been removed, one has a small lake that may not be perennial, and the third contains a permanent lake . A very low rim separates the two craters containing lakes. Their walls contain welded horizons of

olivine-rich, glassy black agglutinate containing olivine phenocrysts as large as 5 mm in diameter. The northwestern crater with the smaller lake is located in a larger and older crater with a very low rim that is partially surrounded by a lava flow.

Sediments in the larger of the crater lakes (Cagaloq Lake) have been core-drilled for palynological studies (Colinvaux, 1967, 1981). As well as palynology, radiocarbon age determinations were also done on a 14 m sediment core from Cagaloq Lake (Colinvaux, 1967, 1981). The greatest radiocarbon age was 17,800 ± 700 years, determined from a sample between 10.5 and 10.8 m depth on the 14 m core. Ages determined from below this level (13.0-13.2 m) were anomalously young, likely due to the introduction of modern carbon brought in by the flow of ground water (Colinvaux, 1967). Therefore, the age of the Lake Hill complex is greater than 17,800 ± 700 years. Small pits located around the low rim of the northwestern crater are the vestiges of bunkers dug during World War II. A few of these diggings are also located in the southeastern crater.

The morphology of Lake Hill is differs from most other monogenetic cinder cones on St. Paul in that its cone is areally extensive considering its height. Although the Lake Hill cinder cone (1.75 km in greatest diameter) covers nearly as much area as the Polovina Hill cone, Lake Hill rises only about 200 feet (60 m) above surrounding lava flows. In comparison the Polovina Hill cone rises twice as high (~390 ft or 120 m) above its lava shield. Vents at Lake Hill appear to be aligned on two different trends (Fig. 26) and they are widely separated, compared with vents at other monogenetic centers.

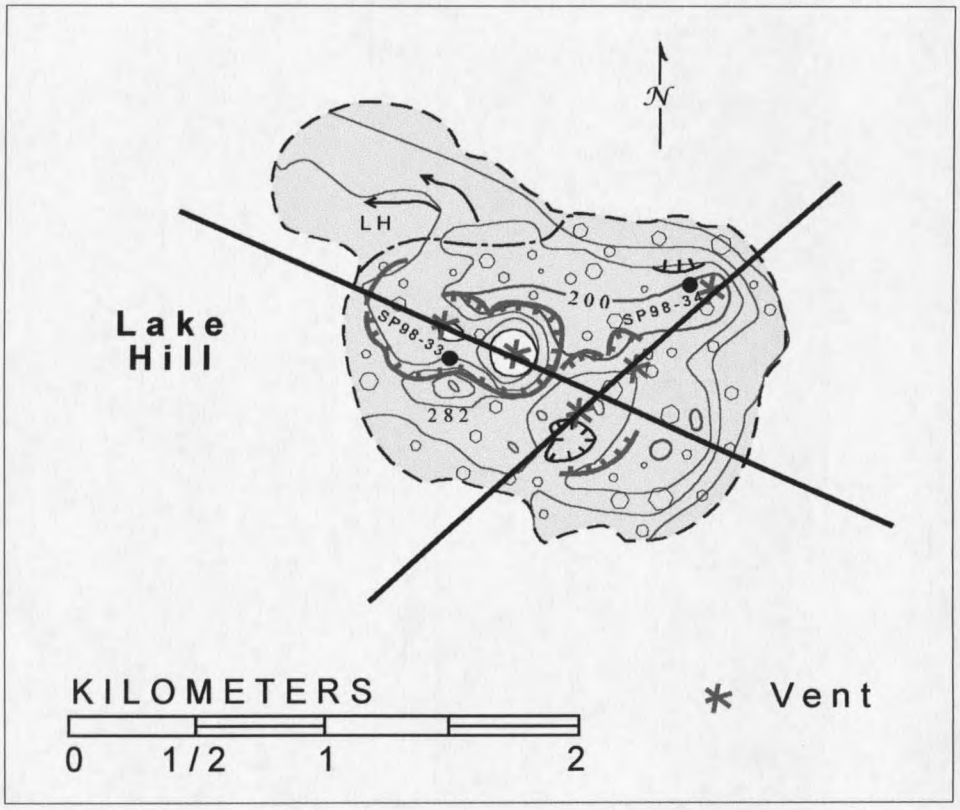


Figure 26. At Lake Hill, vents are located on intersecting NE-SW and NW-SE lineaments.

Lake Hill lava is an unevolved (11.20 wt% MgO), vitric, olivine basalt (SP98-33) with a seriate texture. Olivine phenocrysts are plentiful (12 modal %), but generally small (<2 mm greatest diameter). Olivine is euhedral to anhedral and frequent columnar crystals are weakly aligned with sparse plagioclase microlites in the black glassy groundmass. Plagioclase and clinopyroxene phenocrysts are rare in this sample (< 1 modal %).

Lake Hill (LH) Interpretation

It is inferred that the Lake Hill scoria cone complex was formed in several eruptive phases: (1) serial Strombolian eruptions from a group of vents aligned on intersecting feeder dikes formed nested scoria cones; (2) within the previously formed volcanic edifice, penecontemporaneous explosive eruptions from three or more vents began forming three intersecting craters and overlapping cones; (3) as the degree of explosivity waxed and waned, layers of spatter and agglutinated lava were deposited on the growing cone rims; and (4) following the cone construction, the effusive eruption of degassed lava breached the northwest crater wall and formed a lava flow. It is inferred that the unusually broad, low edifice of Lake Hill cinder cone is related to the widely spaced locations of its vents

Ridge Hill (RiH) Description

The Ridge Hill cinder cone is located on the western end of the island between Cone Hill and Rush Hill. The cone is breached to the southwest and is nearly surrounded by its own lava flows. The north side of the Ridge Hill cone is considerably steeper than the east, west, and especially the southern aspect (see Plate 1). A unique feature among St. Paul cinder cones is the widespread southern base of Ridge Hill. Surrounding the more gently sloping sides of the cone is a hummocky field of low, rounded mounds of scoria, some of which extend to Fox Hill where they are covered by Fox Hill scoria. Ridge Hill lavas extend south and southwest to the coast and are partially covered by the younger

lava flow of Fox Hill. Lava exposed directly beneath Fox Hill lava at Southwest Point is petrographically very similar to Ridge Hill lava.

Ridge Hill (SP98-77) is an unevolved (11.04 wt% MgO) olivine-rich (17 modal %) vitrophyric trachybasalt with a weakly trachytic texture. Large (≤ 5 mm) olivine and clinopyroxene phenocryst are euhedral to subhedral. A spongy texture in clinopyroxene phenocrysts and the glassy groundmass indicate quenching during rapid cooling.

Ridge Hill (RiH) Interpretation

The formation of Ridge Hill is interpreted as a Strombolian eruption that constructed a cinder cone during the explosive phase, which was followed, or accompanied, by the effusive eruption of lava. The presence of low mounds of scoria partially surrounding the cone is interpreted as the result of lateral spreading of the cone base. The rapid effusion of degassed lava may have facilitated cone base spreading. In this scenario, dense lava effused into the crater and burrowed out (Kuntz et al., 1982) at the cone-substrate interface [it is the rare cinder cone that lacks a lava flow originating at its base (Wood, 1980a)]. Lateral spreading of the cone is inferred to have been accomplished by the slump-like collapse of the cone base as it was rafted outward on flowing lava at the cone-substrate interface (Fig. 27). Sumner (1998) describes a similar process at Izu-Oshima, in Japan, where the lateral extrusion of flowing clastogenic lava beneath the cone base facilitated the lateral spreading. Lava beneath the Fox Hill flow at Southwest Point is inferred to be a part of the Ridge Hill lava flow on the basis of stratigraphy and petrography.

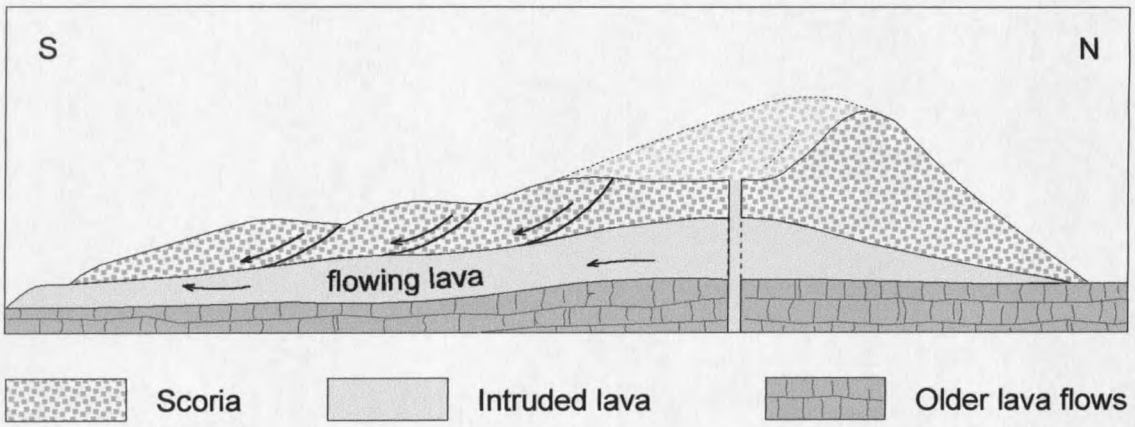


Figure 27. Schematic diagram of Ridge Hill cinder cone and proposed mechanism for basal cone spreading (Kuntz et al., 1982). Diagram adapted from Sumner (1998).

Rush Hill (RuH) Description

Rush Hill, located on the west end of St. Paul, is the largest cinder cone complex on the island. Its summit, the highest point on the island, rises to 203 m (665 feet) above sea level and 140 m above the surrounding lava flows. The greatest width of the cone complex is about 2 km. Rush Hill consists of at least 5 overlapping scoria cones, indicating a complex eruptive history. The craters intersect one another and all are breached. Lava flows issuing from Rush Hill extend northeast to Lincoln Bight and north and west along the coast where they are well exposed in the sea cliffs.

Relative to the other cinder cone complexes on the island, the Rush Hill complex is significant in that the subsurface marginal interior of a Strombolian eruptive center is exposed in cross-section in the Einahnuhto Bluffs. The relationship between the Rush Hill volcano and structures through which it has intruded have been described and illustrated by Barth (1956) (Fig. 28), who apparently had access by boat to study the face

of the cliff. At Einahnuhto Bluffs, Barth (1956) illustrated the layered platform lavas dipping away from the vicinity of Rush Hill and described the disruption of the platform lavas related to the eruption of Rush Hill and its subsurface intrusions. Barth (1956) specifically describes an intrusive dike that he sampled (sample no. 17; Fig. 28), and the same dike was described and sampled in this study (see the section on UPL – Undifferentiated platform lavas, above). Compositionally, samples from this dike (SP98-18 and Barth's (1956) no. 17), are similar to Rush Hill samples from the northwest point of the island (SP98-23), and from the Rush Hill summit (SP98-78). Rush Hill lavas (SP98-18, SP98-23, SP98-78) have the highest K_20 contents (2.29 to 2.56 wt%) of all rocks analyzed in this study (Table 1).

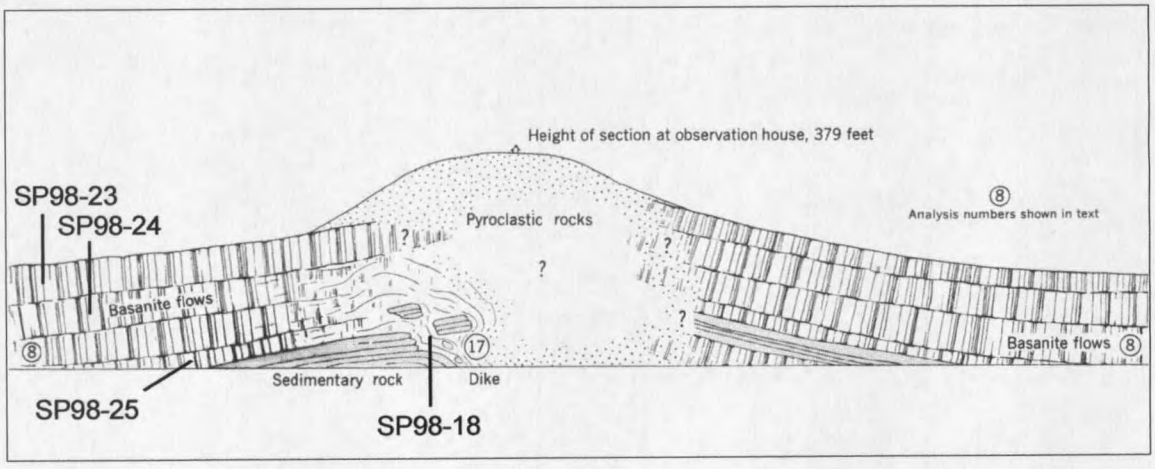


Figure 28. Schematic diagram of section through Rush Hill and Einahnuhto Bluffs on the west coast of St. Paul Island (Barth, 1956). Circled numbers are sample locations from Barth (1956). Observation house is no longer on Rush Hill. Sample numbers from lava flows sampled in this study are included. The dike is described in the text.

Rush Hill lavas range from basanite to tephrite (Table 2) and are compositionally and petrographically similar with glassy to fine-grained groundmasses and small (usually much less than 1 mm) skeletal olivine phenocrysts. SP98-78 is vesicular with a black glassy groundmass and contains an altered diorite xenolith (15 mm greatest diameter). SP98-18 has a pronounced trachytic texture with very small (often <<1 mm) skeletal olivine phenocrysts in a fine-grained groundmass. Also present in this sample are a few rounded clinopyroxene megacrysts (<3 mm in greatest diameter) that, because of their rounded appearance, are interpreted as xenocrysts. A glassy vesicular bomb collected near the summit of Rush Hill (SP98-78) contains a diorite xenolith 1.5 cm in diameter.

Rush Hill (RuH) Interpretation

Similar to many other vent complexes on St. Paul Island, the Rush Hill complex is inferred to have formed during a Strombolian-style eruption that progressed from explosive ejection of gas-rich spatter and scoria to effusive outpouring of gas-poor lava flows and breaching of early-formed tephra cones. As evidenced by the numerous overlapping cones and intersecting crater rims that form the complex, the location of the active vents during this eruption shifted, and it is possible that multiple vents may have been simultaneously active.

Barth's (1956) interpretation of the vertically exposed section of Rush Hill suggests that the tremendous pressure associated with the Rush Hill eruption uplifted layered platform lavas by approximately 100 m and caused lateral penetration of adjacent lava flows and intercalated sediments by Rush Hill magma (Barth, 1956) (Fig. 28). The

explosion that formed Rush Hill burst through lava flows in the vicinity, depositing pyroclastic material as it moved upward to construct the Rush Hill cinder cone complex (Barth, 1956). The explosive eruption was followed by the effusive discharge of lava that breached the overlapping cones and craters of Rush Hill and flowed west and north toward the sea.

Interpretations from this study, and by Barth (1956), have inferred that the platy jointed unit exposed in the bluffs represents a subvolcanic intrusion (possibly a feeder dike) for the Rush Hill complex. This interpretation is confirmed by the new geochemical data for this intrusion and other Rush Hill units presented in this thesis (Table 1). Specifically, K_2O contents of the intrusion are elevated (at a given SiO_2 content) relative to other volcanic units on the island, and they are similar to unambiguous Rush Hill units. Rush Hill thus formed from a highly explosive eruption of the most alkalic lavas on St. Paul Island. Their low MgO contents (7.36 to 6.46 wt%), low modal olivine (5 to 6%), and Ni and Cr contents similar to Fox Hill lavas, suggest that Rush Hill magma, like Fox Hill magma may have undergone crystal fractionation prior to eruption (Feeley and Winer, 1999).

Ridge Wall (RW) Description

Ridge Wall (RW) is a breached tephra cone complex located on the south coast between Zapadni Point and Southwest Point. Ridge Wall has four vents aligned on a NE-SW trend, which is parallel to the main Cone Hill trend (described below). All cones within the complex have breached to the southeast and a lava flow extends to the east and

south to the coast. On the lava flow are large, often intact, chunks of crudely bedded scoria, some of which are exposed in cross-section in the sea cliff. As much as 15 m of rafted tephra is located atop the Ridge Wall flow at the highest part of the sea cliff south of Ridge Wall. Below the tephra in the vertical cliff face are exposures of three lava flow layers or lobes, varying from 1 to 3 m thick, with layers of volcanic breccia and tephra beneath each layer. The lower two lava layers contain conspicuous ultramafic inclusions (up to 5 cm in diameter) and disaggregating granitoid xenoliths as large as 12 cm across.

Ridge Wall tephra is distinct from that at other scoria cones observed on St. Paul. While pyroclasts at other cones are generally irregular chunks of scoria with a stony luster, Ridge Wall has an abundance of ribbon and cow-dung bombs with vitreous luster. Ridge Wall's distinct tephra is well exposed in a borrow-pit or quarry (see Plate 1 for location). Tephra in the walls of the borrow-pit, located in a large and partially rafted cone segment, varies from welded to unconsolidated and has a large component of very glassy, red and black ribbon bombs. Tachylyte cow-dung bombs are common on the cone surface. These pyroclasts are very lightweight and fragile.

On the surface of the Ridge Wall lava flow, south of the road that runs between Ridge Wall and the sea, is a formation that, because of its silhouette as seen from the road, is locally referred to as the "Praying Aleut" (Fig. 29). This outcrop is composed of a rafted segment of Ridge Wall tephra.

The upper two lava flows [SP98-42 (upper) and SP98-43 (middle)] are petrographically very similar olivine vitrophyres. Sample SP98-42 is a vesicular, compositionally unevolved (11.76 wt% MgO), and olivine-rich (~12 modal %) basalt.

Olivine phenocrysts are euhedral to subhedral and mostly small (1 mm or less in largest diameter), with a few subhedral olivine megacrysts (5 mm greatest in diameter), set in a mostly glassy, microlite-poor groundmass (Fig. 30). A microlite-rich streak in SP98-42 may represent flow structure. A granitoid xenolith in sample SP98-34X (from the middle flow near SP98-43), appears to be disaggregating along its border with the host basalt (Fig. 31).



Figure 29. Praying Aleut. On the Ridge Wall lava flow is an outcrop formed from a section of rafted scoria cone from Ridge Wall's breached cinder cone. Because of its distinctive silhouette, the outcrop is known as the Praying Aleut. It is located south of Ridge Wall between the road and the coast.

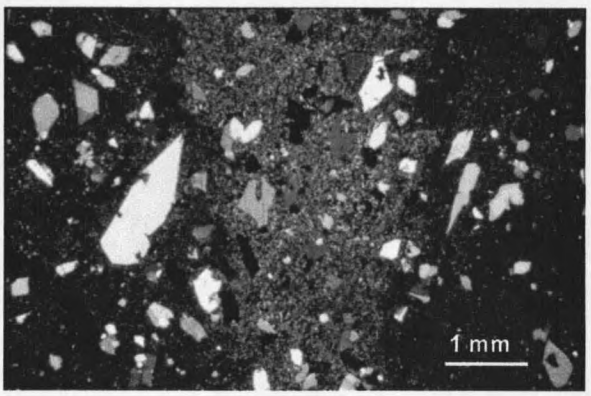


Figure 30. Photomicrograph of Ridge Wall olivine basalt (SP98-42). Crossed polars.

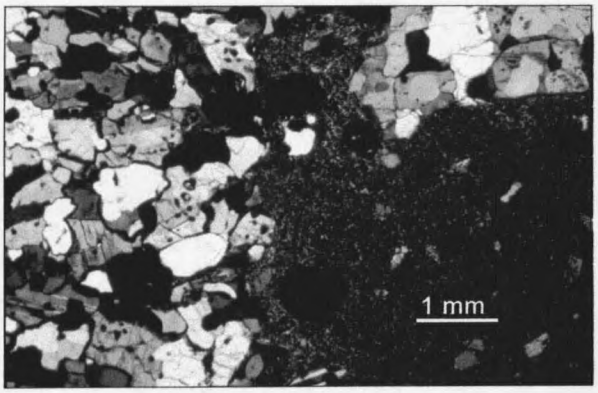


Figure 31. Photomicrograph of granitoid xenolith (left and upper right) in Ridge Wall lava (SP98-43X). Crossed polars.

Ridge Wall (RW) Interpretation

The Ridge Wall complex probably began as a fissure eruption that localized to four points to form four aligned vents erupting as Hawaiian style fire fountains. It is inferred that a high effusion rate (magma volume per unit time) with rapid rate of ascent (greater that ~1m/s), high volatile content, high temperature, and lava with very low viscosity (10-100 P) (Vergniolle and Mangan, 2000), combined to produce the lava fountains that formed the abundance of discrete, glassy clasts at Ridge Wall (Wolff and Sumner, 2000; Head and Wilson, 1989; Wood, 1980a). Eruptions from all four vents formed an elongate cone (Wood, 1980a) of variably welded, to minimally welded, to unconsolidated tephra around the periphery of the fountains (Wolff and Sumner, 2000). It is likely that molten pyroclasts from the optically dense and hot center of the fountains steadily added to the amount of fluid lava in the vents, forming lava ponds and near-vent clastogenic flows (Wolff and Sumner, 2000), which caused wholesale breaching of the entire

southeast side of the NE-SW trending cone. Lava flowed seaward from the ruined cone, rafting away large chunks of tephra now preserved as the bedded scoria deposits. At least two flow lobes were emplaced where they are now exposed in the sea cliffs. The first flow lobe and its cover of tephra was overrun by a second flow lobe and yet another layer of tephra. The presence of mantle xenoliths in Ridge Wall lava flows attests to the magma's rapid ascent from the mantle (Walker, 2000). Granitoid xenoliths were torn from the walls of the volcanic conduit and entrained in the rapidly rising magma (Wylie et al., 1999).

Hutchinson Hill (HH) and Northeast Point Description

The Hutchinson Hill eruptive center is a low shield volcano (elevation 30 m) located on Northeast Point (Fig. 32A). The interior of Hutchinson Hill is constructed of scoria and welded spatter that is mantled by sheets of clastogenic lava. The eruption that formed the summit of Hutchinson Hill deposited successive thin (< 1 m) layers of basaltic lava flows that dip gently away from the summit (Fig. 32B). Earlier deposits of oxidized scoria and welded spatter are exposed in a crater-like feature on the flank of Hutchinson Hill. Small lava tubes are exposed in the bottom of this cavity.

Surrounding Hutchinson Hill is a low-lying shield of lava flows, basalt boulders, hard-packed sediments, and unconsolidated sand. Southwest of Hutchinson Hill, along the coast, curiously contorted and indurated sandy sediments are packed into interstices between blocks and boulders of basalt. Northeast Point is the largest seal rookery on St.

Paul Island. Elliott (1881) estimated the number of seals on Northeast Point at 750,000 when he first visited St. Paul.



Figure 32. Hutchinson Hill located on Northeast Point. A. Silhouette of Hutchinson Hill showing its low shield form. View is from the north coast. B. Thin clastogenic lava flow lobes on summit of Hutchinson Hill. Length of hammer is 0.6 m.

Hutchinson Hill basalt is evolved (7.54 wt% MgO), plagioclase-rich (SP98-04 has 22 modal %), and contains both equant phenocrysts and laths of plagioclase. Olivine and clinopyroxene phenocrysts, occurring in smaller modal percentages (7 and 3 respectively), are euhedral to anhedral and generally <1.5 mm in greatest diameter.

Hutchinson Hill lava is relatively crystal-rich (Table 1) with an intergranular, intersertal, sometimes trachytic texture (Fig. 33).



Figure 33. Photomicrograph of crystal-rich Hutchinson Hill basalt (SP98-04). Crossed polars.

Hutchinson Hill (HH) Interpretation

Hutchinson Hill appears to have begun as a scoria cone built by modestly explosive eruptions. As the erupting magma became depleted in volatiles and less explosive the eruption changed to a lava fountain, forming successive, thin, clastogenic lava flows that cascaded down the gentle slopes of the cone. The low-lying lava flows that surround Hutchinson Hill may have formed in two different ways: (1) from a fissure eruption prior to its localization at the Hutchinson Hill vent or (2) their source may have been the clastogenic flows formed on Hutchinson Hill.

The low aspect ratio of Hutchinson Hill and its plagioclase-rich lava indicate that its magma generally ascended relatively slowly to the surface. The slow ascent of the

magma facilitated the escape of volatiles and led to the formation of lava flows. The formation of the abundant plagioclase phenocrysts may be related to shallow, low-pressure crystallization during the slow rise of the magma. The evolved nature of the lava and relatively small size of olivine phenocrysts suggests that fractionation of large olivine phenocrysts may also have occurred. The location of Hutchinson Hill may be responsible for the slower rise of magma at this site; differential stress may be smaller at its location off-axis of the main E-W trend of the central highland.

The hole in the side of Hutchinson Hill may be an explosion crater or, alternatively, a man-made excavation that exposed lava tubes the within it. The presence of lava tubes and scoria suggests that the eruption at Hutchinson Hill was alternately effusive and explosive in the early stages of the eruption. The contorted sediments south and west of Hutchinson Hill may have a novel geomorphic agent—that of millions of seals over thousands of years packing sediments into the interstices between the rocks.

Airport Lava Field (ALF) Description

The Airport lava field (ALF) is comprised of a group of small eruptive centers with similar geochemistry and petrography. ALF vents are located in and adjacent to the Bogoslof Hill lava flows (BHVC). However, their higher MgO contents distinguishes them from Bogoslof lavas, which are lower and more restricted in MgO. ALF lavas are chiefly surface- and tube-fed coalescing flows. Low scoria mounds with discontinuous covers of welded spatter surround the source vents.

ALF lavas are moderately evolved (MgO wt% 8.23 (SP98-31) to 8.05 (SP98-75) basanites with intersertal to intergranular textures. They are plagioclase-rich (up to 26 modal %), containing both laths and zoned equant phenocrysts. A common feature of ALF lavas is their large plagioclase laths, some greater than 5 mm in length. Olivine and clinopyroxene phenocryst range up to 3 mm in diameter. ALF lavas are similar to Hutchinson Hill lavas not only in composition and modal phenocryst assemblages (Table 1), but also in eruptive style in that lavas from both units are only mildly explosive, building low volcanic edifices.

Airport Lava Field (ALF) Interpretation

ALF lavas appear to have been only slightly more explosive than the Hutchinson Hill lava. The low spatter/cinder cones and lava flows of the Airport lava field, with their high plagioclase contents, are also interpreted to have formed from slowly rising, shallow crystallizing, relatively degassed magmas. The relatively slow rise of ALF magma, rather than being related to their off-axis location like Hutchinson Hill, may be related to the ALF's stratigraphically young age and proximity of its vents to Bogoslof Hill and the E-W trending central highland. In this spatial and temporal location, the slower rise of ALF magmas may be a result of the combination of a longer lived magma supply with a higher magma supply rate, resulting in the formation of magma chambers (Takada, 1999 and 1994b) in the proximity of Bogoslof Hill, where stalling of magma occurs.

Cone Hill Volcanic Complex (CHVC) Description

The Cone Hill volcanic complex on western St. Paul Island is composed of numerous lava flows surrounding a slightly curved zone of volcanic vents and related features. Cinder cones, lava tubes, spatter cones, calderas, pit craters, feeder dikes, and fissures are exposed and aligned along a NNE trending ridge that culminates at Cone Hill proper, for which the complex is named. Cone Hill, at 168 m (551 ft), is the third highest point on the island following Rush Hill and Bogoslof Hill. Included in the Cone Hill complex is an enigmatic lava dome adjacent to Cone Hill on the east.

Locations along with brief descriptions of the main features of the Cone Hill complex are presented in Plate 2. Two important points not evident in Plate 2 are: (1) the strong petrographic and compositional similarities between the Cone Hill caldera lava (SP98-56) and lava forming the carapace of the dome adjoining Cone Hill on the east (SP98-46); and (2) beginning at the southwest end of the Cone Hill ridge, in the vicinity of the lake-filled caldera, the ridge surface is smoother and more vegetated than the northeast end of the ridge where lava surfaces are much better exposed. The caldera lake (Plate 2E and Fig. 34) on southwestern Cone Hill ridge is locally referred to as "Kittiwake Lake" because of the great numbers of red- and black-legged kittiwakes that come to the lake to collect nesting materials.

Another feature of the Cone Hill volcanic complex that requires further description and illustration is the fissure (Plate 2, F, G, and I) and some features that lie along its trend. The Cone Hill volcanic complex fissure that connects several eruptive vents along the Cone Hill ridge is a few meters wide and partially filled with lava boulders (Fig. 35).

Southwest of the main Cone Hill caldera the fissure is inferred to be covered by clastogenic lava erupted from the caldera vent. Directly down-ridge from the Kittiwake Lake spatter cone is an exposure of what is interpreted to be a feeder dike at the ridge center (Plate 2C; Fig. 36, A and B). The width of this dike is similar to dikes in Hawaii that are also about 1 m wide (Walker, 1987). Other, less obvious exposures of similar feeder dikes are located in small craters along the trend of the fissure. Two areas of roof collapse over a lava tube are located on the northwest flank of the low cinder cone at the southeast end of the Cone Hill ridge. The photograph in Figure 37 shows the scale of the tube collapse feature.

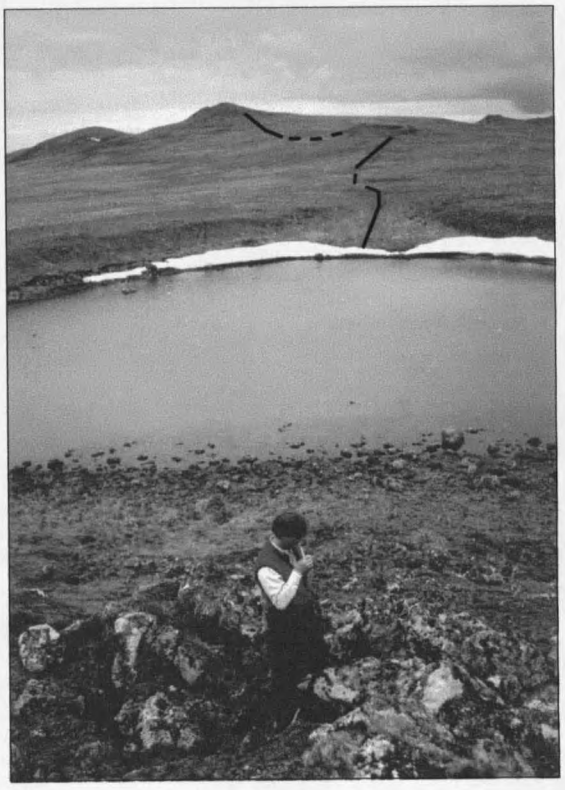


Figure 34. View from Kittiwake Lake caldera looking northeast along the Cone Hill ridge. Fissure location is shown by black line. Note change in trend of fissure at small spatter cone. Geologist T. Feeley in foreground.

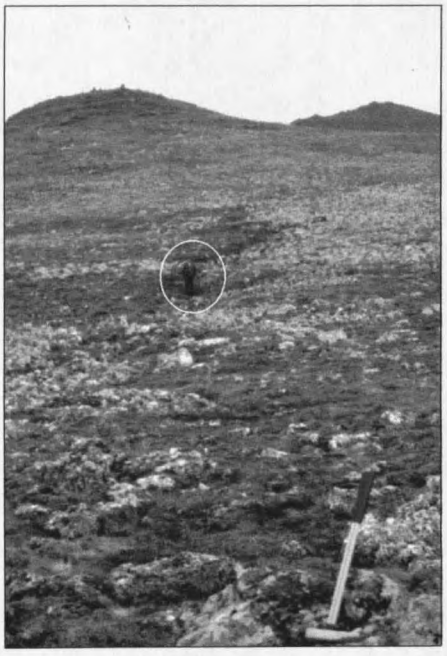


Figure. 35. Fissure on Cone Hill ridge. Hammer in foreground and figure in white circle (center) for scale. Spatter cone on left horizon is described in Plate 2H. Cone Hill on right in background.

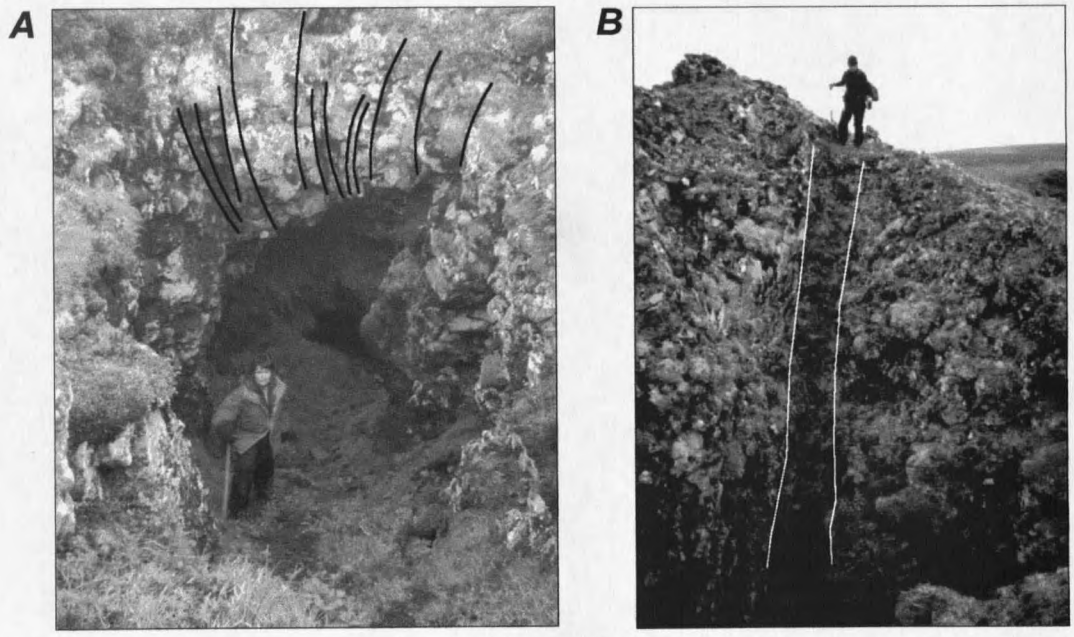


Figure 36. Exposures of feeder dike in Cone Hill ridge. A. Opening along fissure exposes feeder dike (top) with vertical jointing. Black lines are added to better show position of joints. B. Feeder dike (outlined in white) is about 1 m wide in this vertical exposure. See location on Plate 2C.



Figure 37. Collapsed lava tube on southwestern Cone Hill ridge. Collapse in mid-distance is about 20 m wide and 20 m deep. Hill 255 is on the distant horizon. See Plate 2B for location and further description.

Lavas of the Cone Hill volcanic complex range from trachybasalts to tephrites. All samples of CHVC lavas contain distinctive aggregates of plagioclase (Fig. 38A). Plagioclase glomerocrysts composed of tightly clustered, stubby plagioclase laths (<1 mm in length) often form discrete clusters 1 to 1.5 mm in diameter, that are set in glassy to fine-grained intersertal to intergranular groundmasses. The least evolved CHVC lavas (SP98-46 and SP98-56) contain 7 to 10 modal percent clinopyroxene, often in large glomerocrysts (5 mm in diameter) that are sometimes cored by olivine phenocrysts (Fig. 38B); as in other St. Paul lavas the clinopyroxene is a titanium-rich augite (titanaugite) that appears brown to brownish-mauve in thin section in plane-polarized light. These samples also contain large (≤6 mm in diameter), often euhedral olivine phenocrysts (7 to 10 modal %). With decreasing MgO values in CHVC lavas, modal olivine and clinopyroxene also decrease (<6 and <3 modal % respectively) (Table 1). Cone Hill

lavas are, as a group, the second most evolved (7.56 to 6.40 wt% MgO) lavas (after Bogoslof lavas) on St. Paul Island.

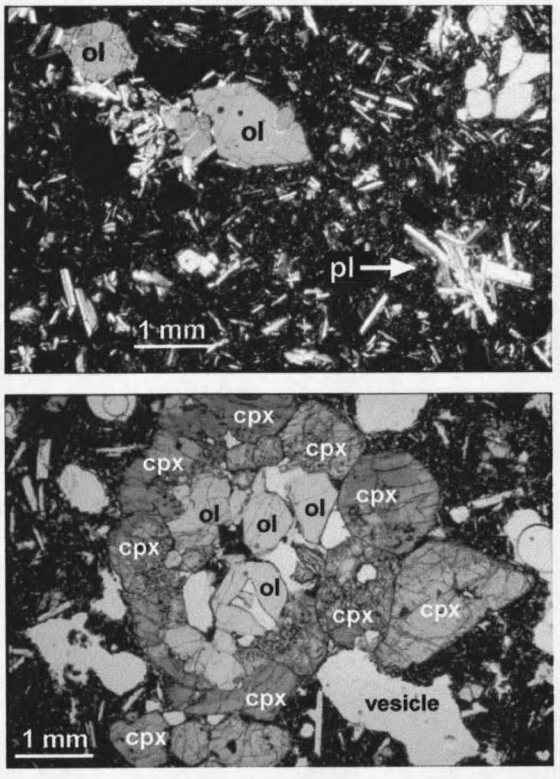


Figure 38. Photomicrograph of glomeroporphyritic CHVC lavas. A. All CHVC lavas contain distinctive small glomerocrysts of plagioclase as seen in lower right. B. Clinopyroxene glomerocrysts are also common in CHVC lavas. This one is cored with olivine.

Cone Hill Volcanic Complex (CHVC) Interpretation

The Cone Hill volcanic complex is interpreted as a compositionally evolved polygenetic eruptive center with numerous aligned vents that appear to have been active at different intervals over an extended period of time. The diverse display of volcanic structures along the Cone Hill ridge (Plate 2, A to M) suggests that they were formed by a

variety of volcanic processes. Eruptive activity likely began with a curtain of fire erupting along a magma-filled fissure and soon localized to one or several points along the fissure. Explosive tephra-forming eruptions were followed by, and perhaps even accompanied by, effusive outpourings of lava that flowed to both sides of the fissure as pahoehoe. Vents were established with conduits that would be reused in the future, especially toward the northeastern section of the fissure where Cone Hill proper is the site of a caldera. During periods of sustained effusion of low viscosity lava, lava tubes along the Cone Hill ridge fed growing pahoehoe fields. Some of these tubes are now exposed by roof collapse (Plate 2B; Fig. 37).

The two largest calderas along the ridge are located (1) just below and partially encircled by Cone Hill proper (Plate 2J) and (2) at Kittiwake Lake (Plate 2E and Fig. 34), adjacent to the remnants of a faulted and dissected spatter cone. It appears that the cones adjacent to the calderas were built initially of scoria and spatter, followed by agglutinated and clastogenic lavas. It is inferred that as these calderas formed, probably by roof collapse, sections of the cones foundered and collapsed into the calderas. At the Cone Hill caldera, clastogenic lava flows covered the top of the ridge and flowed down the northwest to the break-in-slope.

The Cone Hill volcanic complex is structurally highest at Cone Hill proper, where repeated eruptions from the same vent, or vents, built the largest edifice of the complex, while flank eruptions formed minor edifices along strike of the Cone Hill fissure. The smoothed and well vegetated area around and down-ridge from the Kittiwake Lake caldera suggests that this is an older area of the vent complex where, over time, eolian

sediments have settled into the interstices in the scoria and between the lava boulders and now support the vegetation. The accumulation of sediments in the caldera at Kittiwake Lake may also be responsible for sealing the caldera floor and allowing accumulation of water. Because of the cover of vegetation, any lava flowing from the Kittiwake Lake caldera is not as evident as that at the inferred younger Cone Hill caldera.

The cinder cone adjacent to Cone Hill proper (Plate 2L) is the older of the two features because clastogenic lava erupted from Cone Hill spills over a solidified lava lake contained in the older cone. It appears as if this lava lake formed within a formerly higher standing crater, and that lava from this lake spilled over its crater rim, eroding it on three sides and leaving turret-like ramparts on the northwest and eastern side sides of the cone. The flat surface in the central area of the cone suggests that the lava lake did not drain back into its conduit, but cooled in situ.

In Figure 36A, the area in the center of the photograph is believed to be the surface exposure of a vertical feeder dike. This interpretation is based on the closely spaced vertical jointing and the more extensive exposure of the same feature in a wall adjoining this opening (Fig. 36B).

The low dome of lava that abuts Cone Hill on its east side (Plate 2M) is of uncertain origin. The dome is underlain by olivine-rich welded spatter (SP98-45), exposed on the southern portion of the dome, that is petrographically distinct from Cone Hill lavas. One possibility for the formation of the dome is that the underlying structure initially formed as an unrelated, relatively low-lying, structurally strong, olivine-rich tephra cone (SP98-45), and subsequently filled with a clinopyroxene-rich lava from a separate source.

Because the clinopyroxene-rich lavas in the dome carapace (SP98-46) are indistinguishable from lavas at the Cone Hill caldera (SP98-56), these units probably have the same source. Given this evidence, the following mechanism (Geist et al., 1999) is proposed for formation of the dome (Fig. 39). During an eruption at the Cone Hill caldera, stress effects near the Earth's surface caused a magma-filled crack (a dike) to break out of the main northwest trending Cone Hill feeder dike, or possibly the magma chamber, at shallow depths. The break-out then propagated along a more energy-efficient E-W pathway that, by chance, erupted Cone Hill lava within the crater of a pre-existing olivine-rich monogenetic cone. An effusive eruption of Cone Hill lava then filled the crater of the older structure and overtopped it, spilling lava down the sides. Because the original structure was an extinct monogenetic cone, there was no magma mingling or mixing involved during filling. This method for the intrusion of magma from one volcano into an adjacent volcano by lateral dike propagation has recently been described in Galápagos volcanoes by Geist et al. (1999). In another study, lateral transport of magma occurred at the Katmai volcanic cluster during the great eruption of 1912 (Hildreth and Fierstein, 2000). Here, juvenile ejecta from Novarupta is presumed to have been withdrawn from a reservoir beneath Mount Katmai and transported by an unknown subterranean route to the Novarupta vent (Curtis, 1968; Hildreth and Fierstein, 2000). An alternative and more simple interpretation of the CHVC lava dome would be that lava spilled over from Cone Hill and filled the pre-existing crater. However, a topographically low area that separates Cone Hill from the dome negates this

interpretation. Phreatic explosions likely formed the small craters on the north end of the cone.

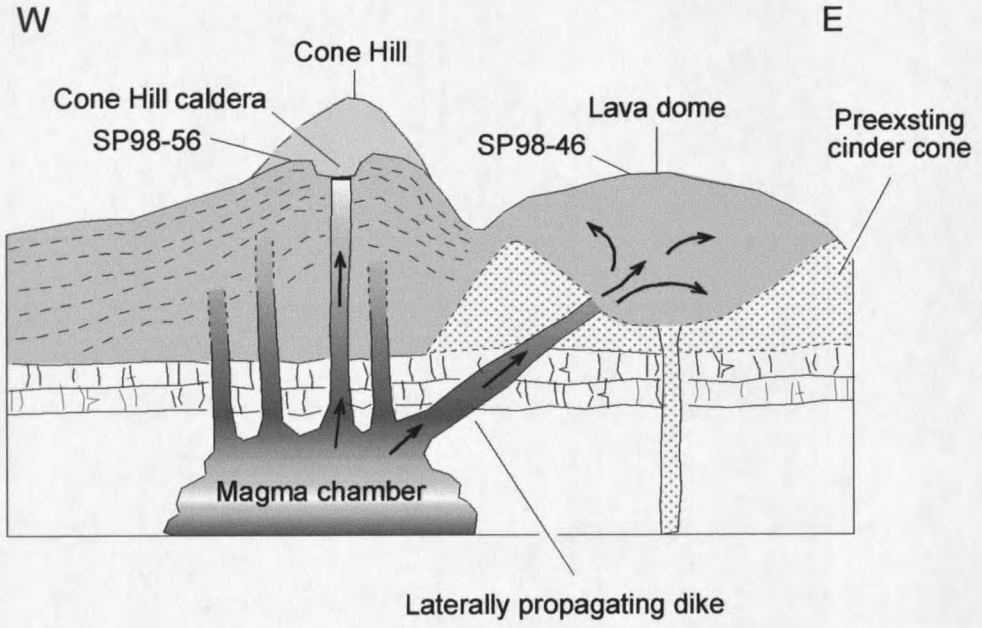


Figure 39. Proposed mechanism for formation of lava dome in Cone Hill volcanic complex. In this schematic diagram, a laterally propagating dike carries Cone Hill magma to the crater of a pre-existing cinder/spatter cone (Plate 2M) that is unrelated to the Cone Hill magmas. Lava samples from the rim of the Cone Hill caldera (SP98-56) and the lava dome (SP98-46) are compositionally and petrographically indistinguishable. Diagram is vertically exaggerated. Adapted from Geist et al. (1999).

The various volcanic features of the Cone Hill volcanic complex suggest that this is a polygenetic volcano with a relatively long-lived magma source of sufficient volume to supply the repeated eruptions that have occurred here (Walker, 2000). Beneath Cone Hill it is possible that the coalescence of fluid filled cracks (Takada, 1994a) at the level of neutral buoyancy has formed one or several shallow crustal magma chambers (Takada, 1994a, 1994b; Nakamura, 1999). Degassing of the magma at shallow levels may be

responsible for the less explosive eruptions that built spatter cones and formed clastogenic and effusive eruptions that fed the pahoehoe flows surrounding the Cone Hill ridge. The exposure of feeder dikes and pit craters and the development of fissures and faults along the ridge are evidence of extension that accompanied and post-dates eruptions along the Cone Hill ridge.

Bogoslof Hill Volcanic Complex (BHVC) Description

Bogoslof Hill is located at the center of St. Paul Island and its northwest summit is the second highest point (180 m or 590 ft) on the island. Constructed mostly of pahoehoe lava flows with small amounts of intercalated scoria, the Bogoslof Hill shield volcano has a double summit of two cone-shaped vents (Fig. 40). Bogoslof Hill's gently sloping



Figure 40. Profile of Bogoslof Hill as seen from Lake Hill. The high northwest cone is on the right. Note the broad shield shape that steepens at the summit cones.

flanks (<8°) steepen abruptly to 30° on the summit cones, which are formed mostly of spatter with minor amounts of scoria. At the northwest vent is a truncated cone of spatter

(Fig. 41A) and layered agglutinate with a shallow crater that is mostly surrounded by a rim of agglutinated spatter (Fig. 41B). A lava lake, ponded in the crater, has partially drained through a breach in the north crater rim. The southeast cone is composed mainly of spatter and agglutinate and has no developed crater. The northwest and southeast

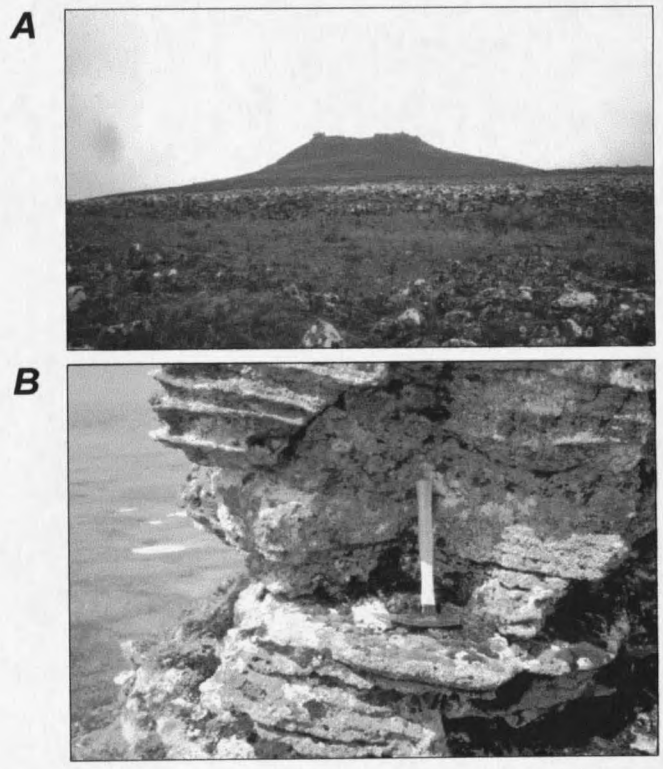


Figure 41. Northwest cone on Bogoslof Hill. A. Slope of Bogoslof Hill steepens sharply at the northwest spatter cone summit. B. Jagged crater rim of spatter cone is constructed of agglutinate composed of large flattened and welded pyroclasts.

cones are surrounded by flows of lava. In the saddle between the cone-shaped vents is a crater that is approximately 30 m in diameter, with a low spatter rampart around its rim; a small ejecta blanket of scoria overlies a lava flow on the north side of the crater rim. The depth of this crater could not be determined as it was filled with snow at the time field

work was done. Minor vents and openings to lava tubes are located on the flanks of the volcano. Bogoslof Hill is elongate to the east and west and a pronounced tongue of lava extends eastward from it toward Lake Hill. This flow tongue has an area on its eastern and southern border that has a smoothed and more vegetated surface than the major portion of the tongue; a small amount of tephra is located in this area. Extensive east-west fissuring occurs across Bogoslof Hill.

A set of subparallel and en echelon fissures extends westward from the terminus of the east-flowing lava tongue, through the Bogoslof saddle (Fig. 42). These fissures diverge to pass north and south around the southeast cone (Plate 1) and continue westward across the Bogoslof Hill edifice, striking toward Slope Hill. The surface expressions of fissures on the lava tongue are 3 to 5 m wide and are offset, down to the south, by approximately 1 m. Although partially obscured by the lava boulders that nearly fill them, the fissures on the lava tongue are estimated to be open to a depth of at least 7 m; this determined by dropping rocks down through cracks and estimating how far they fell. Portions of the fissures are buried by young lava flows in the immediate vicinity of southeast cone. The trend of the fissures extends westward through the southern part of Slope Hill and also eastward beyond the lava tongue, extending toward Lake Hill as a small graben (Plate 1).

A normal fault, parallel to the fissures and faults described above (Plate 1) defines the straight southern edge of the lava tongue. The western part of this fault is covered by lava that appears to have issued from the southeast cone. This fault cuts a small wedge of

lava from the southeast extremity of the tongue where it intersects a northeast trending fault that defines the border of an adjacent part of the tongue.

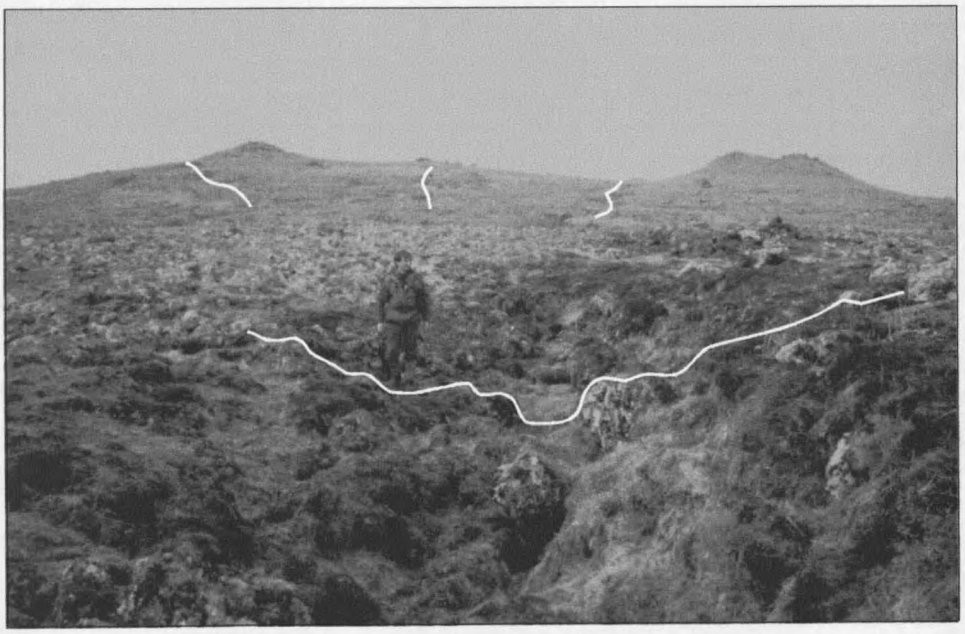


Figure 42. Fissure in lava tongue on the east flank of Bogoslof Hill strikes E-W across Bogoslof summit. Fissure is several meters wide and nearly filled by loose boulders. White lines show fissure profile in foreground and fissure traces on Bogoslof summit.

Openings to several lava tubes are located on the slopes of Bogoslof Hill. Access to the largest tube is located just south of the northwest crater and in line with a fissure that extends to the west of the southeast cone. People who have explored this tube describe it as being "many meters" wide and high (R.M. Sherwood and A.J. Stepetin, 2000, personal commun.) and several hundred feet long (Robinson, 1982). The presence of snow in craters and tube openings prevented exploration of tubes when field work was done.

The most aerially extensive of all recent lava flows on St. Paul Island extends in every direction from Bogoslof Hill and covers approximately 16 km^2 of central St. Paul

Island from Lake Hill to the Cone Hill complex. The flow completely surrounds Slope Hill and partially surrounds Hill 404 and Crater Hill to the northwest. It approaches English Bay to the south. The estimated average thickness of the flow is about 4 m and the flow volume about 0.1 km^3. This large flow was dubbed the "chunky flow" during field studies because of distinctive features on the flow surface that are peculiar to this flow. It is characterized by the random, yet ubiquitous, distribution of "chunks" or blocky jointed formations of lava on the flow surface, occurring particularly on shallow slopes. These formations range in size from 3 to 20 meters in diameter and 4 to 10 m in height. They rise abruptly from the flow surface and some have columnar jointing and central clefts. The lava that forms them appears in hand sample similar to that on other surfaces of the flow: grey, crystal-poor basalt with sparse olivine (<3 modal %) and small plagioclase crystals. In thin section, however, the lava (SP98-47) has >13 modal % clinopyroxene glomerocrysts, but these are generally less than 1 mm in diameter and, therefore, are not obvious in hand sample.

The lava flows near Bogoslof Hill are characterized by patchiness defined by regions of plagioclase-rich lava next to regions of more plagioclase-poor lava, distributed in a random manner. The scale of these regions ranges from centimeters to tens of meters. For example, plagioclase-rich and plagioclase-poor domains may be found in hand-sample sized pieces of lava from the southeast cone. On the larger scale, on the south flank of Bogoslof hill, patches of plagioclase-rich and plagioclase-poor lava appear to be scattered in a random fashion. In the hand-sample example (SP98-27), spatter from Bogoslof's southeast cone is composed of two distinct types of lava; a dense (degassed),

plagioclase-rich lava forms part of the sample and welded to this is a vesicular (volatile-rich), plagioclase-poor lava.

Varying textures of Bogoslof lavas are shown in Figure 43, A to C. Geochemically, Bogoslof lavas (excepting the extremely rare trachyte from Polovina Hill) are the most evolved of all rocks sampled in this study. Bogoslof lavas range from trachybasalt

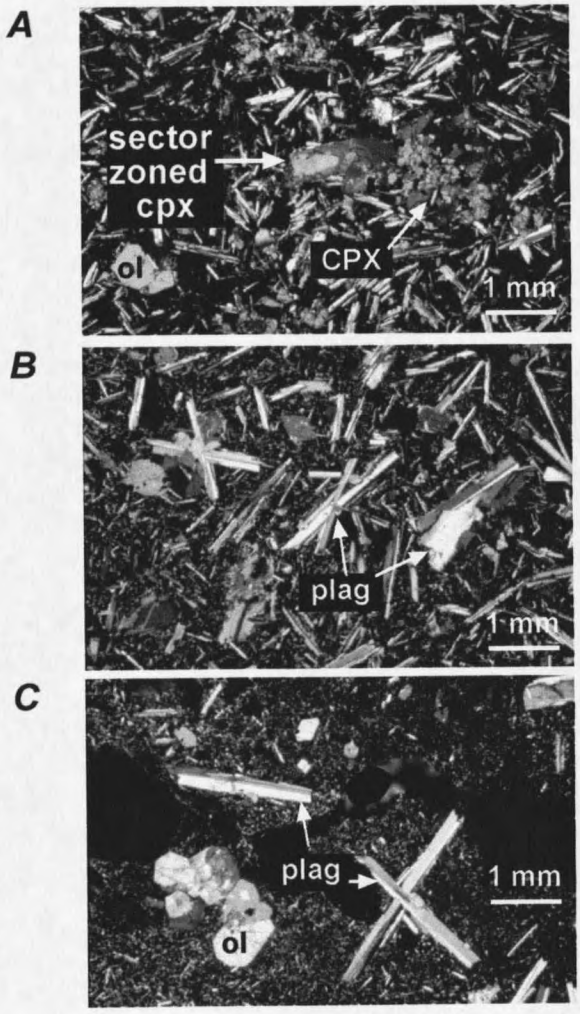


Figure 43. Photomicrographs of BHVC lavas. A. High clinopyroxene content in the largest BHVC lava flow (SP98-47) is related to presence of numerous clinopyroxene glomerocrysts (right center). Sector zoning in clinopyroxene phenocrysts (center) is common. B. and C. Varying percentages of modal plagioclase content in the youngest Bogoslof lavas are illustrated in B (SP98-26) and C (SP98-27). Darkest areas in C are vesicles.

(SP98-47) to tephrites (SP98-73, SP98-26, SP98-72, SP98-27), becoming more evolved up section, decreasing in MgO (from 6.01 to 4.25 wt%) and increasing in K_2O (from 1.63 to 2.22 wt%) toward the top of the pile. Lee Wong et al. (1979) noted that Bogoslof lavas are well defined by their low MgO values. Bogoslof lavas are also lowest in olivine content (5 to 2 modal %) with small olivine phenocrysts (<1 mm in diameter) tending to occur in clusters. Varying modal contents of plagioclase (30 to 9%) may be explained by the patchy occurrence of plagioclase, described above and interpreted below.

Bogoslof Hill Volcanic Complex (BHVC) Interpretation

Eruptions that formed the Bogoslof Hill shield volcano probably began with basaltic lava erupting along an east-west trending fissure. Evidence for this interpretation is in the E-W elongation of Bogoslof Hill and the presence of E-W trending fissures that traverse the Bogoslof volcanic edifice. The eruption localized at the site where the fissure appears to intersect with a northeast-trending fault, and there formed the nucleus of Bogoslof Hill (Plate 1). Three main eruptive vents were established at (1) the northwest crater, (2) the southeast spatter cone, and (3) the centrally located saddle crater. Flows of lavas erupted, possibly randomly, from the three summit vents. Over time, repeated eruptions of low viscosity lavas and minor amounts of tephra formed the gentle slopes of Bogoslof Hill. During eruptions, advancing fronts of pahoehoe were emplaced over previous Bogoslof flows as well as over flows associated with nearby cinder cones and even over the lower flanks of these cinder cones.

Large lava tubes developed on the steeper slopes of Bogoslof Hill, directing the flowing lava to a complex network of smaller tubes feeding the flow-fields on the gentle gradients surrounding the main edifice (Calvari and Pinkerton, 1999; Peterson, 1994). Evidence for the tube system is seen in the numerous tube openings exposed on the flanks of Bogoslof Hill. From the presence of lava tubes and pahoehoe flow fields in the BHVC, it can be inferred that effusion rates of Bogoslof eruptions were less than 5-10 m^3/s [at higher effusion rates (>5-10 m^3/s), aa flows form] (Rowland and Walker, 1990).

Fissuring across Bogoslof Hill continued through the late stages of construction of the edifice. The most recent of the lava flows erupted from the southeast cone have covered the fissures that diverge to pass around the base of the cone. They have also partially covered the normal fault that defines the southern edge of the lava tongue on the eastern side of Bogoslof Hill and offsets Slope Hill to the west.

Slope angles on shield volcanoes are increased by addition of lava chiefly to shield flanks, whereas the growth of surrounding lava fields through tube systems does not appreciably change slope angles (Peterson et al., 1994). Bogoslof Hill's greater steepness at its northwest and southeast summits is probably related to the construction of summit cones composed of spatter, agglutinate, and clastogenic lavas with high angles of repose. These deposits may be the result of a decreasing effusion rate and spatter formation following the initial higher effusion rate of more fluid lava (Kuntz et al., 1982).

Distinctive field aspects of the Bogoslof lava flows are the "chunky" formations and the "patchiness" of lavas. Based on literature reports, the chunky outcrops are similar to formations described as tumuli, lava rises, and pop-ups, all associated with tube fed flows

(Greeley and Hyde, 1972; Walker, 1991; Yilmaz et al., 1998). The chunky formations are interpreted as sections of uplifted lava flow crust that, before uplift, cooled sufficiently to form columnar joints. The lava rises or pop-ups, the perimeters of which are defined by columnar joints, appear to have been uplifted by a piston-like action where injection of lava through lava tubes beneath an already rigid crust was causing increased hydrostatic pressure (Walker, 1991; Hon et al., 1994; Calvari and Pinkerton, 1999).

Patchy lavas are interpreted to be the result of mixing, in a subvolcanic magma chamber, of magmas at different stages of crystallization. In this scenario, magma ascends to high levels, degasses, cools, and crystallizes acicular plagioclase. This is rapidly followed by the ascent of another batch of compositionally similar, but volatile-rich and less crystallized, magma that triggers an eruption. Evidence for mingling of magmas at different stages of crystallization is located at Bogoslof's southeast crater summit where "patchy" lava occurs on a small scale (i.e., the same hand sample described above). Patchiness in lavas on the larger scale could possibly be explained by breakouts or ephemeral vent formation whereby tube-fed flows are emplaced in a random manner in previously deposited flows. This may be accomplished by exploitation of tubes from previous flows by later erupted lavas, and their emplacement in a chaotic fashion within existing pahoehoe flow fields (Peterson et al., 1994; Calvari and Pinkerton, 1999).

The compositional evolution of Bogoslof lavas is interpreted as being related to the development of a shallow crustal magma chamber beneath the volcano. Coalescence of magma-filled cracks is the mechanism, as described by Takada (1994a and 1994b), for

magma chamber formation beneath polygenetic volcanoes, such as Bogoslof Hill, in regions of crustal extension. Crystal-liquid fractionation of olivine in the proposed shallow crustal magma chamber beneath Bogoslof Hill would account for the progressive eruption of more evolved lavas (Wilson, 1993). The increase in alkali content over time is predicted by Moll-Stalcup (1994a and 1994b), who suggests that the more alkalic lavas may be more explosive. However, eruptions of alkali-rich lavas from Bogoslof Hill have not been highly explosive, perhaps because of degassing in shallow crustal magma chambers prior to eruption.

Fox Hill (FXH) Description

The youngest eruptive center on St. Paul Island is Fox Hill, a breached cinder cone complex located on southwestern St. Paul Island. The Fox Hill lava flow issues from Fox Hill and extends for 2.5 to 3 km to the sea at Southwest Point (Fig. 44; Plate 1). A one-meter thick layer of organic carbon-bearing sediments is exposed in the coastal cliff beneath the lava flow. Sample SP98-64, collected from this site (Fig. 45), yielded an AMS C^{14} radiometric age-date of 3230 ± 40 years, confirming the suspected youthfulness (Cox et al., 1966) of the Fox Hill lava flow. The Fox Hill cone breached to the southeast, perpendicular to the NE-SW trend of its multiple aligned vents. Lava flowing from at least four separate vents coalesced to form one lava flow. Greater than half of the Fox Hill cone was removed during breaching and many chunks of fairly well consolidated scoria and welded spatter of varying sizes are found on the surface of the lava flow (Fig. 46). The height of some of these structures is as great as 4 m. Chunks of the cinder cone

are exposed along the entire length of the lava flow, to the edge of the sea cliff at Southwest Point. The lava flow surface has pronounced levees (Fig. 44) that developed along flow margins. The flow levees and the flow channel between them are easily observed just east of Southwest Point where the road crosses the eastern lobe of the lava flow.

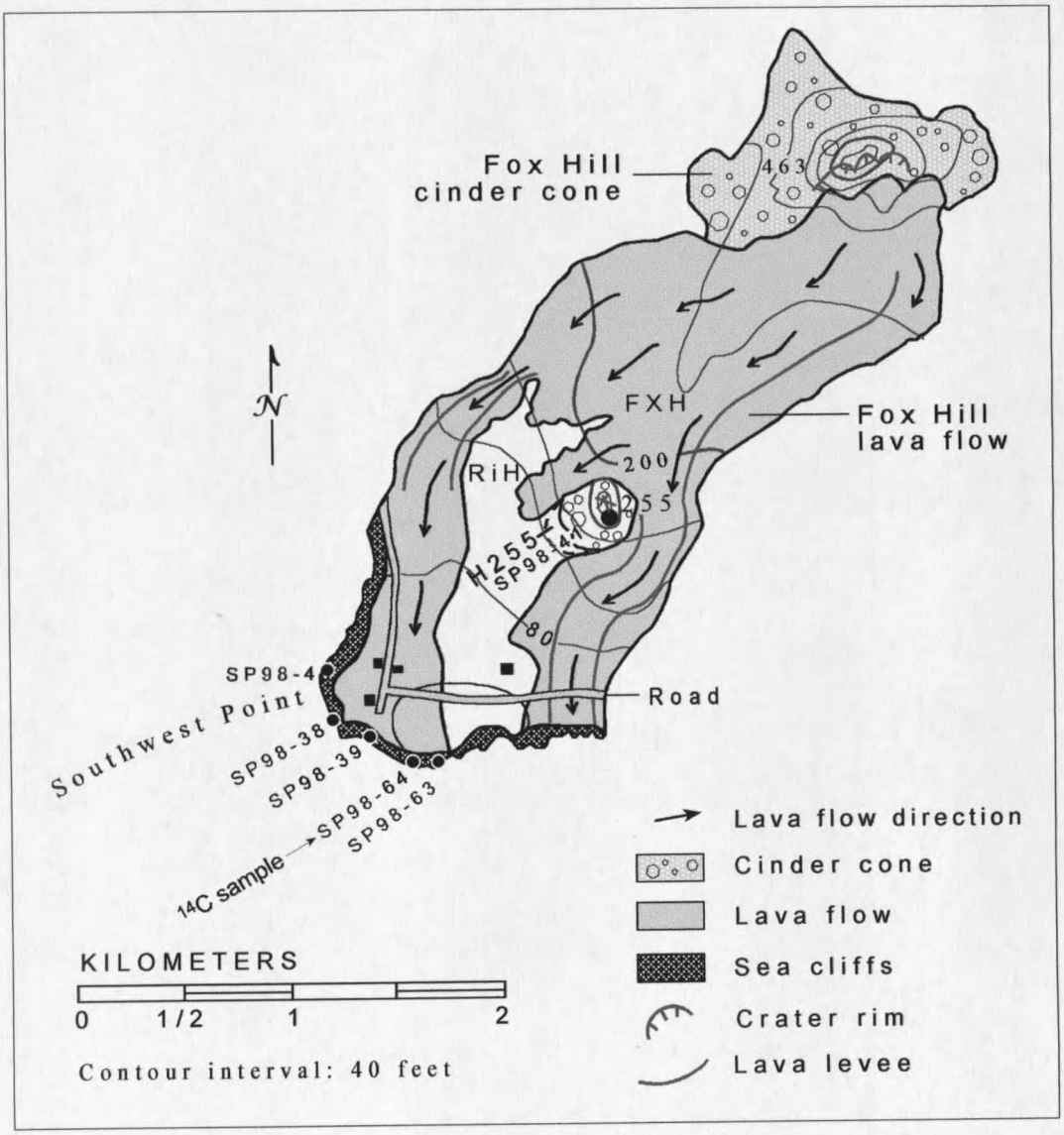


Figure 44. Fox Hill cinder cone and lava flow (FXH).

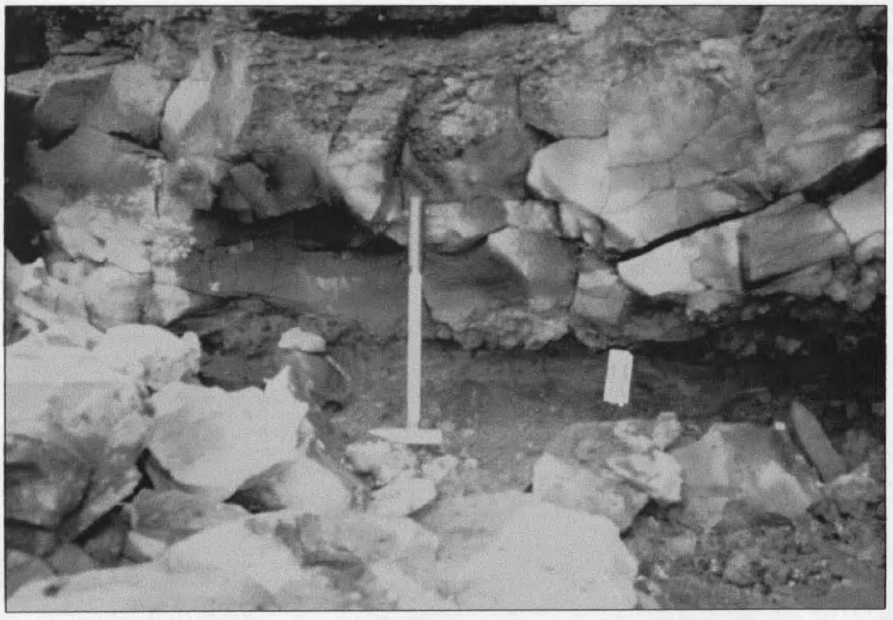


Figure 45. Sample site for ^{14}C in layer of sediment beneath Fox Hill lava flow (SP98-64).

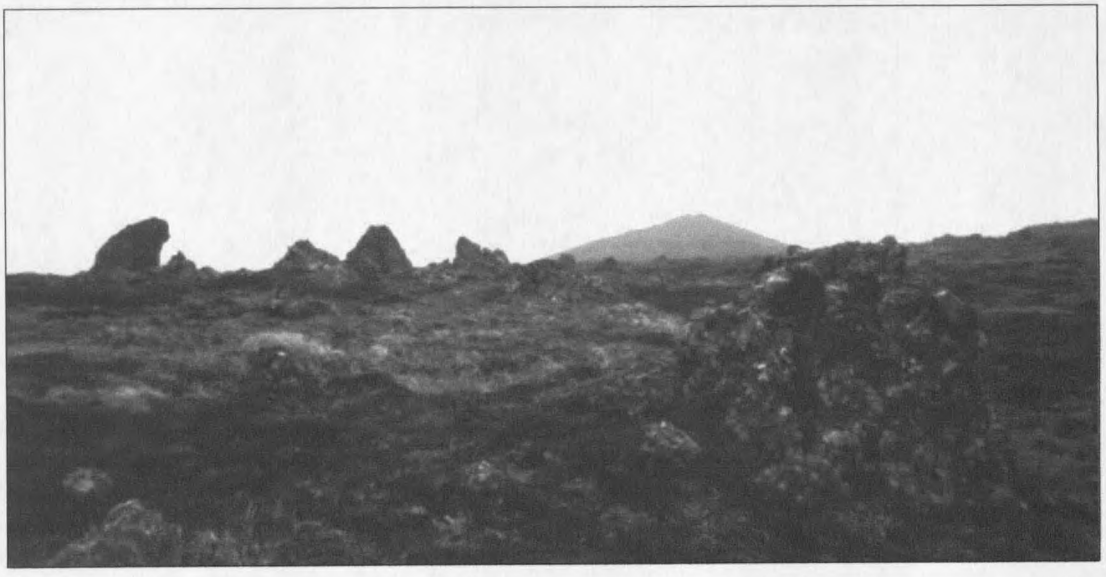


Figure 46. Segments of the breached Fox Hill cinder cone that have been rafted along on the Fox Hill lava flow. Some of these cone chunks are several meters tall. Hill 255 is in the background.

Compared with older lava flows on the island, the young Fox Hill lava flow has less eolian sediment cover and less vegetation than observed on other flows. Surface features such as levees and cone chunks are thus very well preserved. The lava flow appears to be unfaulted, although its surface, like the other lava flows on the uplands of the island, is fractured into boulder sized chunks. Linear fractures reported by Cox et al. (1966) were not observed.

The thickness of the Fox Hill lava flow at Southwest Point, where it is truncated and exposed in cross-section at the sea cliffs, is about 2.5 to 4 m (Fig. 47). The average thickness of the lava flow is estimated to be 3.25 m and its area is approximately 2 km^2. Therefore, allowing for lava that ran into the sea or eroded from the sea cliffs, the minimum estimate for the volume of the Fox Hill lava flow is 0.01 km^3. This volume is comparable to the smaller lava flows at the Craters of the Moon lava field, Idaho (Kuntz et al., 1986a).

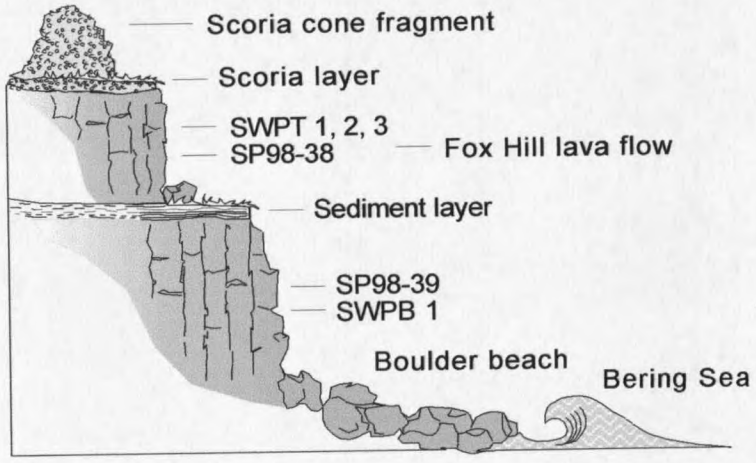


Figure 47. Fox Hill lava flow at Southwest Point. A fragment of the breached Fox Hill cinder cone rests on its lava flow at Southwest Point. The Fox Hill flow is separated from the lower flow by a 1-1.5 m layer of organic carbon bearing sediment. Height of section is about 15 m.

Four whole-rock analyses of Fox Hill lava (SWPT1, SWPT2, SWPT3, and FXH1) were performed. Compositional differences among all samples are minimal and within analytical error (Feeley and Winer, 1999) (Table 1). Fox Hill lavas are crystal-poor and evolved (7.40 to 7.20 wt% MgO) compared with most monogenetic centers. Skeletal forms of olivine phenocrysts and groundmass mixing of microlite-rich and glassy microlite-poor areas are common in Fox Hill lavas (Fig. 48). Large olivine phenocrysts in Fox Hill lavas are notably lacking. A previous study shows evidence of crystal fractionation, mainly of olivine, in Fox Hill lava (Feeley and Winer, 1999).

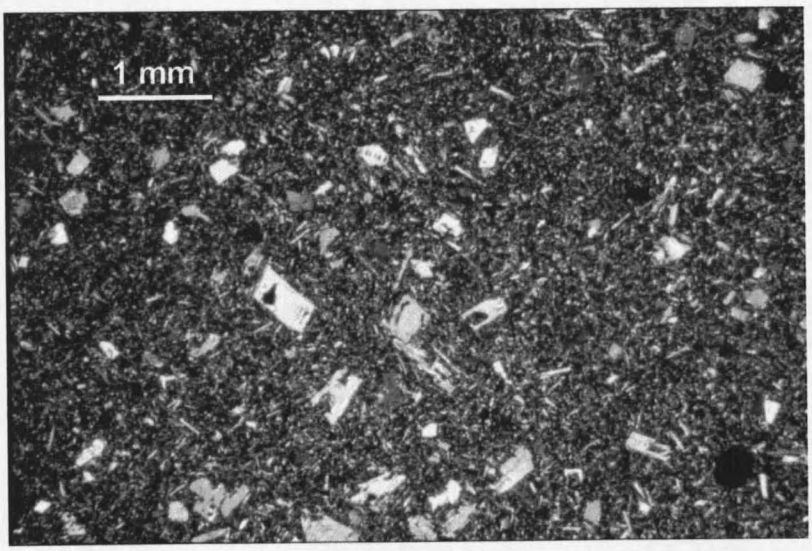


Figure 48. Photomicrograph of fractionated Fox Hill lava. Small skeletal phenocrysts of olivine are common in Fox Hill lavas.

Fox Hill (FXH) Interpretation

The Fox Hill scoria cone is interpreted to have formed during a Strombolian eruption from multiple closely spaced vents that localized along a SW-NE trending fissure. Wholesale breaching of the southeast wall of the cone probably occurred with waning of the explosive phase and establishment of the effusive phase of the eruption. Chunks of the breached cone wall were rafted away on the lava that flowed from as many as four vents. The formation of levees on the Fox Hill lava flow is related to a decrease in lava flow rate along cooling flow borders (Hulme, 1974). As described by Hulme (1974) and Rowland and Walker (1990), lava flowing next to the stagnated flow borders builds levees by the process of accretion. Velocity of the flowing lava then increases, as it is concentrated between the levees (Rowland and Walker, 1990).

The evolution of the Fox Hill eruptive center appears to be fairly similar to that for many of the other scoria cones on the island. In particular, apart from the abundance of vitric tephra, the evolution of the Fox Hill vent complex and lava flow is very similar to that at the Ridge Wall complex cone and lava flow. For example, Fox Hill and Ridge Wall are nearly the same size and they have a similar number of aligned vents located on nearly parallel NE-SW striking fissures. Also, both the Fox Hill and Ridge wall cones have undergone major breaching to the southeast, and sections of their sundered cones are preserved on their lava flows. However, the Fox Hill complex is unique because it is young and the vents are located along the central highland, as opposed to Ridge Wall, which is older and located near the coast. Because of its young age and its location, features of the Fox Hill cone and lava flow are very well preserved and allow insight into

(1) the volume of the lava flow, (2) how far breached material may be carried away from the vent, and (3) the formation of flow levees.

The compositional similarity of the four analyzed lava samples of Fox Hill lava indicates that there is minimal interflow variation and the lava is probably from a homogeneous magma. The presence of skeletal olivine phenocrysts is likely due to rapid quenching as the lava flow cooled. The crystal-poor nature and low MgO content of Fox Hill lava suggests that magma at this young eruptive center may have resided temporarily in a shallow crustal magma chamber, where it underwent crystal fractionation prior to eruption (Feeley and Winer, 1999).

Surficial Deposits (Sd) Description

All mapped sedimentary deposits on St. Paul Island are included in the Surficial deposits unit (Sd). Thin and discontinuous deposits of loess and eolian sand that partially cover lava flows and tephra deposits are not mapped. Surficial deposits are undifferentiated and include colluvium, sand dunes, sandy beaches, and sand and loess deposits thick enough to totally obscure the lava flows beneath them. Colluvium includes boulder beaches. Dune sands and beach sands (SP98-66, SP98-67, SP98-68) are medium- to coarse-grained, subangular to well rounded, well-sorted, and composed mainly of olivine and basalt. The sand is inferred to be derived from quenching and shattering of lava flowing into the sea (Moore et al., 1973) and from mechanical weathering of olivine-rich St. Paul lavas in the pounding surf. The olivine imparts a golden color to the sand when it is dry and sunlit. The extensive deposit of sand and sand

dunes located on eastern St. Paul Island in the area around Polovina Hill and Little Polovina Hill may represent more evidence for the Kotzebuan transgression on St. Paul Island. A string of dunes that follows a subtle break-in-slope, curving around the east and north sides of Polovina Hill and the south and west sides of Little Polovina Hill (Plate 1) at approximately the same elevation as Hopkins' (1967a) Kotzebuan age wave-cut notch on Tolstoi Point (see Introduction).

Faulting and Fissuring

Faults and fissures occur in various places on St. Paul Island. Faults with many meters of offset are restricted to the older platform lavas, while fissures with little if any offset cut some of the youngest lavas on the central highland (Plate 1). As noted by Cox et al. (1966) and Hopkins (1976), the density and magnitude of fault separation has a general correlation with the age of the faulted units. Offsets are the largest in the undifferentiated platform lavas (UPL) exposed in the southern promontories of Reef Point, Tolstoi Point, and Zapadni Point. For example, a fault with about 30 m offset is located at Zapadni Point. However, more common in the older lavas are extensional faults with offsets of 5 to 15 m, such as those located on Tolstoi Point and Reef Point (Plate 1; Fig. 49). Faulting in the Kaminista area is described above in the section on undifferentiated platform lavas (UPL).

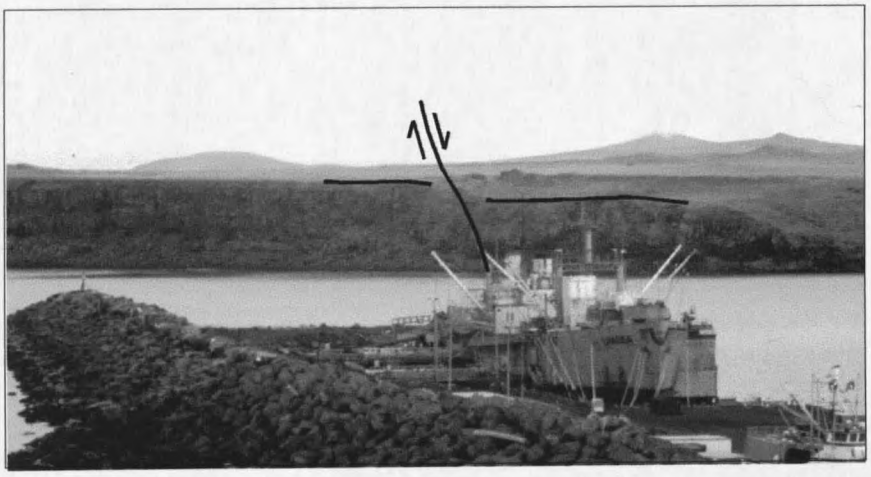


Figure 49. Faulting of platform lavas on Tolstoi Point. View from above the harbor. Lines and arrows show location of fault and sense of motion.

Located in platform lavas just NNE of Zapadni Point is an area of uplifted basalt with provocative features including a scissor fault that is easily visible from the road. The scissor fault has offset of approximately 20 m toward the southwest and tapers to the northwest, disappearing beneath lava flows from Bogoslof Hill (see Plate 1). Gaping, northwest striking extensional faults in the southwest corner of the uplifted area southwest of the scissor fault may be tension gashes on the apex of a flexural bulge, created during uplift. The faults have sharp edged, steep scarps and are as great as 30 m deep, with as much as 10 m offset. The scissor fault strikes at 043°, straight toward the center of Bogoslof Hill. Bogoslof lava appears to be broken by the continuation of this fault at a site between the scissor fault and the summit of Bogoslof Hill. The normal fault that borders the road south of the scissor fault [the road is on the downthrown block] appears to be a continuation of the Zapadni Point fault, albeit, with a different sense of offset. Interpretation of this locus of complex faulting is beyond the scope of this study.

The least displacement is in the series of linear fissures that cut relatively recent lava flows located on the central highland. Fissures that strike E-W across Bogoslof Hill and NE-SW between vents on the Cone Hill ridge have offsets of less than about 1 m. Fissures are generally a few meters wide and are partially filled with lava boulders (Fig. 50). In places the fissures are open with no evidence that they are eruptive fissures and in others, fissures are covered by lava flows that appear to post-date their formation, i.e., near the southeast summit of Bogoslof Hill and just southwest of the main Cone Hill summit caldera. The shallow emplacement of dikes may cause a fissure to form on the surface whether or not an eruption occurs along the fissure (Hughes et al., 1999)



Figure 50. Fissure on Bogoslof Hill. Southeast summit cone in background.

Volcanic and Structural Lineaments

On St. Paul Island, many volcanic vents are localized along the trend of linear fissure systems and faults and some of these trends may be extrapolated to nearby islands and shoals. A major E-W lineament extends from Walrus Island on the east, across St. Paul Island, and offshore to a shoal on the west (Fig. 51). This E-W trend is a locus of source vents for the young eruptive centers of the central highland, e.g., Bogoslof Hill, Cone Hill, and Fox Hill. Also located along the E-W trend are Lake Hill and Polovina Hill. Trending NE-SW across St. Paul is a set of nearly parallel alignments of faults, fissures, and vents. The longest of these extends NNE from Otter Island, located south of St. Paul, through the village hill, Polovina Hill, Northeast Point, and offshore to another shoal. Barth (1956) suggested that shoals in the area of St. Paul Island are of probable volcanic origin.

Vent locations on St. Paul Island appear to be controlled by faulting and fissuring. Evidence for this interpretation is seen in (1) the fissures located on Bogoslof Hill and the Cone Hill ridge, and (2) multiple aligned vents at single eruptive centers (Fig. 52). In the first case, fissures traverse the volcanic edifices of Bogoslof Hill and the Cone Hill ridge, striking toward volcanic vents. Note that these large polygenetic centers are located at intersecting trends of faults and fissures (see arrows in Fig. 52). In the second case, evidence for the localization of multiple aligned vents along an eruptive fissure is located at Fox Hill and Ridge Wall, two cinder cones in which closely spaced aligned vents have been exposed by breaching . The aligned vents at Fox Hill and Ridge Wall are roughly

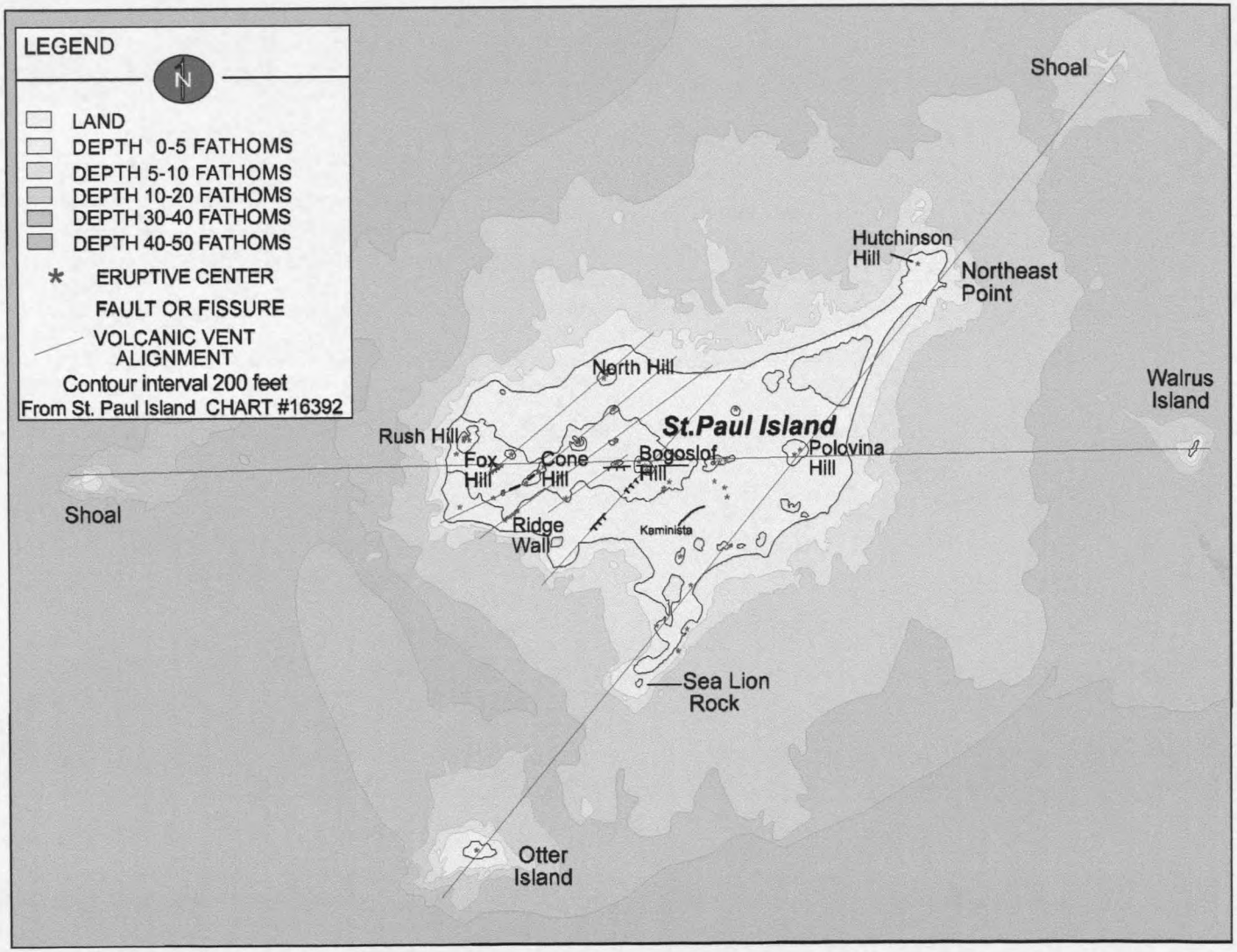


Figure 51. Volcanic and structural lineaments on St. Paul Island and surrounding area.

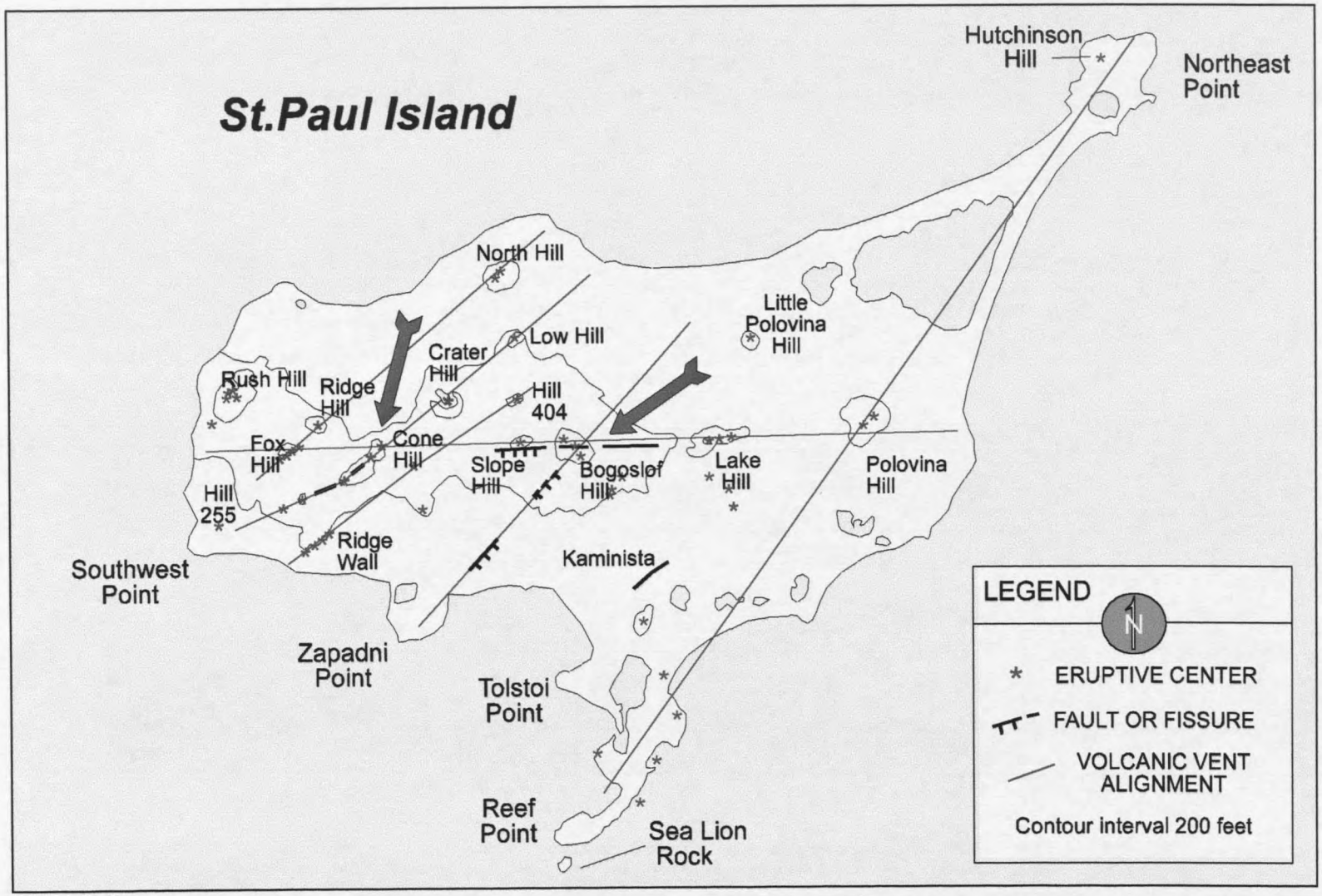


Figure 52. Lineaments of volcanic vents, fissures, and faults on St. Paul Island. Arrows indicate locations of polygenetic shield volcanoes.

parallel to each other and also to the strike of aligned fissures and vents on the Cone Hill ridge. In addition, other vents are located along strike of multiple vent alignments, for example, the location of Ridge Hill and North Hill along strike of the Fox Hill vents.

Directional trends of fissures, cone breaching, faults, and vent alignments on St. Paul Island are shown on rose diagrams in Figure 53. Data for fissures (Fig. 53A) is taken from the Bogoslof Hill and Cone Hill volcanic complexes where open fissures and exposed dikes occur, and from Fox Hill and Ridge Wall where the alignments of multiple related vents are obvious (see Plate 1 and Fig.44). Cone breaching directions are taken from breaching directions of simple cinder cones (e.g., Little Polovina Hill and Hill 404), and from complex cones where breaching of multiple crater rims has occurred (e.g., Lake Hill and North Hill). Most cone breaching directions on St. Paul Island are inferred to be parallel to strike of the magma feeding plane or fissure (Tibaldi, 1995), however, at Fox Hill and Ridge Wall, breaching has occurred perpendicular to the strike of the aligned vents (Tibaldi, 1995). This is illustrated in Figure 53B, where southwest breaching occurs at approximately 90° to the main northeast trend. Most data on faulting (Fig. 53C) is from older platform lavas exposed on the southern part of the island. The relationship of these fault trends to emplacement of younger fissures and dikes is unknown. Vent alignments (Fig. 53 D) are taken from any three or more aligned vents without regard for cone breaching directions. In vent alignments of 105° to 180°, cone breaching bears no apparent relationship to fissure trends In contrast, breaching direction and fissure trends have a noticeable correlation in the northeast quarter.

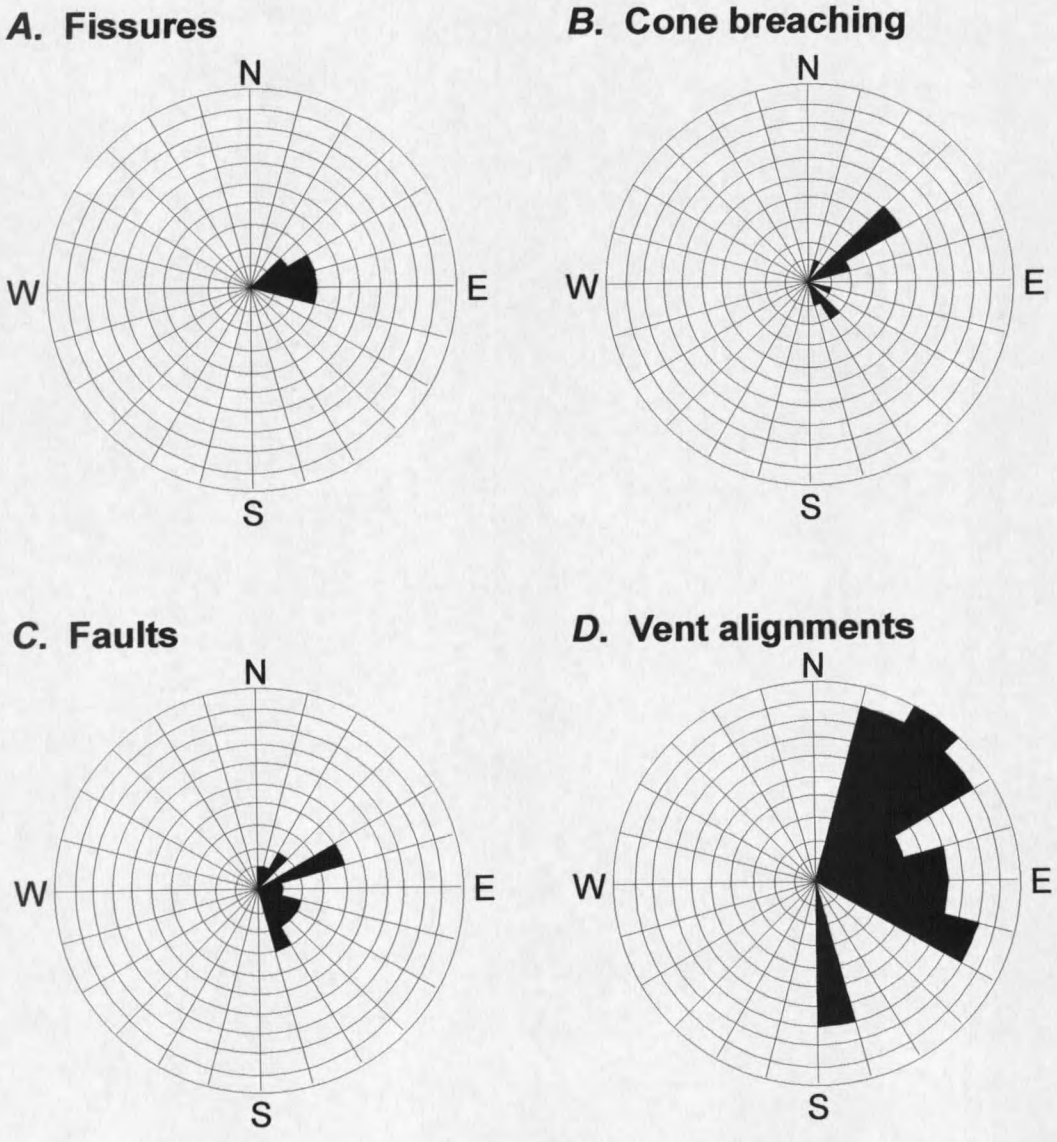


Figure 53. Rose diagrams showing directional trends of A: fissures; B: cone breaching; C: faults; and D: vent alignments.

On St. Paul Island, as in other basaltic volcanic fields [e.g., the Eastern Snake River Plain (Greeley and King, 1977; Hughes et al., 1999)], the alignment of volcanic vents is very common (Connor and Conway, 2000). Tibaldi (1995) suggests that vent alignments along the strike of faults or fissures occur most often in regions [such as St. Paul Island (Nakamura, 1977)] that are located in transtensional tectonic settings [e.g., the Transmexican Volcanic Belt (Bullard, 1984; Scarth, 1999)] where dikes are intruded under extensional stress conditions (Takada, 1999). In regions of extension, fissures or crack planes which facilitate the transport of magma tend to form perpendicular to the direction of minimum compressional stress (Takada, 1994b). At St. Paul Island, the local stress field may be too complicated to correspond most lineaments to the regional stress. However, regarding the E-W trend, Plafker et al. (1994) infer N-S extension in the Pribilof area.

Xenoliths in St. Paul Lavas

On St. Paul Island, lavas from monogenetic centers were found bearing both mantle and crustal xenoliths (see Figs. 25 and 31). [No xenoliths were found in lavas from polygenetic volcanoes.] The occurrence of ultramafic and granitoid xenoliths is related to the relatively rapid ascent velocity of alkali basalts (Rutherford and Gardner, 2000). The estimated minimum ascent velocity for alkali basalts ranges from 2 to 10 m/s (Rutherford and Gardner, 2000). Xenolith bearing magmas ascend in dikes as the lithosphere undergoes fracturing in regional tensional environments. The tensional

environment is greater for monogenetic volcanoes, where xenoliths are found, than for polygenetic volcanoes (Maaløe, 1998). The ascending magma, already carrying mantle xenoliths (e.g., the lherzolite xenolith from Crater Hill), may incorporate crustal xenoliths (e.g., the granitoid xenoliths at Crater Hill and in the Ridge Wall lava) as the magma-filled fracture propagates through the crust (Maaløe, 1998) and the shear stress exerted on the fissure walls by the rising magma causes brecciation of wall rock (Wylie et al., 1999). Xenoliths in magmas that rise rapidly from their source indicate that the magma did not pause on its way to the surface, allowing the xenoliths to settle (Walker, 2000).

The presence of the lherzolite xenolith (SP98-50 from the Crater Hill lava flow) is regarded as evidence for the asthenospheric mantle source suggested by Kay et al. (1978) for St. Paul lavas. This finding also has implications for the St. Paul magma source depth; Wilson (1996) suggests that the source for lherzolite xenoliths in alkalic basaltic magmas is likely less than 70 to 80 km. The granitoid xenoliths verify the presence of continental crust beneath the island.

SUMMARY

Volcanic Evolution of St. Paul Island

Volcanism at St. Paul Island has occurred in three distinct, though gradational, stages and distinctive volcanic landforms are associated with each stage. The stages are: (1) the early, mostly effusive eruptions that produced the platform lavas, (2) the more explosive Strombolian style eruptions that emplaced the monogenetic cinder cones and their coalescing lava shields upon the platform lavas, and (3) the more effusive and less explosive eruptions at the polygenetic shield volcanoes on the central highland. Although the styles of eruptive activity overlap both temporally and spatially, they are distinctive enough to warrant the division of volcanic activity on St. Paul Island into three separate stages: (1) the platform building stage, (2) the monogenetic cinder cone stage, and (3) the polygenetic shield stage.

Platform Building Stage

The early platform building stage began with the first subaerial eruptions at St. Paul sometime after 780 Ka (Cox et al., 1966) and at least as early as the oldest lava flows dated by Cox et al. (1966) at around 360 Ka. Based on descriptions of UPL and ULF in the chapter three, Geology of St. Paul Island, early, unevolved, olivine-rich, low viscosity lavas, with minor amounts of associated tephra, erupted through extensional fissures and

point sources to construct the relatively flat-lying, discontinuous—but coalescing, stacked lava flows that form the platform of the island (Fig. 54).



Figure 54. Platform lavas on the west coast. The cliff on the left rises about 35 m above sea level. View is looking north from Southwest Point. Rush Hill is on the horizon at right.

In the island platform, the great volumes of effusive lavas, minimal amounts of tephra, and lack of evidence for volcanic constructs of any great height, suggest that eruptions of platform lavas were similar to that at the younger Hutchinson Hill on Northeast Point. At Hutchinson Hill the volume of tephra is minimal compared with the volume of effusive or clastogenic lava. Low viscosity lava forms the thin multiple flow lobes on the gentle slopes of the hill and the nearly flat-lying flows that surround it. The compound flow units of this low monogenetic shield resemble the lower units of the platform lavas. This contrasts with the high aspect cinder cones that have much greater proportions of tephra to lava. Because of the subdued topography and compound, nearly

flat-lying lava flows with minimal amounts of tephra, it is inferred that the platform lavas are similar to the complex, coalescing pahoehoe flows and low shields of plains style volcanism on the ESRP (Greeley, 1977a; Hughes et al., 1999). A more detailed comparison of the platform lavas at St. Paul island with plains volcanism of the ESRP is located in the interpretation of undifferentiated platform lavas (UPL) in Chapter 3. Old, eroded cinder cones among the platform lavas on south central St. Paul are evidence for the gradual change from the platform building stage to the cinder cone stage of volcanism.

Monogenetic Cinder Cone Stage

The second stage in the volcanic evolution of St. Paul Island is the monogenetic cinder cone stage, during which the eruptive style changed from the mostly effusive eruptions of platform lavas to the more explosive Strombolian eruptions that formed numerous cinder cones and their associated lava flows. A few early-erupted cinder cones mingle with the platform lavas on southern St. Paul, but the majority are emplaced upon the platform and many of them played an important part in the formation of the central highland of the island

Monogenetic basaltic cinder cones are located on all areas of St. Paul Island. Such volcanoes are generally located in regions of tectonic extension with relatively high rates of differential stress (maximum principal stress minus least principal stress) and relatively small magmatic input (Takada, 1994a and 1994b; Walker, 2000; Alaniz-Alvarez, 1998). They tend to localize along magma-filled fissures with a strong

correlation between regional differential stress and vent alignment (Connor and Conway, 2000) (Fig. 55). Based on their stratigraphic and spatial locations, geomorphology, and radiogenic carbon age dating (described above in Chapters 2 and 3), the ages of monogenetic cinder cones on St. Paul appear to span most of the eruptive history of the island, beginning during the platform building stage and ending with the most recent eruption at Fox Hill.

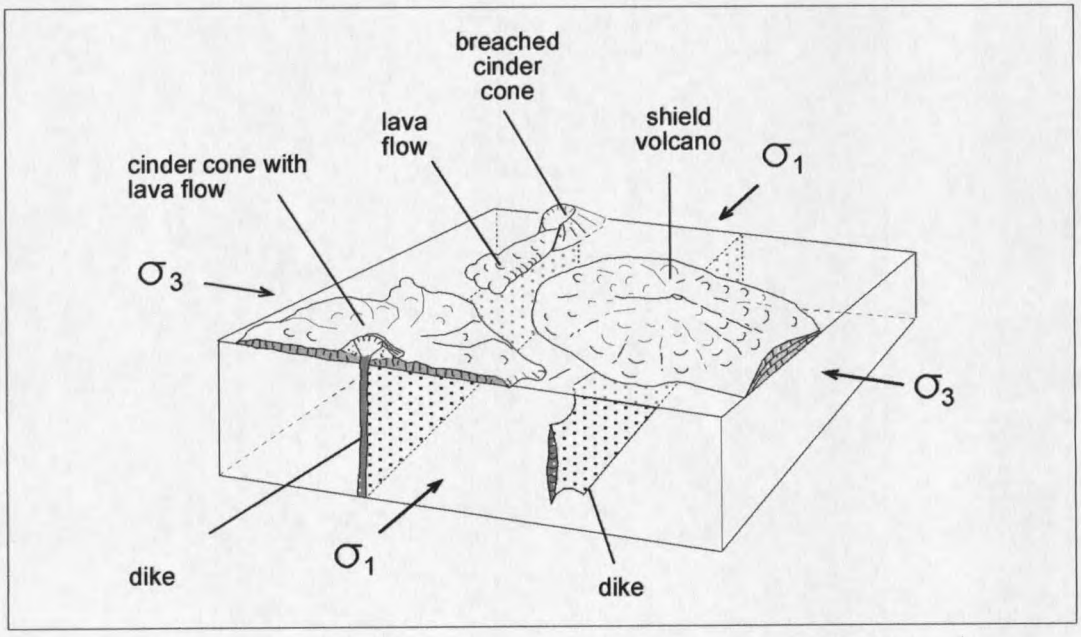


Figure 55. Schematic diagram of a monogenetic volcanic field. Monogenetic volcanoes are located along dikes or fissures where magma-filled cracks intercept the Earth's surface. Note dikes forming perpendicular to the least principal stress (sigma-3). Figure adapted from Walker (2000).

Monogenetic volcanoes on St. Paul range in size from the large, complex cinder cones of Polovina Hill on eastern St. Paul and Rush Hill on the west coast, to the small spatter/cinder cones of the Airport lava field and the Hutchinson Hill lava shield (Plate

1). Most of the cinder cones have associated mappable lava flows, but several do not. In the cases of cones with no apparent lava flows it appears, because of cone breaching, that many of these did produce lava flows that have since been buried by younger deposits (e.g., on the central highland), or they may have been lost to erosion (e.g., the village hill).

Most cinder cones on St. Paul, especially on the central highland, are morphologically young with sharp to relatively sharp profiles and well preserved craters. The stratigraphically and morphologically oldest cinder cones are located on the southern part of the island, from Telegraph Hill southward, near exposures of platform lavas. The craters of these old cones have been obliterated by erosion, or perhaps by breaching, and some have undergone major mass wasting where they have been exposed to the heavy surf of the Bering Sea.

At a few sites, the relationship between the faulted platform basalts, marine sediments, and an overlying cinder cone is exposed in cross-section. For example, beneath the west side of the village hill, along the coast, a fault with approximately 2.5 m of offset cuts the platform lava flows. Here the downthrown block is covered with layered sediments to the level of the upthrown block, at which point, both lava flows and sediments are covered with the scoria that forms the village hill, an eroded cinder cone (Fig. 56, A and B). The village hill cinder cone has undergone major erosion and no sign remains of any former crater. Based on the dip of the scoria layers in the village hill, the site of the vent is presumed to lie offshore.

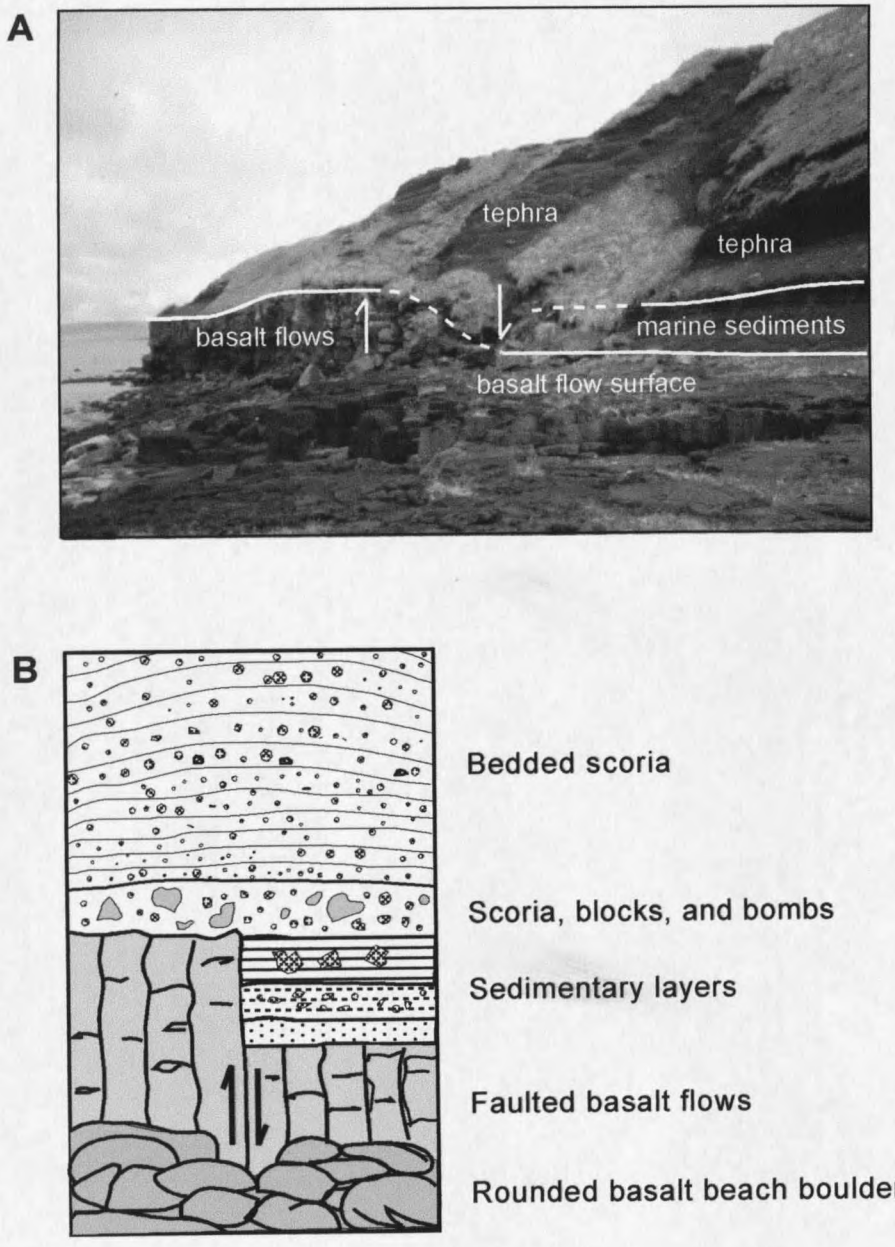


Figure 56. Relationship of Village Hill cinder cone to platform lavas. A. View of west side of Village Hill; note offset in basalt flows shown by white lines and arrows. B. Schematic representation of photograph in A. Offset on fault (shown by arrows) is approximately 2.5 m.

At a second site, on the eastern shore of the Reef Point peninsula, a small outcrop of consolidated scoria, a cone remnant too small to map, rests upon a base of breccia that overlies faulted and tilted pahoehoe lava (Fig. 57, the site of samples ERP1, ERP2, SP98-11, and SP98-12). The breccia layer is interpreted to be the product of a vent clearing explosion and contains very angular lithic blocks (≤1 m in diameter) mixed with scoria. The interpreted sequence of events at this site is: (1) the emplacement of the pahoehoe lava flow, which was later faulted and tilted, (2) a vent-clearing explosion of rock and ash, which deposited the breccia layer, and (3) the explosive Strombolian eruption and deposition of the scoria. Further interpretation must be limited, given the advanced state of erosion and the small size of the cone remnant and outcrop exposure. Again, the vent is presumed to lie offshore (see Plate 1).

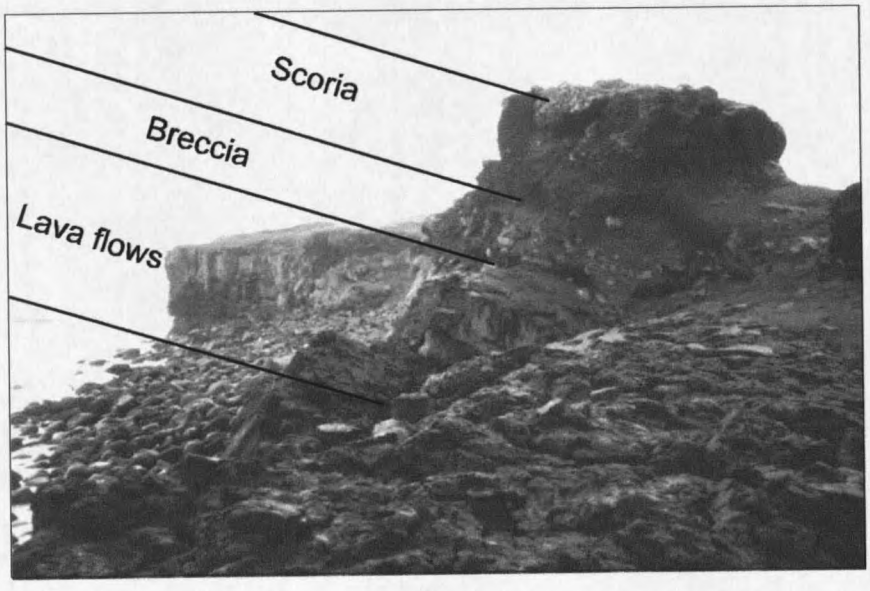


Figure 57. Remnant of scoria cone on lava flows on east Reef Point.

Magmas from the monogenetic cinder cone stage become less olivine-rich with a gradual decrease in MgO from older to younger units. Compositionally, the monogenetic centers range from primitive to evolved (Table 1) with MgO contents of 12.36 wt% at North Hill (SP98-37), decreasing to 6.46 wt% at Rush Hill (SP98-23). Olivine contents in monogenetic centers vary from strongly picritic with olivine megacrysts, e.g., North Hill (SP98-37; Fig. 23), to those fractionated of large olivine phenocrysts, with mostly quenched skeletal olivine remaining, such as Fox Hill (Feeley and Winer, 1999) (Fig. 48).

Shifts in the locus of cinder cone volcanism over time are common in small (<50 vents distributed over <1000 km^2) basaltic lava fields, for example the San Francisco, Springerville, and Cima volcanic fields (Connor and Conway, 2000). On St. Paul, the shift has been from the old eroded cones on south-central St. Paul toward the north and especially to the aligned vents of the central highland, where the morphologically young cinder cones and their coalescing and overlapping lava flows are closely associated with [and in the case of Fox Hill even post-date the most recent eruptions of] volcanoes of the third stage of volcanism on St. Paul, the polygenetic shield stage.

Polygenetic Shield Stage

The development of the polygenetic shield stage characterizes a change in the style of volcanism on St. Paul Island and a change in land forms from the steep edifices of the cinder cones to the broad, low-angle slopes of the polygenetic shield volcanoes (see Fig. 40). Polygenetic volcanoes differ from monogenetic volcanoes in that they erupt

repeatedly from the same vent or closely spaced vents and their gentle slopes are formed by repeated effusive eruptions of tube-fed pahoehoe lava flows. Eruptive activity on St. Paul has become increasingly localized at the Bogoslof Hill and Cone Hill volcanic complexes where large shield volcanoes have formed. These polygenetic centers are located at the intersections of major vent lineaments and faults on the central highland (see Fig. 52).

Compared with monogenetic volcanoes, polygenetic volcanoes tend to develop in areas with less differential stress and higher rates of magma supply (Takada, 1994b). The formation of polygenetic volcanoes on St. Paul Island appears to be related to their locations at intersecting faults and fissures, cracks in the lithosphere, through which magma is transported (Takada, 1999). It is inferred that at the intersections of these zones of crustal weakness, local differential stress is relieved by the injection of dikes grids to shallow crustal levels beneath polygenetic volcanoes (Takada, 1994b). These dikes then coalesce to form magma chambers at the level of neutral buoyancy (LNB) (Fig. 58), the level at which magma density is equal to the surrounding crust (Takada, 1994b; Maaløe, 1998; Takada, 1999; Watanabe et al., 1999). The depth of the LNB is thought to be at about 10 km for unvesiculated basaltic magma, while the apparent LNB for vesiculated magma may be located within the volcanic edifice itself, or just below the uppermost crust of the volcano (Takada, 1999). Through thermal conditioning, polygenetic volcanoes establish stable magma paths or conduits through which repeated

eruptions occur (Walker, 2000), building larger volcanic edifices than those of the monogenetic volcanoes (Francis, 1996; Takada, 1994; Nakamura, 1977).

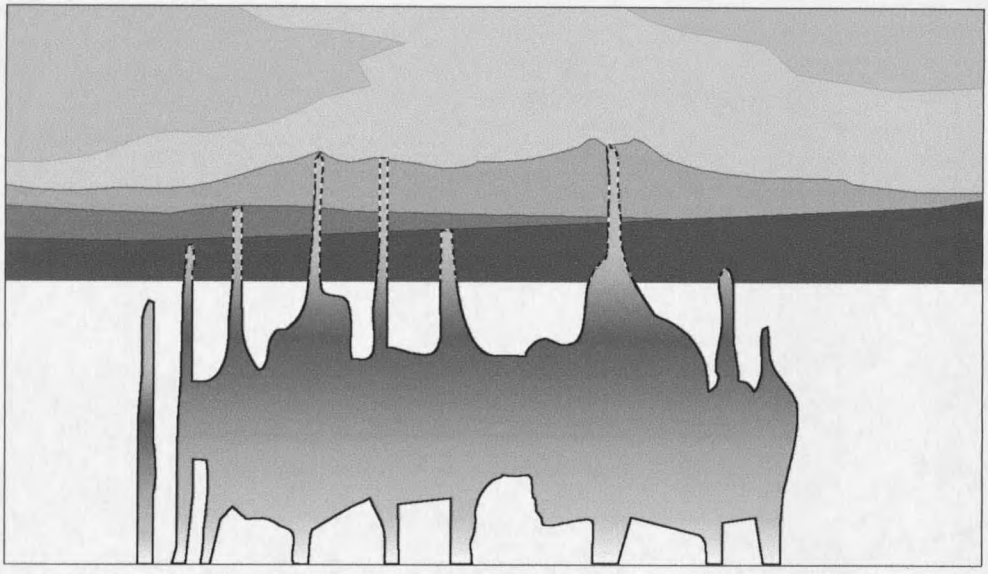


Figure 58. Schematic diagram of coalescing dikes forming a shallow crustal magma chamber beneath Bogoslof Hill.

The Bogoslof Hill and Cone Hill volcanic complexes are defined as polygenetic volcanoes based on multiple separate eruptions over time and evidence (i.e., fractionation of olivine and eruption of degassed, plagioclase-rich lava) for the existence of shallow crustal magma chambers beneath them. Some of the most recent lava flows on the island are the products of repeated eruptive episodes from these two polygenetic shield volcanoes. The construction of these centers is related to the development of long-lived, periodically replenished, shallow crustal magma chambers beneath St. Paul Island (Walker, 2000; Feeley and Winer, 1999). Compositionally, the polygenetic centers range

from evolved (7.56 wt% MgO) to most evolved (4.25 wt% MgO) of St. Paul lavas (Table 1), with Bogoslof Hill being the most evolved.

Eruptions at the polygenetic centers are interpreted to have been only mildly explosive, with minor amounts of ash and scoria, fire fountains depositing spatter and agglutinated lava near their vents, and clastogenic and effusively erupted lava forming flows and complex systems of lava tubes, which feed their increasingly evolved lavas to their surrounding lava shields. This eruptive style is analogous to Hawaiian style eruptions described by Wolff and Sumner (2000) and Vergniolle and Mangan, (2000).

Compositional and Petrologic Evolution of St. Paul Island

The integration of geochemical and petrologic data are combined with geologic mapping, geochronology, and construction of a stratigraphic column to reconstruct the volcanic evolution of St. Paul Island. This approach is used to determine long-term compositional trends that relate to the evolution of the St. Paul volcanic system and also to ascertain the bearing of such trends on future eruptive styles and volcanic hazards.

In general, St. Paul lavas become increasingly compositionally evolved (decreasing MgO and increasing K_2O) with decreasing age (Fig. 59A). This trend is reflected in the modal mineralogy, which shows a steady decrease in modal olivine (Fig. 59B) with decreasing MgO content. For both clinopyroxene and plagioclase (Fig. 59, C and D), the platform lavas with highest modal abundances of these minerals are anomalous and are seen in the platform lavas with holocrystalline groundmasses, described in the previous

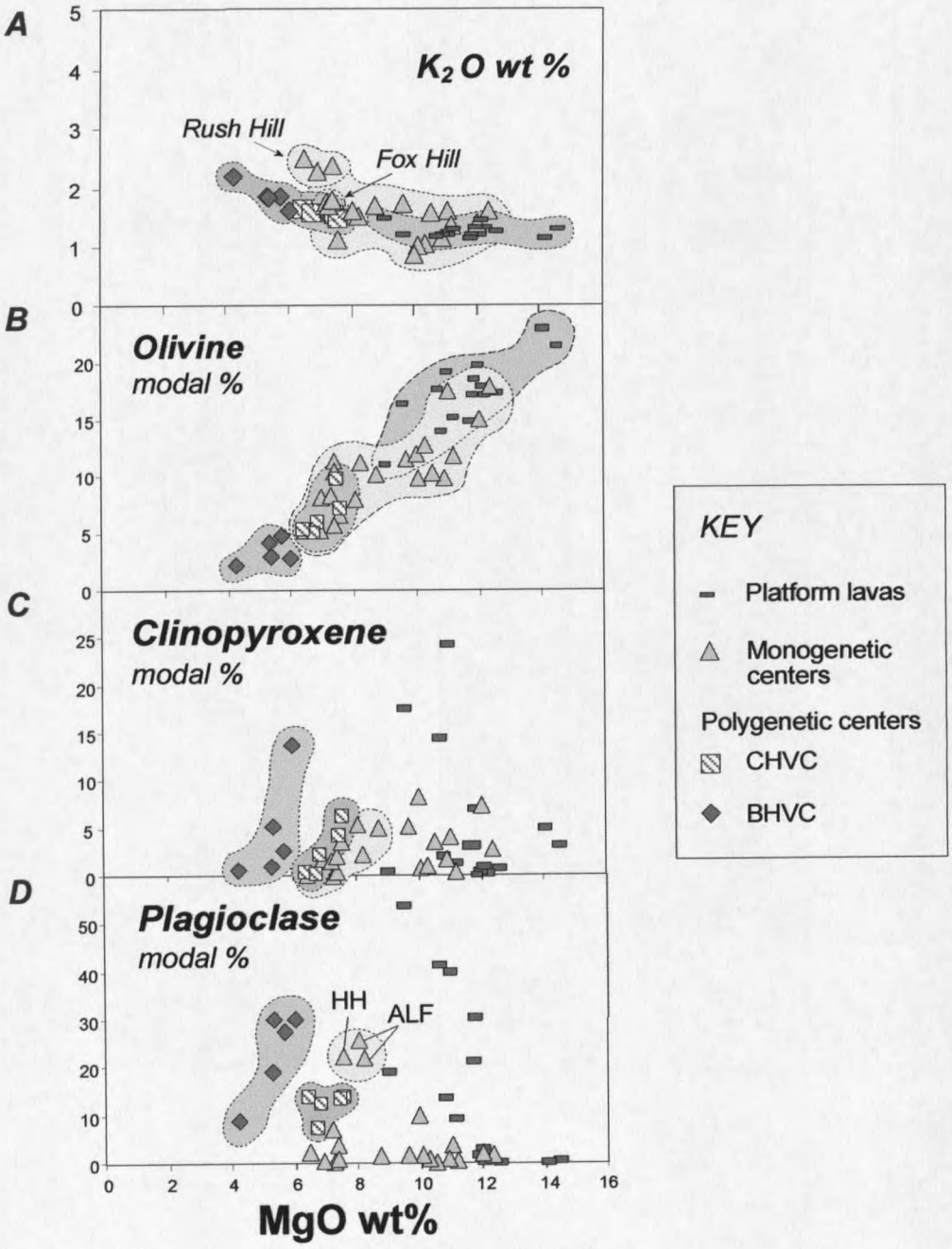


Figure 59. Variation diagrams show increasing evolution and fractionation of lavas from platform to monogenetic to polygenetic centers. Variations of (A) wt% K_2O and modal percentages of (B) olivine, (C) clinopyroxene, and (D) plagioclase vs. wt% MgO are discussed in the text.

section. The high phenocryst content of these lavas are possibly related to post-eruptive protracted cooling. Overall, modal clinopyroxene (Fig. 59C) shows no clear trend. Modal plagioclase generally increases with decreasing MgO (Fig. 59D), especially in polygenetic centers and in monogenetic centers (Hutchinson Hill and the Airport lava field) that are only mildly explosive and have formed low volcanic edifices. On the variation diagrams, lavas from monogenetic centers overlap with platform lavas and also with lavas from polygenetic centers, in both composition and modal mineralogy.

Magmas erupted during the earliest stage of subaerial volcanic activity, the platform building stage, are predominantly unevolved, olivine-rich basalts and basanites that generally become more evolved upsection (Fig. 59A). A petrological description of these early lavas is included in the section on undifferentiated platform lavas in Chapter 3. Overlying the platform lavas are deposits of lava and tephra of the monogenetic cinder cone stage of volcanism. Compositions of magmas from this stage range from olivine-rich and unevolved (e.g., North Hill, Table 1, Fig. 23) to the evolved and fractionated lavas of Fox Hill (Feeley and Winer, 1999), and, apparently, Rush Hill (Fig. 59A). Like the platform lavas, lavas from the monogenetic cinder cone stage, generally become increasingly evolved with decreasing age. Finally, lavas erupted at the young Bogoslof Hill and Cone Hill volcanic complexes of the most recent stage of volcanism, the polygenetic shield stage, are the most evolved lavas in the St. Paul Island volcanic system, becoming increasingly depleted in MgO and olivine contents and increasingly rich in plagioclase and K_2O. This trend is especially noticeable at Bogoslof Hill, the large polygenetic shield volcano located at the center of St. Paul Island. Future

voluminous lava flows from Bogoslof Hill may pose the most formidable volcanic hazard on the island.

POTENTIAL VOLCANIC HAZARDS AND RELATED RISKS

Introduction and Definitions

St. Paul Island is a live, though currently dormant, volcanic center. A live volcanic center, as defined by Decker and Decker (1991), is one at which volcanism is *potentially active* and future eruptions are *probable*. However, because St. Paul is presently dormant with no apparent precursory signs of an eruption (e.g., seismic, ground deformation, or fumarolic activity), predictions, or forecasts, and risk assessments are appropriately long-range, that is, related to coming years, decades, or longer (Newhall, 2000).

In the field of volcanology, prediction is done for two reasons; (1) to identify hazards related to eruptive processes and, (2) to assess related risks to people living in the area (Chester, 1993). Long-range predictions, called *general predictions*, are used for volcanoes such as St. Paul Island, where an eruption does not appear to be imminent. The term *general prediction* is defined by Walker (1974) as the study of historical patterns of a volcano to determine its eruptive interval as well as magnitude and style of previous eruptions in order to identify areas of high risk. In volcanic hazard and risk assessment the terms *hazard* and *risk* are more narrowly defined than in common usage where they are often used as synonyms (Peterson and Tilling, 2000).

In the study of volcanoes, *hazards* are defined as potentially dangerous phenomena associated with eruptive and post-eruptive volcanic activity that might occur in the foreseeable future in the area under consideration (Newhall, 2000). Examples of hazards

that may occur on St. Paul are lava flows, pyroclastic fallout, and emissions of volcanic gases. Volcanic *risks* are a measure of the adverse effects of volcanic hazards. These include the degree of probability of damage to property, loss of productive capacity, or loss of life related to the hazardous volcanic process (Peterson and Tilling, 2000). A third term, *vulnerability*, is defined as the susceptibility of people, property, and economic activity to be affected by the volcanic hazard (De La Cruz-Reyna et al., 2000). *Hazard* and *vulnerability* are elements of *risk* and the fundamental equation of risk is [hazard × vulnerability = risk] (Blong, 2000).

As described by Peterson and Tilling (2000), the hazard posed by a lava flow on an uninhabited region of St. Paul would be the same as the hazard if the flow threatened the village. In contrast, the risk would be negligible if the lava flow were far from the village, but risk, in human terms, could be significant if the flow were near the village where vulnerable people, property, and productive capacity were threatened. Risk is not strictly related to the size or violence of the eruption (the hazard), but rather to the proximity (vulnerability) of the community and its infrastructure (harbor, roads, airport, U.S. Coast Guard LORAN Station, and the National Weather Service Station) to the hazard (Pareschi & Bernstein, 1989). Even a relatively small eruption near the village could have a high risk. On St. Paul Island, volcanic risk may also apply to the great herd of northern fur seals, their rookeries, and rich and varied bird life including nesting colonies of seabirds that make St. Paul an international tourism destination.

In this study, a general prediction is approximate concerning the timing, nature, and size of a future eruption at St. Paul Island. Its purpose is to outline possible hazards and

risks that could be associated with a future eruption. Knowledge beforehand of possible volcanic scenarios will allow local authorities to consider appropriate responses in the event that the volcanic center exhibits signs of impending eruption, or even if an eruption should begin unannounced.

Hazard Assessment

The key to hazard assessment at a dormant volcano is knowledge of its eruptive history, as past behavior is the best indicator of future eruptive activity (Fisher et al., 1997; Decker and Decker, 1991; Wright and Pierson, 1992; Chester, 1993). In this study, methods used to interpret the volcanic history of St. Paul Island include (1) detailed geologic mapping, (2) description of volcanic units and interpretation of eruptive styles, (2) geochemical and petrographic studies to document changes in magma composition that may indicate increasing explosivity in future eruptions, (3) determination of relative ages of volcanic vents and lava flows using methods such as stratigraphic relationships between volcanic deposits, degree of weathering and sediment cover on lava flows, and morphology of cinder cones, and (4) estimation of volumes of areas covered by recent lava flows.

In hazard assessment, it is assumed that the pattern of future activity will follow that of the most recent past. On St. Paul Island, the most recent volcanic activity has been located on the central highland where the youngest events have ranged from the explosive cinder cone building eruption and quiet effusion of lava at Fox Hill, to the less

explosive eruptions that formed the spatter cones and the pahoehoe lava flows at the Bogoslof Hill and Cone Hill volcanic complexes. Because of the locations of the most recent eruptions on the central highland, the greatest risk associated with a future eruption would likely be from lava flows.

Potential Volcanic Hazards

The principal hazards from the most recent style of eruptions on St. Paul Island are those from pyroclastic fallout and lava flows. A modern example of a Strombolian eruption is that of the volcano Paricutín in the Trans-Mexican volcanic belt. The eruption of Paricutín began in 1943. Although the eruption of Paricutín was unusually prolonged (nine years as compared with the usual life-span of one year or less for a monogenetic eruption), the hazards associated with this eruption are similar to what may occur at future eruptions on St. Paul Island. Within one week, the explosive eruption had constructed a cinder cone about the height of Polovina Hill. During the first year of Paricutín's eruption, fallout of ash created a hazard in a town 48 km away (Bullard, 1984). Effusive eruptions of lava that issued from the base of the cone eventually covered an area of nearly 25 km^2. In comparison, a lava flow from Bogoslof Hill covers an area of approximately 16 km^2, which is approximately 15% of the area of the island of St. Paul. The young Fox Hill flow on southwest St. Paul covers an area of about 2 km^2,

and flows approximately 3 km from Fox Hill to the sea. This flow would likely have covered more area had it not flowed into the sea.

Although future eruptions may be expected to follow recent trends, a Surtseyan eruption in the near vicinity of the community of St. Paul Island occurred in the past at Black Bluffs, and the possibility of a future eruption of this style cannot be ruled out. A modern example of a possible future scenario at St. Paul is the eruption that occurred near the coast of Iceland in 1963, forming the island of Surtsey. Compared with Strombolian eruptions, a Surtseyan eruption presents a formidable hazard. The greatest hazard associated with Surtseyan eruptions is the *base surge*. Base surges from Surtseyan-style eruptions are gravity controlled, highly turbulent, pyroclastic density currents that expand radially with hurricane-velocity [as great as 100 m/s (Moore, 1967)] in all directions from the locus of a hydrovolcanic explosion (Cas and Wright, 1995). Base surges can cause extensive damage and loss of life within a few kilometers of the vent and can sandblast objects up to 8 km away (Cas and Wright, 1995).

Estimate of Eruptive Intervals and Prediction

An estimate of the frequency of volcanic eruptions on St. Paul Island was made using a count of forty separate vents, thought to represent separate eruptions. These eruptions were considered by Hopkins (1976) to be somewhat regularly spaced during a period of about 300,000 years (K-Ar age date from Cox et al., 1966). Using this estimation along

with the most recent eruption on St. Paul, the Fox Hill eruption, dated at about 3230 years before the present, the estimated mean occurrence rate is then

$40 / (300{,}000 - 3230 \text{ yrs}) = 0.135 \times 10^{-3}$ eruption/year

and the estimate of the eruptive interval is approximately 7400 years. The probability of an eruption (Mattox, 1999) within the next five years is approximately 0.10%. Because there are likely to be buried vents that were not counted, the value of 0.135×10^{-3} eruption per year may be an underestimate of the true mean occurrence rate. A more accurate evaluation of the occurrence rate and eruption interval will be possible when radiogenic Ar^{40}/Ar^{39} age determinations on eruptive units are completed. These analyses have been delayed by equipment problems, but are in progress.

Based on the above recurrence rate and the most recent volcanic history of St. Paul Island, a general prediction of future volcanic activity can be made. If the volcano follows recent trends, about 4000 years from now, an eruption may occur on the central highland. However, because the geochronology is not well constrained and many buried vents may be uncounted, the possibility of an eruption in the near future cannot be ruled out A future eruption would probably be either a monogenetic, Strombolian, cone-building eruption with an associated lava flow, at some location on the central highland, or a Hawaiian style eruption with fire fountains and lava flows originating at one of the existing polygenetic volcanoes. Because the eruptive style on St. Paul appears to be trending toward polygenetic centers with evolved lavas, especially at Bogoslof Hill, a future eruption at this volcanic complex appears to be the most likely future event.

Volcanic Hazard Characteristics and Associated Risks on St. Paul Island

The description of volcanic hazards and related risks that may occur on St. Paul Island during future eruptions is made using modern, well-studied examples of volcanism such as: (1) explosive and effusive eruptions at Parícutin in the extensional Transmexican volcanic belt (Bullard, 1984; Scarth, 1999); (2) fissure eruptions and pahoehoe flows with lava channels and tubes at Kilauea, Hawaii (Peterson et al., 1994), and at Mount Etna, Sicily (Calvari and Pinkerton, 1999); (3) the violent hydrovolcanic eruption at Surtsey, the emergent volcanic island near Iceland (Kokelaar, 1983); and (4) the eruption of Eldfell at Heimaey, Vestmannaeyjar, Iceland (Williams and Moore, 1983). The following list of hazards and risks is modified for St. Paul from the format of volcanic hazards from Blong (1996).

Lava Flows

- The temperature of flowing lava, 750-1100° C, is hot enough to ignite many materials.
- Flow rate is viscosity dependent and flow-front velocities may vary from a few tens of m/hr to a few tens of km/h depending on effusion rate and steepness of terrain.
- Flows follow topographic depressions or may spread widely like the flows surrounding Bogoslof Hill. Lava tubes enhance distances traveled; the flow field

surrounding Bogoslof Hill was likely emplaced by lava tubes that could be reactivated during a subsequent eruption.

- A haze of noxious gases may be associated with sustained lava flows. Downwind from the eruption acid rain and air pollution could be a persistent problem.
- Lava flows often crush or bury objects in their paths.
- There is danger from small explosions when hot lava enters seawater.
- Phreatic explosions may result from lava flows running over saturated ground or small ponds, creating a serious risk to unsuspecting onlookers.
- Lava flows in winter may rapidly melt enough snow to cause flooding that washes out roads.
- Lava tubes, such as those around Bogoslof Hill, increase the hazards from pahoehoe flows since tubes insulate the lava allowing it not only to flow much farther before cooling, but also to appear at unexpected locations.

Tephra Falls

Tephra is solid fragmented matter ejected by a volcano, often extremely rapidly; it includes ash, lapilli ("little stones"), and larger bombs, and blocks (Thornton, 2000).

- Eruption column height can reach >6 km as it did, for example, at Parícutin, where ash brought traffic to a halt and threatened to collapse rooftops 25 km away (Scarth, 1999).
- Visibility may be severely limited (less than a meter) by high fall-rate of tephra.

- Ash may compact, especially when wet, to a density of 1.6 ton/m^3 (Blong, 1996) and has potential for collapsing roofs.
- Ash, when inhaled by humans, causes respiratory irritation and distress and aggravates symptoms of asthma (Baxter, 2000).
- Swirling ash, as at Parícutin (Scarth, 1999), may, on St. Paul, batter birds, clog the lungs of animals (seals and reindeer) and cover reindeer's food supply.
- Highly abrasive fallen ash may be readily re-entrained by wind.
- Airborne ash damages engines, especially aircraft engines, which may stall or be rendered inoperative.
- Distribution and amount of ashfall is difficult to predict in advance.

Ballistic Ejecta

Ballistic ejecta are tephra fragments large enough to be little effected by wind; they follow ballistic trajectories and fall near the vent, building a cone.

- Circular area around vent is affected—usually limited to 3-5 km radius; wind direction and velocity have little effect on scoria and bombs, which are common in explosive eruptions on St. Paul.
- Bombs and blocks much larger than 10 cm diameter have high impact energies—a spindle bomb about 2 m in length was found on the outer slopes of Polovina Hill.
- Bombs may be hotter than ignition temperature of many materials.

Volcanic Gases

- Fumes may cause asphyxiation in close proximity to the source (vent or lava flow) and exacerbate respiratory disease, such as asthma, over a larger region (Rymer, 2000).
- They may result in acid rain from the incorporation of CO_2 and SO_2 into raindrops; acid rain has an adverse effect on wildlife and vegetation as well as on humans.
- Basalt emits more sulfur dioxide (SO_2) per unit mass than more evolved lavas (Carey and Bursik, 2000) and could pose a significant risk downwind from an explosive eruption or degassing lava flow on St. Paul. Even short-term overexposure to SO_2 can cause inflammation of eyes and the respiratory tract, causing coughing and respiratory distress (Williams-Jones and Rymer, 2000).

Ground Deformation

- Ground uplift and cracking related to magma movement
- Subsidence may follow eruption

Earthquakes: Seismicity of Volcanic Origin

Volcanic earthquakes occurring at or near volcanoes may be related to volcanic processes (McNutt, 2000).

- Pre-eruptive earthquakes related to shear fracturing of overlying rock in the vicinity of moving magma may be of short duration at basaltic volcanoes (such as St. Paul) and be closely followed by the eruption (McNutt, 1996). Volcanic tremor is a common and important short-term precursor to volcanic eruptions (McNutt, 1996). These tremors usually, but not always, occur beneath the site of the impending eruption (McNutt, 1996).
- Basaltic volcanic centers often have energetic post-eruptive earthquake swarms (McNutt, 1996).
- A tectonic earthquake may trigger an eruption if one is imminent.

Tsunami

- May be triggered by sector collapse with submarine landslide related to earthquakes accompanying an eruption—or even without an eruption. Examples of this phenomenon have occurred in Hawaii.

Base Surge

- Associated with Surtseyan eruptions, a base surge may be located near the shore of St. Paul and destroy everything within one to a few kilometers of the vent.

Factors That May Exacerbate Risks on St. Paul Island

Because of St. Paul's remote location in the storm-lashed Bering Sea, risks related to volcanic hazards are greater than they would be in a different setting. The risk from volcanic hazards on St. Paul Island is heightened by the following factors:

- Weather in the Bering Sea is infamous for its storms and risks from volcanic hazards could be exacerbated by wind, fog, and rain. On St. Paul Island, winds are often strong and cover all points of the compass with no particular prevailing wind direction (W. Burson, National Weather Service, St. Paul Island, Alaska, 2000, personal commun.). Wind speeds average 17.3 mph with gusts up to 84 mph, heavy cloud cover occurs 286.7 days per year (nearly 80% of the time), visibility is limited to ¼ mile or less about 57 days per year (fog is most prevalent during the summer months), and precipitation (0.01 inches or more) occurs 205 days per year (data from the National Weather Service, St. Paul Island, Alaska).
  - Severe storms and heavy fog can make transportation to and from the island, by air and by sea treacherous, if not impossible.
  - Fog may interfere with rescue work and with the ability to monitor the eruption. In addition, fog may become acidic as it combines with volcanic gas emissions such as CO_2 and SO_2 and is carried downwind.
  - Frequent precipitation increases the risk of acid rain, which could have an adverse effect on vegetation as well as on wildlife.
  - Rain may settle volcanic ash, but ash can become very slippery when wet.

- Wind carries volcanic ash for many kilometers from the eruption cloud. High winds may also whip fallen ash into blinding, highly abrasive clouds. Wind direction is difficult to predict on St. Paul.

- Traffic between the town of St. Paul and the airport could be severely compromised by lava flows crossing the road to the airport.
- Lava flowing across the single runway, e.g., from Bogoslof Hill could prevent landing of all fixed-wing aircraft.
- A lava flow or heavy deposit of tephra could close the harbor.
- Location of the town of St. Paul is restricted to a small area with no housing available outside this area and the nearest community is on St. George Island, 70 km SSW of St. Paul. In counterpoint, the location of the village appears to be sheltered by topography from a lava flow, unless its source was very near the town.
- Medical facilities are limited to clinic with one or two physician's assistants on staff.

Hazard Mapping

The assessment of volcanic hazards on St. Paul Island is complicated by the volcanic history of the island. St. Paul Island, with the exception of sand dunes and a few small sandy beaches, is entirely constructed from the products of volcanic eruptions with vents located all over the island. Therefore, it is impossible to accurately predict the location of the next vent. However, given the polygenetic behavior of Bogoslof Hill, it seems likely that the next eruption could be from this eruptive center (Fig. 60). Flows from Bogoslof

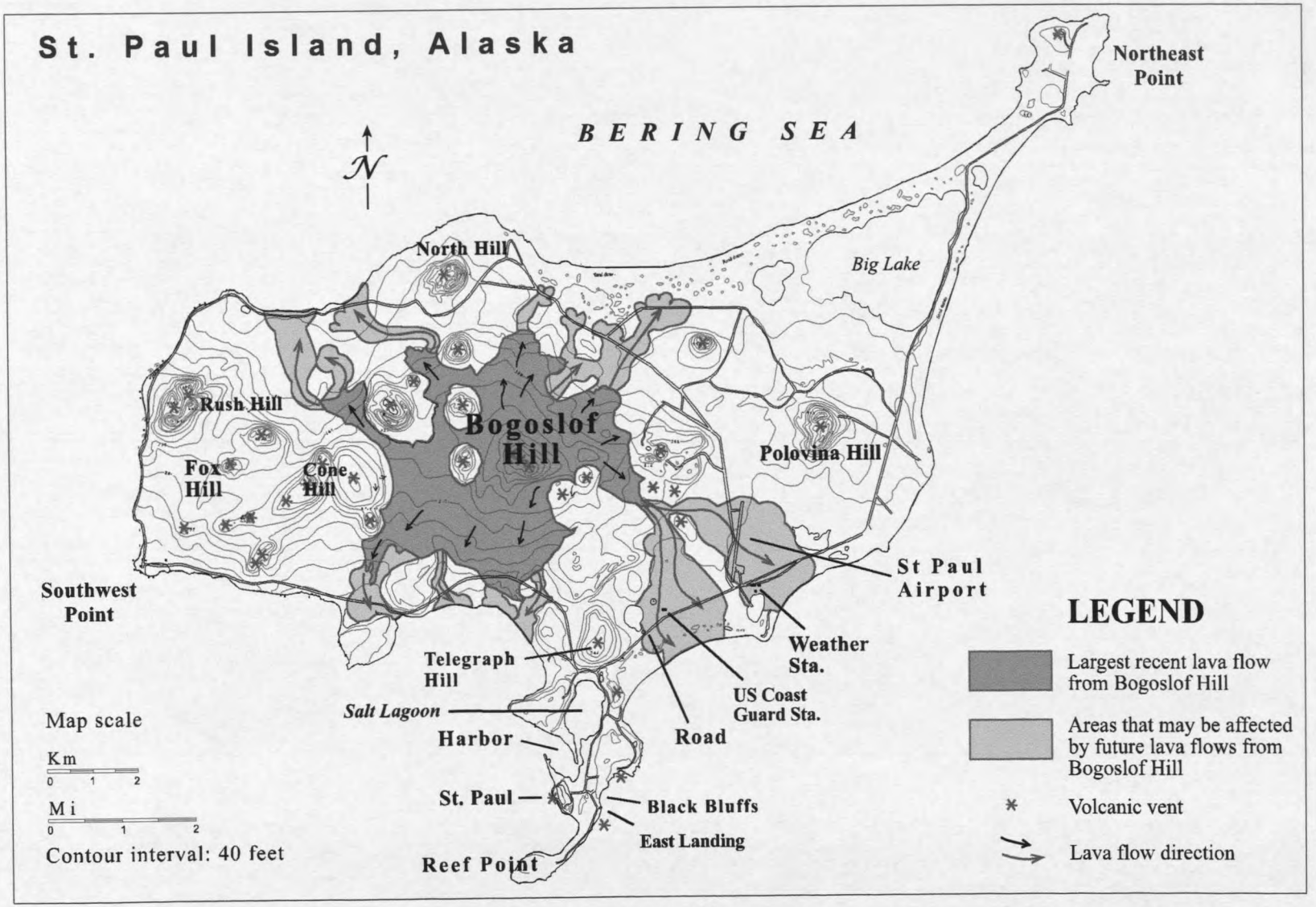


Figure 60. Area of possible future lava flows from Bogoslof Hill volcano.

Hill could feasibly flow directly south toward English Bay and cross the road to Southwest Point, flow east and southeast crossing the road near the US Coast Guard station and/or flow across the airport landing strip. Areas that may be covered by a future lava flow from Bogoslof Hill are shown in Figure 60. Note that the town of St. Paul is well situated in the event of a future eruption on the central highland. The town would be protected by topography as the nearest lava flows would be diverted to the east or west of Telegraph Hill, and flow toward the sea at Lukanin Bay and/or English Bay, a distance of 3 to 4 km from town.

Suggestions for Dealing with Future Volcanic Eruptions

While there is no control over the hazard related to volcanic phenomenon, risk can be mitigated by preparedness to lessen vulnerability (De La Cruz-Reyna, 1996). Earthquakes, ground deformation, and possibly faulting and fumarolic activity are precursory signs that may precede a volcanic eruption on St. Paul Island (Kuntz, 1978). If any such premonitory signs should occur, they should be carefully monitored by geophysicists and volcanologists such as the staff at the Alaska Volcano Observatory (AVO) at the University of Alaska-Fairbanks. If any of the aforementioned precursory activity should occur, the AVO should be notified immediately. The staff at the AVO is prepared to monitor a hazardous volcano and to assess the nature, timing, and likelihood of an eruption. They also assess volcanic hazards associated with anticipated activity, including effects of the hazards and areas at risk. Another objective of the AVO staff is

to provide timely and accurate information on volcanic hazards, and warnings of impending dangerous activity, to local officials and the public, and also to implement public safety measures (AVO, 2000).

CONCLUSIONS

(I) Volcanism at St. Paul Island is tectonically controlled and is related to continuing subduction of the Pacific plate beneath the North American plate along the Aleutian subduction zone.

(II) Locations of volcanic lineaments are tectonically controlled by faulting and fissuring

(III) Eruptive styles on St. Paul Island include fissure eruptions, Surtseyan eruptions, Strombolian eruptions, and Hawaiian style eruptions.

(IV) The St. Paul Island basaltic lava field has evolved from the (1) mostly effusive platform building stage, to (2) the more explosive monogenetic Strombolian cinder cone stage, and finally to (3) the mildly explosive polygenetic shield building stage.

(V) Styles of volcanism on St. Paul Island are controlled by a combination of extension rates, magma supply rates, and sometimes, interaction of magma and water.

(VI) The development of polygenetic volcanoes on St. Paul Island is related to their locations at intersections of faults and fissures.

(VII) Polygenetic shields on St. Paul Island are only the latest phase of a complex volcanic evolution.

(VIII) The combination of spatial, temporal, and compositional changes on St. Paul Island suggests that the magmatic system as a whole is trending toward more evolved compositions related to the progressive development of shallow crustal magma chambers in which crystal fractionation and magmatic differentiation are occurring

(IX) The most recent volcanic eruption on St. Paul Island occurred 3,230 ± 40 ybp at Fox Hill.

(X) Potentially large lava flows from Bogoslof Hill may create the greatest volcanic hazard on St. Paul Island.

(XI) Future eruptions may be expected at St. Paul Island, putting at risk this unique environment and the heart of the Aleut culture.

REFERENCES CITED

Alaniz-Alvarez, S.A., Nieto-Samaniego, Á.F., Ferrari, L., 1998, Effect of strain rate in the distribution of monogenetic and polygenetic volcanism in the Transmexican volcanic belt: Geology, v. 26, no. 7, p. 591-594.

Alaska Volcano Observatory, 2000, <http://www.avo.alaska.edu/avo3/cover/coop.htm>

Ansfield, V.J., 1990, Olivine dominated sand beach, Mahana Bay, Hawaii: Geological Society of America Abstracts with Programs, p. A57.

Barth, T.F.W., 1956, Geology and petrology of the Pribilof Islands, Alaska: Geological Survey Bulletin 1028-F, 56 p.

Baxter, P.J., 2000, Impacts of eruptions on human health, *in* Sigurdsson, H., editor-in-chief, Encyclopedia of Volcanoes: New York, Academic Press, p. 1035-1043.

Blackburn, E., Wilson, L., and Sparks, R.S.J., 1976, Mechanisms and dynamics of strombolian activity: Journal of the Geological Society of London, v. 132, p. 429-430.

Blong, R.J., 1996, Volcanic hazards and risk assessment, in Scarpa, R., and Tilling, R.I., eds., Monitoring and mitigation of volcano hazards, Springer-Verlag, p. 675-698.

Bullard, F.M., 1984, Volcanoes of the Earth: 2nd edition, The Dan Danciger Publication Series, Austin, Texas, University of Texas Press, 629 p.

Calvari, S., and Pinkerton, H., 1999, Lava tube morphology on Etna and evidence for lava flow emplacement mechanisms: Journal of Volcanology and Geothermal Research, v. 90, p. 263-280.

Carey, S., and Bursik, M., 2000, Volcanic Plumes, *in* Sigurdsson, H., editor-in-chief, Encyclopedia of Volcanoes: New York, Academic Press, p. 527-544.

Cas, R.A.F., and Wright, J.V., 1995, Volcanic Successions: Modern and ancient: London, Chapman & Hall, 528 p.

Chester, D., 1993, Volcanoes and society: Sevenoaks, Kent, UK, Edward Arnold (Division of Hodder & Stoughton Publishers), 351 p.

Colinvaux, P.A., 1967, Bering Land Bridge: Evidence of spruce in Late-Wisconsin times: Science, v. 156, p. 380-383.

Colinvaux, P., 1981, Historical ecology in Beringia: The south land bridge coast at St. Paul Island: Quaternary Research, v. 16, p. 18-36.

Cooper, A.K., and Marlow, M.S., 1983, Preliminary results of geophysical and geological studies of the Bering Sea self during 1982: U.S. Geological Survey Open-File Report 82-322, 8 p.

Cooper, A.K., Marlow, M.S., Scholl, D.W., and Stevenson, A.J., 1992, Evidence for Cenozoic crustal extension in the Bering Sea region: Tectonics, v. 11, no. 4, p. 719-731.

Connor, C.B., and Conway, F.M., 2000, Basaltic volcanic fields, *in* Sigurdsson, H., editor-in-chief, Encyclopedia of Volcanoes: San Diego, Academic Press, p. 331-343.

Cox, A., Hopkins, D.M., and Dalrymple, G.B., 1966, Geomagnetic polarity epochs: Pribilof Islands, Alaska: Geological Society of America Bulletin, v. 77, p. 833-910.

Curtis, G.H., 1968, The stratigraphy of the ejecta from the 1912 eruption of Mount Katmai and Novarupta, Alaska, *in* Coats, R.R., et al., eds., Studies in volcanology: Geological Society of America Memoir 116, p. 153-210.

Dall, W.H., 1899, The mollusk fauna of the Pribilof Islands, *in* The Fur Seals and Fur Seal Islands of the North Pacific Ocean, Part 3, p. 539-546.

Dawson, G.M., 1894, Geological notes on some of the coasts and islands of Bering Sea and vicinity: Bulletin of the Geological Society of America, v. 5, p. 117-146.

Decker, R.W., and Decker, B.B., 1991, Mountains of Fire: New York, NY, Cambridge University Press, 198 p.

De La Cruz-Reyna, S., 1996, Long-term probabilistic analysis of future explosive eruptions, *in* Scarpa, R., and Tilling, R.I., eds., Monitoring and mitigation of volcano hazards, Springer-Verlag, p. 599-629.

De La Cruz-Reyna, S., Melli, R.P., 2000, Volcanic crises management, *in* Sigurdsson, H., editor-in-chief, Encyclopedia of Volcanoes: New York, Academic Press, p. 1199-1214.

Elliott, H.W., 1881, The Seal-Islands of Alaska: Washington, Government Printing Office; reprinted, 1976, Kingston, Ontario, Canada, The Limestone Press, 176 p.

Emerson, B.K., 1904, Harriman Alaska Expedition: General geology: Geology, New York, NY, vol. 4, p. 29-42.

Feeley, T.C., and Winer, G.S., 1999, Evidence for fractionation of Quaternary basalts on St. Paul Island, Alaska, with implications for the development of shallow magma chambers beneath Bering Sea volcanoes: Lithos, v. 46, p. 661-676.

Fisher, R.V., Heiken, G., and Hulen, J.B., 1997, Volcanoes: Crucibles of change: Princeton, New Jersey, Princeton University Press, 317 p.

Francis, P., 1996, Volcanoes: A planetary perspective: New York, Oxford University Press Inc., 443 p.

Geist, D., White, W., Naumann, T., and Reynolds, R., 1999, Illegitimate magmas of the Galápagos: Insights into mantle mixing and magma transport: Geology, v. 27, no. 12, p. 1103-1106.

Greeley, R., 1977a, Basaltic "plains" volcanism, *in* Greeley, R., and King, J.S., eds., Volcanism of the eastern Snake River Plain, Idaho: A comparative planetary geology guidebook: Washington, D.C., Office of Planetary Geology, National Aeronautics and Space Administration, p. 23-44.

Greeley, R., 1977b, Volcanic morphology, *in* Greeley, R., and King, J.S., eds., Volcanism of the eastern Snake River Plain, Idaho: A comparative planetary geology guidebook: Washington, D.C., Office of Planetary Geology, National Aeronautics and Space Administration, p. 5-22.

Greeley, R., and Hyde, A., 1972, Lava tubes in the Cava basalt, Mount St. Helens, Washington: Bulletin of the Geological Society of America, v. 83, p. 2397-2418.

Hackett, W.R., and Smith, R.P., 1992, Quaternary volcanism, tectonics, and sedimentation in the Idaho National Engineering Laboratory area, *in* Wilson, J.R., ed., Field Guide to Geologic Excursions in Utah and Adjacent areas of Nevada, Idaho, and Wyoming: Utah Geological Survey, Miscellaneous Publication 92-3, p. 1-18.

Hanna, G.D., 1919, Geological notes on the Pribilof Islands, Alaska, with an account of the fossil diatoms: American Journal of Science, 4th ser., v. 48, p 216-224.

Head, J.W., III, and Wilson, L., 1989, Basaltic pyroclastic eruptions: Influence of gas-release patterns and volume fluxes on fountain structure, and the formation of cinder cones, spatter cones, rootless flows, lava ponds and lava flows: Journal of Volcanology and Geothermal Research, v, 37, p. 261-271.

Hildreth, W., and Fierstein, J., 2000, Katmai volcanic cluster and the great eruption of 1912: Geological Society of American Bulletin, v. 112, no. 10, p. 1594-1620.

Hillhouse, J.W., and Coe, R.S., 1994, Paleomagnetic data from Alaska *in* Plafker, G., and Berg, H.C., eds., The Geology of Alaska: Boulder, Colorado, Geological Society of America, The Geology of North America, v. G-1, p. 797-812..

Hon, K., Kauahikaua, J., Denlinger, R., and Mackay, K., 1994, Emplacement and inflation of pahoehoe sheet flows: Observations and measurements of active lava flows on Kilauea Volcano, Hawaii: Geological Society of America Bulletin, v. 106, p. 351-370.

Hopkins, D.M., 1976, Fault history of the Pribilof Islands and its relevance to bottom stability in St. George Basin, in Environmental Assessment of the Alaskan continental shelf: Boulder, Colorado, Environmental Research Laboratories, v. 13, p. 41-67.

Hopkins, D.M., 1967a, Quaternary marine transgressions in Alaska, in The Bering Land Bridge, Hopkins, D.M.: Stanford, California, Stanford University Press, p. 47-90.

Hopkins, D.M., 1967b, The Cenozoic history of Beringia—A synthesis, in The Bering Land Bridge, Hopkins, D.M.: Stanford, California, Stanford University Press, p. 451-484.

Hopkins, D.M., and Einarsson, Th., 1966, Pleistocene glaciation on St. George, Pribilof Islands: Science, v. 152, p. 343-345.

Houghton, B.F., and Smith, R.T., 1993, Recycling of magmatic clasts during explosive eruptions: estimating the true juvenile content of phreatomagmatic volcanic deposits: Bulletin of Volcanology, v. 55, p. 414-420.

Hughes, S.S., Smith, R.P., Hackett, W.R., and Anderson, S.R., 1999, Mafic volcanism and environmental geology of the eastern Snake River Plain, Idaho, *in* Hughes, S.S., and Thackray, G.D., eds., Guidebook to the Geology of Eastern Idaho: Idaho Museum of Natural History, p. 143-168.

Hulme, G., 1974, The interpretation of lava flow morphology: Geophysical Journal, Royal Astronomical Society, v. 39, p. 361-383.

Jackson, J.A., 1997, Glossary of Geology: Jackson, J.A., ed., Alexandria, Virginia, American Geological Institute, 769 p.

Johnson, S.H., 1982, New Day for Alaska's Pribilof Islanders: National Geographic Society, v. 162, 536-552.

Johnson, D.M., Hooper, P.R., and Conrey, R.M., 1999, XRF analysis of rocks and minerals for major and trace elements on a single low dilution Li-tetraborate fused bead: Advances in X-ray Analysis, v. 41, p. 843-867.

Kay, R.W., Sun, S.-S., and Lee-Hu, C.-N., 1978, Pb and Sr isotopes in volcanic rocks from the Aleutian Islands and Pribilof Islands, Alaska: Geochimica et Cosmochimica Acta, v. 42, p. 263-273.

Kilburn, C.R.J., 2000, Lava flows and flow fields, in Sigurdsson, H., Editor-in-Chief, Encyclopedia of Volcanoes, San Diego, Academic Press, p. 291-305.

Kokelaar, B.P., 1986, Magma-water interactions in subaqueous and emergent basaltic volcanism: Bulletin of Volcanology, v. 48, p. 275-289.

Kokelaar, B.P., 1983, The mechanism of Surtseyan volcanism: Journal of the Geological Society of London, v. 140, p. 939-944.

Kuntz, M.A., 1992, A model-based perspective of basaltic volcanism, eastern Snake River Plain, Idaho, *in* Link, P.K., Kuntz, M.A., and Platt, L.P., eds., Regional geology of eastern Idaho and western Wyoming: Geological Society of America Memoir 179, p. 289-304.

Kuntz, M.A., 1978, Geology of the Arco-Big Southern Butte area, eastern Snake River Plain, and potential volcanic hazards to the radioactive waste storage and reactor facilities and the Idaho National Energy Laboratory, Idaho: US Geological Survey Open File Report 78-691, 77 p.

Kuntz, M.A., Champion, D.E., LeFebvre, R.H., and Covington, H.R., 1988, Geologic map of the Craters of the Moon, Kings Bowl, and Wapi lava fields, and the Great Rift volcanic rift zone, south-central Idaho: Department of the Interior U.S. Geological Survey, Map I-1632, reprinted 1994..

Kuntz, M.A., Champion, D.E., Spiker, E.C., and Lefebvre, R.H., 1986a, Contrasting magma types and steady-state, volume-predictable, basaltic volcanism along the Great Rift, Idaho: Geological Society of America Bulletin, v. 97, p. 579-594.

Kuntz, M.A., Champion, D.E., Spiker, E.C., Lefebvre, R.H., and McBroome, L.A., 1982, The Great Rift and the evolution of the Craters of the Moon lava field, Idaho, *in* Bonnichsen, B., and Breckenridge, R.M., eds., Cenozoic Geology of Idaho: Idaho Bureau of Mines and Geology Bulletin 26, p. 423-437.

Kuntz, M.A., Spiker, E.C., Rubin, M., Champion, D.E., and Lefebvre, R.H., 1986b, Radiocarbon studies of latest Pleistocene-Holocene lava flows of the Snake River Plain, Idaho: Data, lessons, interpretations: Quaternary Research, v. 25, p. 163-176.

Landgrebe, G. 1855, Naturgeschichte der Vulcane: Gotha, Justus Perthes, ester band (v. 1) 499 p.

Lee-Wong, F., Vallier, T.L., Hopkins, D.M., and Silberman, M.L., 1979, Preliminary report on the petrography and geochemistry of basalt from the Pribilof Islands and vicinity, southern Bering Sea: USGS Open-file report 79-1556, 51 p.

Le Maitre, R.W., 1989, A classification of Igneous Rocks and Glossary of Terms: Recommendations of the International Union of Geological Sciences Subcommission on the Systematics of Igneous Rocks: Oxford, Blackwell Scientific Publications, 193 p.

Maaløe, S., 1998, Shape of ascending feeder dikes, and ascent modes of magma: Journal of Volcanology and Geothermal Research, v. 81, p. 207-214.

Marlow, M.S., and Cooper, A.K., 1980, Mesozoic and Cenozoic structural trends under the southern Bering Sea shelf: The American Association of Petroleum Geologists Bulletin, v. 64, p. 2139-2155.

Marlow, M.S., Cooper, A.K., and Fisher, M.A., 1994, Geology of the eastern Bering Sea continental shelf, *in* Plafker, G., and Berg, H.C., eds., The Geology of Alaska: Boulder, Colorado, Geological Society of America, The Geology of North America, v. G-1, p. 271-284.

Mattox, S.R., 1999, An exercise in forecasting the next Mauna Loa eruption: Journal of Geoscience Education, v. 47, p. 225-260.

Marlow, M.S., Scholl, D.W., Cooper, A.K., and Buffington, E.C., 1976, Structure and evolution of Bering Sea Shelf south of St. Lawrence Island: The American Association of Petroleum Geologists Bulletin, v. 60, p. 161-183.

McNutt, S.R., 1996, Seismic monitoring and eruption forecasting of volcanoes: A review of the state-of-the-art and case histories, in Scarpa, R., and Tilling, R.I., eds., Monitoring and mitigation of volcano hazards, Springer-Verlag, p. 99-146.

McNutt, S. R., 2000, Volcanic seismicity, *in* Sigurdsson, H., editor-in-chief, Encyclopedia of Volcanoes: New York, Academic Press, p. 1015-1033.

Moll-Stalcup, E.J., 1994a, Latest Cretaceous and Cenozoic magmatism in mainland Alaska, *in* Plafker, G., and Berg, H.C., eds., The Geology of Alaska: Boulder, Colorado, Geological Society of America, The Geology of North America, v. G-1, p. 589-619.

Moll-Stalcup, E.J., 1994b, The origin of the Bering Sea basalt province, western Alaska, *in* Simakov, K.V., and Thurston, D.K., eds., Proceedings of the International Conference on Arctic Margins, p. 113-123.

Moore, J.G., 1967, Base surge in recent volcanic eruptions: Bulletin of Volcanology, v. 30, p.337-63.

Moore, J.G., Phillips, R.L., Grigg, R.W., Peterson, D.W., and Swanson, D.A., 1973, Flow of lava into the sea, 1969-1971, Kilauea Volcano, Hawaii: Geological Society of America Bulletin, v. 84, p. 537-546.

Nairn, I.A., Kobayashi, T., Nakagawa, M., 1998, The ~10 ka multiple vent pyroclastic eruption sequence at Tongariro Volcanic Centre, Taupo Volcanic Zone, New Zealand: Part 1. Eruptive processes during regional extension: Journal of Volcanology and Geothermal Research, v.86, p. 19-44.

Nakamura, K., 1977, Volcanoes as possible indicators of tectonic stress orientation — principle and proposal: Journal of Volcanology and Geothermal Research, v. 2, p. 1-16.

Nakamura, K., Plafker, G., Jacob, K.H., and Davies, J.N., 1980, A tectonic stress trajectory map of Alaska using information from volcanoes and faults: Bulletin of the Earthquake Research Institute, v. 55, p. 89-100.

Newhall, C.G., 2000, Volcano warnings, *in* Sigurdsson, H., editor-in-chief, Encyclopedia of Volcanoes: New York, Academic Press, p. 1185-1197.

Pareschi, M.T., and Bernstein, R., 1989, Modeling and image processing for visualization of volcanic mapping: IBM Journal of Research and Development, v. 33, no. 4, p. 406-416.

Peterson, D.W., Holcomb, R.T., Tilling, R.I., and Christiansen, R.L., 1994, Development of lava tubes in the light of observations at Mauna Ulu, Kilauea Volcano, Hawaii: Bulletin of Volcanology, v. 56, p. 343-360.

Peterson, D.W., and Tilling, I.R., 2000, Lava flow hazards, *in* Sigurdsson, H., editor-in-chief, Encyclopedia of Volcanoes: New York, Academic Press, p. 957-971.

Plafker, G., and Berg, H.C., 1994a, Introduction, *in* Plafker, G., and Berg, H.C., eds., The Geology of Alaska: Boulder, Colorado, Geological Society of America, The Geology of North America, v. G-1, p. 1-16.

Plafker, G., and Berg, H.C., 1994b, Overview of the geology and tectonic evolution of Alaska, *in* Plafker, G., and Berg, H.C., eds., The Geology of Alaska: Boulder, Colorado, Geological Society of America, The Geology of North America, v. G-1, p. 989-1021.

Plafker, G., Gilpin, L.M., and Lahr, J.C., 1994, Neotectonic map of Alaska, *in* Plafker, G., and Berg, H.C., eds., The Geology of Alaska: Boulder, Colorado, Geological Society of America, The Geology of North America, v. G-1, scale 1:2 500 000.

Robinson, R., 1982, Exploring lava tubes: The Alaskan Caver, v. 7, no. 2, p. 4.

Rowland, S.K., and Walker, G.P.L., 1990, Pahoehoe and aa in Hawaii: volumetric flow rate controls the lava structure: Bulletin of Volcanology, v. 52, p. 615-628.

Rutherford, M.J., and Gardner, J.E., 2000, Rates of magma ascent, *in* Sigurdsson, H., Editor-in-Chief, Encyclopedia of Volcanoes, San Diego, Academic Press, p. 207-217.

Rymer, H., 2000, Volcanic hazards, *in* Sigurdsson, H., editor-in-chief, Encyclopedia of Volcanoes: New York, Academic Press, p. 913-914.

Sapper, K., 1917, Katalog der geschichtlichen vulkanausbrüche: Strassburg, K.J. Trübner, 358 p.

Scarth, A., 1999, Vulcan's fury: Man against the volcano: New Haven, CT, Yale University Press, 300 p.

Simpson, G.L., Vallier, T.L., Pearl, J.E., and Lee-Wong, 1979, Potassium-argon ages and geochemistry of basalt dredged near Saint George Island, southern Bering Sea, *in* Johnson, K.M., and Williams, J.R., eds., The U.S. Geological Survey in Alaska; Accomplishments during 1978: U.S. Geological Survey Circular 804-B, p. B134-B136.

Stanley-Brown, J., 1892, Geology of the Pribilof Islands: Geological Society of America Bulletin, v. 3, p. 496-500.

Sumner, J.M., 1998, Formation of clastogenic lava flows during fissure eruption and scoria cone collapse: the 1986 eruption of Izu-Oshima Volcano, eastern Japan: Bulletin of Volcanology, v. 60, p. 195-212.

Takada, A., 1994a, Development of a subvolcanic structure by the interaction of liquid-filled cracks: Journal of Volcanology and Geothermal Research, v.62, p. 207-224.

Takada, A., 1994b, The influence of regional stress and magma input on style of monogenetic and polygenetic volcanism: Journal of Geophysical Research, v. 99, 13563-13573.

Takada, A., 1999, Variations in magma supply and magma partitioning: the role of tectonic settings: Journal of Volcanology and Geothermal Research, v. 93, p. 93-110.

Tibaldi, A., 1995, Morphology of pyroclastic cones and tectonics: Journal of Geophysical Research, v. 100, no. B12, p. 24,521-24,535.

Vergniolle, S., and Mangan, M., 2000, Hawaiian and Strombolian eruptions, in Sigurdsson, H., editor-in-chief, Encyclopedia of Volcanoes: New York, Academic Press, p. 447-461.

Vespermann, D., and Schmincke, H.-U., 2000, Scoria cones and tuff rings, *in* Sigurdsson, H., editor-in-chief, Encyclopedia of Volcanoes: New York, Academic Press, p. 683-694.

Walker, G.P.L., 1972, Compound and simple lava flows and flood basalts: Bulletin Volcanologique, v. 35, p. 579-590.

Walker, G.P.L., 1974, Volcanic hazards and the prediction of volcanic eruptions, *in* Funnell, B.M., ed., Prediction of Geological Hazards: Geological Society of London, Miscellaneous Paper 3, p. 23-41.

Walker, G.P.L., 1987, The dike complex of Koolau volcano, Oahu: Internal structure of a Hawaiian rift zone, *in* Decker, R.W., Wright, T.L., and Stauffer, P., eds., Volcanism in Hawaii: U.S. Geological Survey Professional Paper, 1350, p. 961-993.

Walker, G.P.L., 1991, Structure, and origin by injection of lava under surface crust, of tumuli, "lava rises", "lava-rise pits", and "lava-inflation clefts" in Hawaii: Bulletin of Volcanology, v. 53, p. 546-558.

Walker, G.P.L., 2000, Basaltic volcanoes and basaltic systems, *in* Sigurdsson, H., Editor-in-Chief, Encyclopedia of Volcanoes, San Diego, Academic Press, p. 283-289.

Washington, H.S., and Keyes, M.G., 1930, Rocks of the Pribilof Islands: American Journal of Science, v. 20, no. 119, p. 321-338.

Watanabe, T., Koyaguchi, T., and Tetsuzo, S., 1999, Tectonic stress controls on ascent and emplacement of magmas: Journal of Volcanology and Geothermal Research, v. 91, p. 65-78.

Williams, R.S., and Moore, J.G., 1983, Man against volcano: The eruption of Heimaey, Vestmannaeyjar, Iceland: U.S. Government Printing Office: 1983-381-618/103, U.S. Department of the Interior/Geological Survey, 26 p.

Williams-Jones, G., and Rymer, H., 2000, Hazards of volcanic gases, *in* Sigurdsson, H., editor-in-chief, Encyclopedia of Volcanoes: New York, Academic Press, p. 997-1004.

Wilson, M., 1993, Magmatic differentiation: Journal of the Geological Society, London, v. 150, p. 611-624.

Wilson, M., 1996, Igneous Petrogenesis: London, England, Chapman & Hall, 466 p.

Winer, G.S. and Feeley, T.C., 1997, Petrography and geochemistry of basaltic lava flows from St. Paul Island, Pribilof Islands, Alaska: Geological Society of America Abstracts with Programs, v. 29, p. A329.

Wolff, J.A., and Sumner, J.M., 2000, Lava fountains and their products, *in* Sigurdsson, H., editor-in-chief, Encyclopedia of Volcanoes: New York, Academic Press, p. 321-329.

Wood, C.A., 1980a, Morphometric evolution of cinder cones: Journal of Volcanology and Geothermal Research, v. 7, p.387-413.

Wood, C.A., 1980, Morphometric analysis of cinder cone degradation: Journal of Volcanology and Geothermal Research, v. 8, p. 137-160.

Worrall, D.M., 1991, Tectonic history of the Bering Sea and the evolution of Tertiary strike-slip basins of the Bering Shelf: Geological Society of America Special Paper 257, 120 p.

Wright, T.L., and Pierson, T.C., 1992, Living with volcanoes: The U.S. Geological Survey's Volcano Hazards Program: U.S. Geological Survey Circular 1073, 57 p.

Wylie, J.J., Helfrich, K.R., Dade, B., Lister, J.R., and Salzig, J.F., 1999, Flow localization in fissure eruptions: Bulletin of Volcanology, v. 60, p. 432-440.

Yilmaz, Y., Güner, Y., and Şaroğlu, F., 1998, Geology of the Quaternary volcanic centres of the east Anatolia: Journal of Volcanology and Geothermal Research, v. 85, p. 173-210.

APPENDIX A

RADIOCARBON SAMPLE PREPARATION AND ANALYTICAL TECHNIQUES

The untreated organic carbon sample (SP98-64) was shipped to Beta Analytic Inc. where pretreatment of the carbon sample was done to eliminate secondary carbon components. The sample was analyzed using the bulk organic carbon after removing any carbonates or rootlets. The surface area of the organic carbon was increased as much as possible. Solid chunks were crushed, fibrous materials were shredded, and sediments were dispersed. Acid (HCL) was applied repeatedly to ensure the absence of carbonates. Chemical concentrations, temperatures, exposure times, and number of repetitions, were applied as necessary for this sample. The sample, for a number of reasons, could not be subjected to alkali washes to ensure the absence of secondary organic acids. The most common reason is that the primary carbon is soluble in the alkali. Dating results reflect the total organic content of the analyzed material. Accelerator-mass-spectrometer (AMS) results were derived from reduction of sample carbon to graphite (100%C), along with standards and backgrounds. The graphite was then measured for ^{14}C in an AMS, followed by verification, isotopic fractionation correction, and calendar calibration. The C13/C12 ratio is –23.4 o/oo and the conventional radiocarbon age [RCYBP (radiocarbon years before the present, "present" = 1950 AD) is 3230 ± 40 BP. The quoted errors represent 1 sigma statistics.

N378
.W7255

Plate 2

Cone Hill volcanic complex (CHVC). The CHVC is composed of pahoehoe lava flows surrounding a linear zone of eruptive vents aligned on a NNE trending ridge that culminates at Cone Hill.

K. Cone Hill is a steep spatter cone, half of which appears to be missing in the area of the adjacent caldera.

J. The Cone Hill caldera is somewhat greater than 100 m in diameter and ~30 m deep with steep to vertical walls; it is floored with basalt boulders. The southern caldera rim is composed of a few meters of partially welded scoria topped by ~5 m of clastogenic lava with crude columnar jointing. Clastogenic lava covers the area around the caldera and also spills down the ridge slope, mostly to the west and northwest.

L. Turret-like remnants of a tephra cone partially enclose a frozen lava lake that fills the central crater and spills over on three sides. The area of the lava lake adjacent to Cone Hill is covered by clastogenic lava from Cone Hill.

I. Fissure strikes NE toward Cone Hill. The trend of the fissure passes through the southern flank of a small cone, composed of scoria overlain by welded spatter, and directly toward the lowest point on the Cone Hill caldera rim.

M. Enigmatic lava dome has a carapace of lava that overlies an older, faulted, welded spatter and scoria cone that is exposed beyond the southern limit of the lava carapace. Two small explosion craters are located on the north end of the dome. No lava appears to have issued from them and no vent is evident on the carapace.

H. Overlapping tephra cones with spatter rims one-to-several m thick emplaced upon a scoria base. A vertical feeder dike is preserved in the NE wall of the NE crater. The dike has quenched glassy borders and a vesicular interior. The cone craters are elongate in the direction of the fissure trend (057°). Lava levees are located on the north end of the north cone rim. Note change in strike of fissure that occurs here.

G. Fissure continues toward two small overlapping cinder/spatter cones with open craters. Fissure is several meters wide and filled with loose boulders; it is offset 0.5 -1 m down to the west.

F. Fissure appears to extend from caldera toward a pit crater formed by stoping above a magma filled fracture.

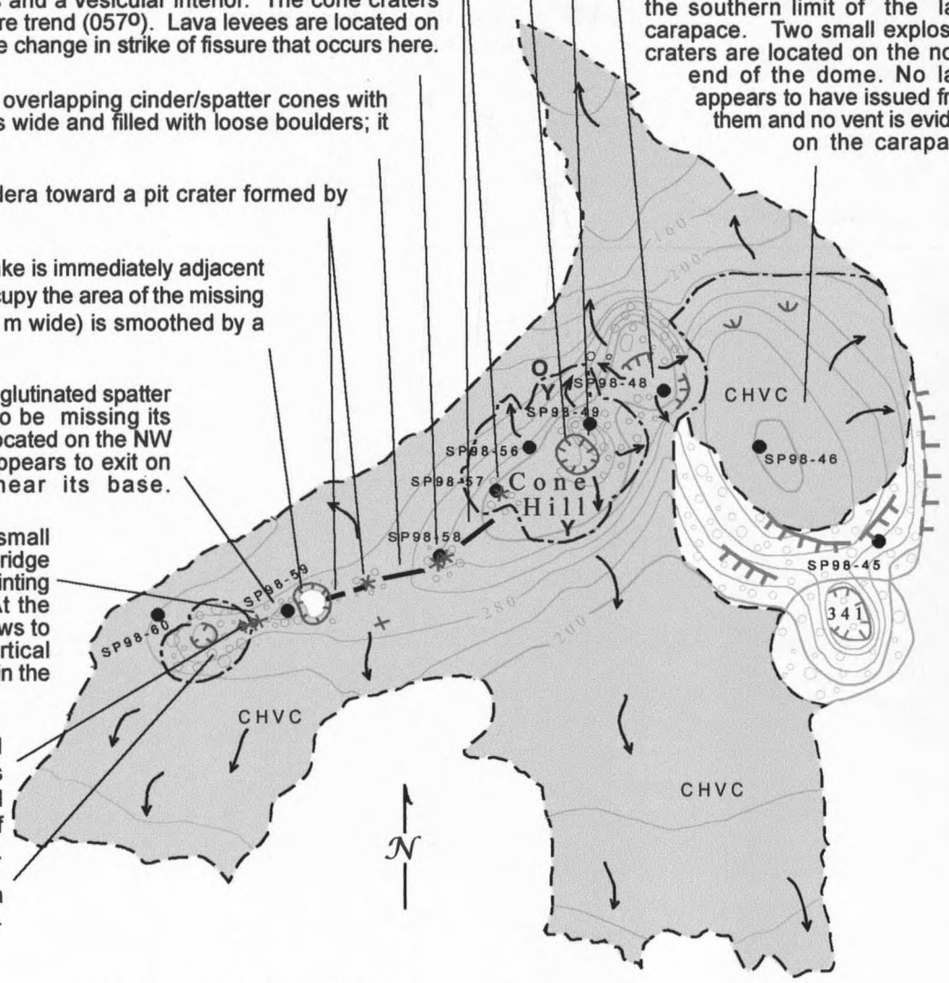
E. Caldera containing "Kittiwake Lake" lake is immediately adjacent to partial spatter cone and appears to occupy the area of the missing part of the cone. The caldera rim (~100 m wide) is smoothed by a cover of sediment.

D. Partial cone composed of layers of agglutinated spatter overlying scoria. The cone appears to be missing its NE half. The opening to a lava tube is located on the NW side of the cone facing the lake and appears to exit on the western side of the cone near its base.

C. A several meter wide opening in a small mound of lava is spanned by a narrow bridge of lava, the center of which has vertical jointing and is interpreted as a feeder dike. At the bottom, 6-8 m down, the opening narrows to a small tube ~2 m in diameter. A vertical section of the 1 m wide dike is exposed in the SW wall of the opening.

B. Lava tube with two closely spaced roof-collapse features. SW collapse is ~20 m wide and 20 m deep. The exposed cross-section of the roof is composed of at least 5 slightly sagging layers of lava.

A. Low rounded cinder cone with a poorly defined breached crater.



Map symbols on Plate 1

KILOMETERS

0 1/2 1 2

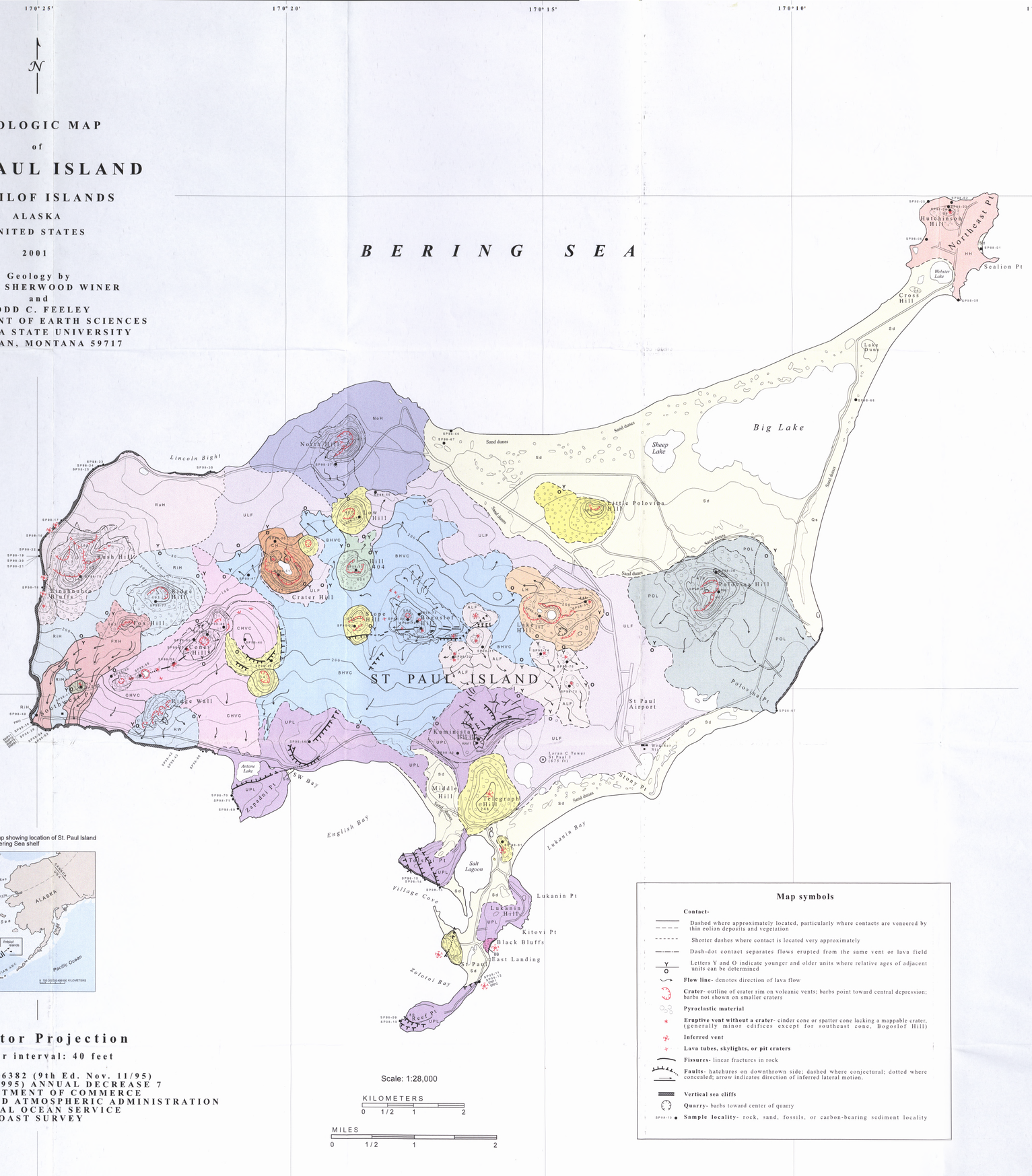
CONTOUR INTERVAL: 40 FEET

Plate 1

GEOLOGIC MAP
of
ST. PAUL ISLAND
PRIBILOF ISLANDS
ALASKA
UNITED STATES
2001

Geology by
GRACE SHERWOOD WINER
and
TODD C. FEELEY
DEPARTMENT OF EARTH SCIENCES
MONTANA STATE UNIVERSITY
BOZEMAN, MONTANA 59717

N278
.W7255



Index map showing location of St. Paul Island on the Bering Sea shelf

Mercator Projection

Contour interval: 40 feet

From map # 16382 (9th Ed. Nov. 11/95)
VAR 11° 30' E (1995) ANNUAL DECREASE 7
U.S. DEPARTMENT OF COMMERCE
NATIONAL OCEANIC AND ATMOSPHERIC ADMINISTRATION
NATIONAL OCEAN SERVICE
COAST SURVEY

Scale: 1:28,000

KILOMETERS
0 1/2 1 2

MILES
0 1/2 1 2

Map symbols

Contact-
- Dashed where approximately located, particularly where contacts are veneered by thin eolian deposits and vegetation
- Shorter dashes where contact is located very approximately
- Dash-dot contact separates flows erupted from the same vent or lava field
- Letters Y and O indicate younger and older units where relative ages of adjacent units can be determined
- **Flow line**- denotes direction of lava flow
- **Crater**- outline of crater rim on volcanic vents; barbs point toward central depression; barbs not shown on smaller craters
- **Pyroclastic material**
- **Eruptive vent without a crater**- cinder cone or spatter cone lacking a mappable crater, (generally minor edifices except for southeast cone, Bogoslof Hill)
- **Inferred vent**
- **Lava tubes, skylights, or pit craters**
- **Fissures**- linear fractures in rock
- **Faults**- hatchures on downthrown side; dashed where conjectural; dotted where concealed; arrow indicates direction of inferred lateral motion.
- **Vertical sea cliffs**
- **Quarry**- barbs toward center of quarry
- SP98-19 ● **Sample locality**- rock, sand, fossils, or carbon-bearing sediment locality

MAP UNITS

All Quaternary in age
Arranged in approximate chronological order

- Sd — Surficial deposits
- FXH — Fox Hill cinder cone and lava flow
- BVC — Bogoslof Hill volcanic complex
- CHVC — Cone Hill volcanic complex
- HH — Hutchinson Hill lava/tephra cone and lava flow
- ALF — Airport lava field
- RW — Ridge Wall tephra cone and lava flow
- RuH — Rush Hill cinder cone and lava flow
- RiH — Ridge Hill cinder cone and lava flows
- LH — Lake Hill cinder cone and lava flow
- H255 — Hill 255 spatter cone and lava flow
- CH — Crater Hill pyroclastic cone and lava flow
- POL — Polovina Hill cinder cone and lava flow
- H404 — Hill 404 cinder cone and lava flow
- NoH — North Hill cinder cone and lava flow
- ULF — Undifferentiated lava flows of uncertain origin
- PyC — Pyroclastic cones with no identifiable lava flows
- BB — Black Bluffs tuff/cinder cone
- UPL — Undifferentiated platform lavas

DESCRIPTION OF MAP UNITS[1]

SURFICIAL DEPOSITS

Sd — **Sedimentary deposits -** Undifferentiated sedimentary deposits; includes colluvium, sand dunes, and sandy beaches. Thin and discontinuous deposits of loess and eolian sand that partially cover lava flows and tephra deposits are not mapped.

LAVA FLOWS AND PYROCLASTIC DEPOSITS

All lava flows mapped are pahoehoe flows; most flow surfaces are broken into boulders by frost riving. The natural color of the rocks is often concealed by a covering of ubiquitous pale-gray lichens, except on lavas exposed along the coast. Volcanic rocks mapped are basanites, basalts, trachybasalts, and tephrites.

FXH — **Fox Hill lava flow and breached cinder cone** - Basanite lava flows from four aligned vents coalesce to form the Fox Hill flow. The pahoehoe flow is studded with chunks of the breached cinder cone. Flow levees and channels are well preserved and the flow surface has little cover from eolian deposits. On the basis of a single high-precision AMS radiocarbon age-date, on carbon-bearing sediment buried by the lava flow (SP98-63), the age of the unit is 3230 +/- 40 y.b.p. Rock is crystal-poor olivine-basalt.

BHVC — **Bogoslof Hill volcanic complex** - A polygenetic shield volcano with a complex eruptive history, Bogoslof Hill is the source of the most voluminous lava flows forming the central highland. Pahoehoe lava flows are surface- and tube-fed. Lava tubes are exposed on the NW, N, and SW flanks of Bogoslof Hill. Rifts trending E-W across Bogoslof Hill are partially covered by younger lava flows. Some Bogoslof lavas are conspicuously plagioclase-rich (~30 modal % plagioclase). The most extensive of the Bogoslof flows, a trachybasalt with abundant very fine groundmass plagioclase, has many blocky outcrops interpreted as tumuli, lava rises, and pop-ups. Most BHVC lavas are tephrites.

HH — **Hutchinson Hill eruptive center** - Hutchinson hill is constructed of scoria, welded spatter, and thin (<1 m) lava flows. Basalts of the Hutchinson Hill field are plagioclase-rich (~22 modal%). The Hutchinson Hill cone and lava field formed an island that has since connected to the main island by a tombolo.

CVHC — **Cone Hill volcanic complex** - A linear array of cinder and spatter cones, clastogenic deposits, surface and tube-fed flows, cauldrons, collapse features, and discontinuous exposures of fissures lie along a northeast trending ridge. A feeder dike is exposed on the southwestern ridge-crest. Cone Hill trachybasalts and tephrites are distinguished by the frequent occurrence of plagioclase and clinopyroxene glomerocrysts. Cone Hill lava covers most of the roundish, flattened dome on the northeastern part of the Cone Hill complex; beneath the carapace of Cone Hill lava, this broad, steep-sided edifice is faulted on its south and southeast flanks where welded spatter and tephra of a pre-existing (PyC) cone are exposed.

ALF — **Airport lava field** - A group of monogenetic vents with similar chemistry, ALF lavas are chiefly surface- and tube-fed, coalescing flows of basanites with conspicuous large plagioclase laths. Low scoria mounds with discontinuous covers of welded spatter surround source vents.

RW — **Ridge Wall cinder cone complex and associated lava flow** - Ridge Wall is a complex breached cinder cone with multiple aligned vents and an associated lava flow. The lava flow has moved a large portion of the cone; as much as 15 m of cone material rests on the lava flow exposed in vertical section in the sea cliff. The basalt in the flow is dark grey and vitrophyric with olivine phenocrysts as large as 5 mm. Ridge Wall's pyroclastic deposit includes a large portion of unwelded, very glassy ribbon and cowdung bombs with colors ranging from brown to red to blue-black.

RuH — **Rush Hill cinder cone complex and associated lava flows** - A large eruptive center on the west end of St. Paul, Rush Hill is the highest point on the island (665'). The multiple nested pyroclastic cones of Rush Hill indicate a complicated eruptive history. The cone complex is breached to the north and west where lava flows extend to the coast. Lava is dark gray olivine basalt and tephrite. Vesicular spatter from the summit of Rush Hill (SP98-78) contains a crustal xenolith.

RiH — **Ridge Hill cinder cone and associated lava flows** - Ridge Hill cone is breached to the southwest and surrounded on the east and south by an apron of low, rounded scoria mounds that appear to be related to lateral spreading of the cone base from "floating" on a layer of lava. Ridge Hill picritic trachybasalt flows extend to the west coast and to the southwest beneath the Fox Hill lava flow.

LH — **Lake Hill cinder cone complex and associated lava flow -** Complex, multiple-vent, nested cinder cones at Lake Hill contain two crater lakes and have an associated lava flow. Glassy black agglutinated basalt in a welded horizon on a crater wall contains large (~ 5 mm) olivine phenocrysts.

CH — **Crater Hill pyroclastic cone and associated lava flow -** The upper Crater Hill cone is armored with spatter and has a sharp edged crater rim that appears to have been truncated by a violent explosion that may have reamed out the inner wall of the cone. A lake and two spatter cones are contained within the crater. Welded spatter on the crater rim contains both granitic and ultramafic xenoliths. A tongue of olivine-basalt lava flows northward from the breached scoria cone.

H255 — **Hill 255** - Hill 255 is a small spatter cone of olivine basalt. Lava has flowed southwest from a notch in the low spatter-rim of its shallow crater. A lava flow of similar composition (SP98-40) (inferred to be from Hill 255) is exposed in the sea-cliff at Southwest Point. This flow is overlain by two younger flows and only a small part of the flow is exposed on the geological map. Hill 255 is locally called the "Halibut's Tail" because of its notched profile.

POL — **Polovina Hill cinder cone complex and lava flow** - Polovina Hill, a nested cinder cone complex with at least two constructional episodes, is composed of crudely stratified, unconsolidated, red and black scoria with block- and bomb-rich layers. Blocks and bombs include dense black tachylite blocks and spindle and breadcrust bombs; some are >1 m in length. Polovina Hill has two craters; both are breached on the southwest side. On the younger crater rim are rare buff-colored, finely-vesiculated trachyte clasts with 62 wt% silica (SP98-35). Polovina Hill basanite lava flows form an extensive shield surrounding its large cone.

NoH — **North Hill cinder cone and associated lava flows** - North Hill is a complex cinder cone on the north coast. A lava flow issues from a breach on the southwest side of North Hill where a section of the cone and crater rim has been moved outward and rotated in a coherent mass. North Hill is surrounded by flows of dark grey, glassy, clinopyroxene- and olivine-phyric basanite.

H404 — **Hill 404 cinder cone and lava flow** - Hill 404 is a simple breached cinder cone with a small lava flow; the flow may be partially buried by younger flows from other centers.

ULF — **Undifferentiated lava flows of uncertain origin** - Vents for these flows have not been identified. Flow surfaces are often mantled by thin and discontinuous layers of eolian sediments and tundra vegetation.

PyC — **Pyroclastic cones** - These cones have no identified associated lava flows. They are constructed of brown, red, and black scoriaceous lapilli and bombs, and welded spatter of basalt and basanite.

BB — **Black Bluffs tuff/cinder cone** - A vertical section of theBlack Bluffs emergent tuff/cinder cone is exposed on the coast east of the village of St. Paul. The lower part of the cone, near sea level, is grey-brown and red-brown, well-stratified tuff composed of rounded lapilli in an ashy matrix; it contains accidental blocks of friable grey mudstone and has bedding plane sags related to block and bomb impacts. Up section the composition changes abruptly to black, crudely-stratified scoria with block-rich layers. The face of Black Bluffs is faulted with offsets as great as 2.5 m.

UPL — **Undifferentiated platform lavas** - Often faulted and tilted, these lava flows of basalts and trachybasalts are best exposed on the island's southern promontories. In other areas thin covers of eolian deposits and tundra vegetation often mantle flow surfaces. Undifferentiated platform lavas have no associated preserved vents; their vents may have been eroded or covered by younger volcanic deposits. The lavas are often characterized by their holocrystalline nature.

[1] Because all map units are Quaternary, the letter "Q" has been omitted from their symbols

MONTANA STATE UNIVERSITY - BOZEMAN
3 1762 10350513 5